Detection Schemes for Multi-Antenna FH/MFSK Systems in the Presence of Multiple Follower Jamming

LIU FANGMING
(B.Eng, Fudan University, P.R. China)

A THESE SUBMIITED
FOR THE DEGREE OF DOCTOR OF PHILOSOPHY
DEPARTMENT OF ELECTRICAL AND COMPUTER ENGINEERING
NATIONAL UNIVERSITY OF SINGAPRE
2010

ACKNOWLEDGEMENT

First and foremost, my deepest gratitude goes to my supervisors, Professor Ko Chi Chung, for his enlightening guidance, supports, encouragement and unending patience throughout the entire period of my Ph.D course and the write-up of this thesis. His invaluable suggestions and discussions are truly rewarding.

Special thanks to my parents, my wife, and my grandparents, who always encourage, support and care for me throughout my life.

I am also grateful to all the colleagues and students in the Communications Laboratory at the Department of Electrical and Computer engineering of National University of Singapore.

CONTENT

SUMMARY

This dissertation focuses on the performance of the frequency hopping spread spectrum (FHSS) *M*-ary frequency shift keying (MFSK) systems in the presence of follower partial band jamming noise (PBJN) over flat fading channels. The thermal and other wideband Gaussian noises are modeled as additive white Gaussian noise (AWGN) at the receiver.

Follower partial band jamming is recognized as an efficient strategy to degrade the performance of FH/MFSK modulation. In this dissertation, three anti-jamming algorithms, based on maximum likelihood-based beamforming (MLBB), an area-based vector similarity metric (VSM), and a volumetric-based algorithm, are proposed to reject follower jamming and carry out symbol detection in slow FH/MFSK systems over quasi-static flat fading channels. In addition, theoretical analysis is derived under a jamming dominant scenario.

The MLBB algorithm which consists of a two-element array first uses an ML-based approach to obtain an ML estimate of the ratio of the jamming fading gains. Based on this ML estimate, a simple beamforming structure is employed to place a null toward the follower jamming source, and symbol detection is then performed by the ML technique. Theoretical and simulated

results show the effectiveness of the proposed algorithm in combating follower jamming.

Using the principle of vector similarity, an area-based VSM algorithm is formulated to give an estimate of the unknown spatial correlation of the received jamming components at the two receiver antennas. The jamming signal can then be removed in the symbol detection process. The improved performance of the VSM algorithm is verified by analysis under a jamming dominant environment as well as using simulated bit error rate (BER) results.

The volumetric-based algorithm uses a multi-element array, and is proposed to reject multiple follower jamming signals and to carry out symbol detection in slow FH/MFSK systems over quasi-static flat fading channels. Specifically, with the use of the proposed algorithm, which can provide an estimate of the unknown spatial correlation of the received multiple jamming components at the receiver antennas, jamming can be removed in the symbol detection process. The jamming rejection capability of this algorithm is verified by analysis under a jamming dominant environment as well as by the much improved BER obtained in simulation studies.

In summary, the MLBB and VSM methods can reject a single jammer by using a two-element antenna. The volumetric algorithm can reject multiple jammers by using a multi-elements antenna. Finally, these three proposed

algorithms can attain highly reliable bit detection with low BER values over a wide range of signal and jamming power ratios.

LIST OF TABLES

LIST OF FIGURES

LIST OF ABBREVIATIONS

AWGN	additive white Gaussian noise
BER	bit error rate
DSSS	direct sequence spread spectrum
FH	frequency hopping
FHSS	frequency hopping spread spectrum
i.i.d	independent identically distributed
MAI	multi-access interference
MFSK	*M*-ary frequency shift keying
ML	maximum likelihood
MLBB	maximum likelihood-based beamforming
MTJ	multi-tone jammer
OFDM	orthogonal frequency-division multiplexing
PBJN	partial band jamming noise
SJR	signal-to-jamming power ratio
SJR_i	signal to the *i*th jamming power ratio
SMI	sample matrix inversion
SNR	signal to noise power ratio
TFD	time-frequency distribution
VSM	vector similarity metric

LIST OF SYMBOLS

α_i	phase shift and attenuation of the *i*th hop for desired signal
β_{kp}	phase shift and attenuation of the *i*th hop for jamming signal
d_p	pilot symbol
E_b/N_0	ratio of bit energy of the signal to white noise energy
f_d	frequency spacing between two adjacent MFSK tones
f_i	hopping frequencies of the *i*th hop
σ^2	variance of the white noise
L	number of samples the receiver received
N	sampling symbol rate
$n_j(t)$	baseband equivalent band-limited signal
P_e	theoretical BER rate
R	information rate
T	duration of one information bit
T_c	chip duration
T_d	data modulator output symbol duration
T_s	sampling period
T_y	symbol duration
$\Gamma(d)$	cost function
V	number of samples per hop

$\mathbf{v}_p$	jamming components of the received signal
W	bandwidth
$w(n)$	additive white Gaussian noise
X	number of jamming signals
Z	number of chips that the MFSK modulator is subdivided into

CHAPTER 1

INTRODUCTION

1.1 Introduction of Spread Spectrum Systems

Spread spectrum signals used for the transmission of digital information are distinguished by the characteristic that their bandwidth W is much greater than the information rate R in bits/s. Spread spectrum signals can be used for combating or suppressing the detrimental effects of interference such as jamming signal, signal transmitted by other users of the channel, and self-interference due to multipath propagation.

There are two fundamental types of spread spectrum systems: direct sequence spread spectrum (DSSS) system and FHSS system. A wideband spread spectrum signal is generated from a data modulated carrier by modulating the data a second time using a very wideband spreading signal. The spreading modulation may be a phase modulation or from a rapidly changing carrier frequency or a combination of these and other techniques. When spectrum spreading is accomplished by phase modulation, the resultant signal

is called a DSSS signal. When the spectrum spreading is accomplished by rapid changing of the carrier frequency, the resultant signal is called an FHSS signal.

1.2 A Literature Review of FHSS

In FHSS, each carrier frequency is typically chosen from a set of 2^C (C is a positive integer) frequencies that are spaced approximately over the width of the data modulation spectrum available, although neither condition is absolutely necessary. The spreading code, in this case, does not modulate the data-modulated carrier directly but is used to control the sequence of carrier frequencies. In the receiver, the frequency hopping is removed by mixing with a local oscillator signal that is hopping synchronously with the received signal. Block diagrams of the transmitter and receiver are shown in Fig. 1.1 [1].

Although PSK modulation gives better performance than FSK in an AWGN channel, it is difficult to maintain phase coherence in the synthesis of the frequencies used in the hopping pattern. Consequently, FSK modulation with noncoherent detection is usually employed with FHSS signals [2].

Due to the advantages of combating narrowband interference and multi-access interference (MAI), FHSS has been used in military applications,

wireless personal communications [3], and satellite communications [4-6].

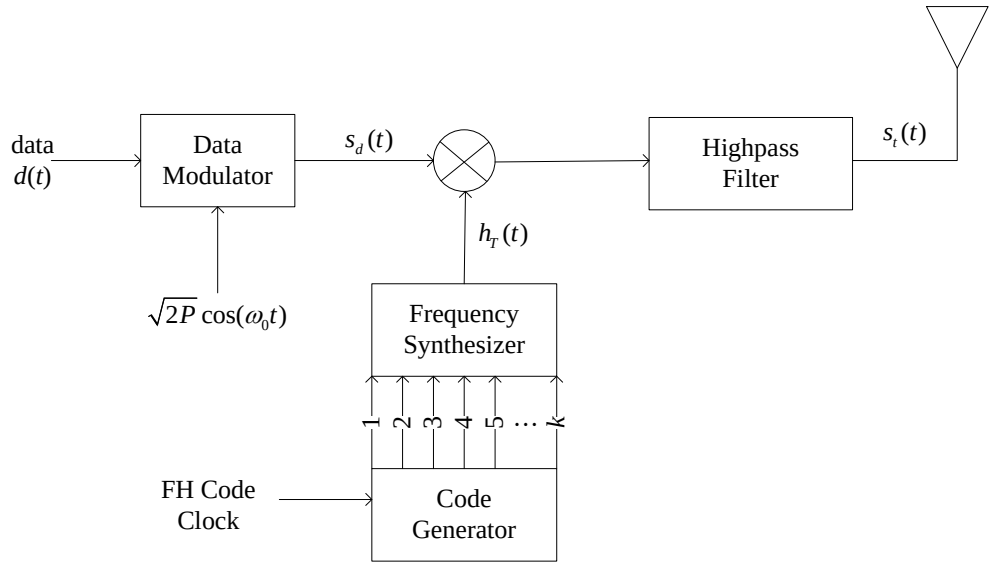

(a) Transmitter

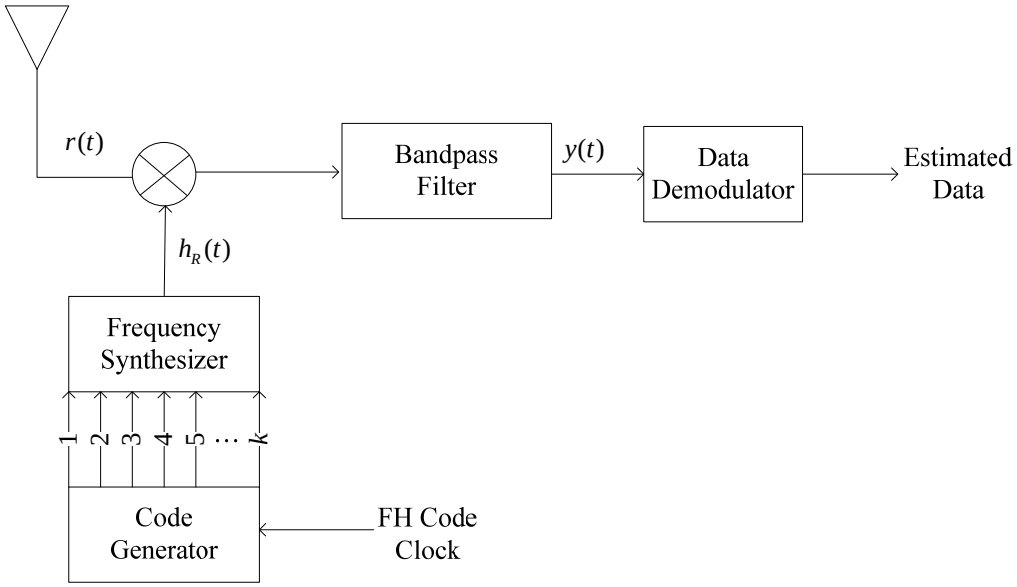

(b) Receiver

Fig. 1.1: FHSS system modem

1.2.1 Slow FHSS Systems

Consider an MFSK data modulation for FHSS systems. The data modulator outputs one of 2^C tones, each lasting CT seconds, where T is the duration of one information bit. Usually, these tones are spaced far enough apart so that the transmitted signals are orthogonal. This implies that the data modulator frequency spacing is at least $1/CT$ and that the data modulator output spectral width is approximately $2^C / CT$. Assume that, in each T_c seconds, or one hop duration, the data modulator output is transmitted to a new frequency by the frequency-hop modulator.

When $T_c \geq CT$, the FHSS system is called a slow frequency hopping system.

1.2.2 Fast FHSS Systems

In contrast to the slow FHSS systems when the hop frequency band changes more slowly than symbols coming out of the data modulator, the hopping frequency band can change many times per symbol in fast FHSS systems. A significant benefit of fast FHSS is that frequency diversity gain is

achieved in each transmitted symbol, which is particularly beneficial in a partial band jamming environment.

Assume that the output of the MFSK modulator is subdivided into Z chips. After each hop, the MFSK modulator output is hopped to a different frequency. Because the chip duration T_c is shorter than the data modulator output symbol duration T_d, the minimum tone spacing for orthogonal signals is now $1/T_c = Z/CT$.

The data demodulator can operate in several different modes in fast FHSS systems. One mode is to make a decision on each frequency hopping chip as it is received and to make an estimate of the data modulator output based on all Z chip decisions. The decision rule could be a simple majority vote. Another mode would be to calculate the likelihood of each data modulator output symbol as a function of the total signal received over Z chips and to choose the largest value. A receiver that calculates the likelihood of each symbol is optimum in the sense that minimum error probability is achieved for a given E_b/N_0. Each of these possible operating modes performs differently and has different complexity. The spread spectrum system designer must choose the mode of operation that best solves the particular problem under consideration.

1.2.3 Synchronization of FH Systems

FH communications require the spreading waveforms of the transmitter and receiver to be synchronized. If the two waveforms are not synchronized within as little as one chip, insufficient signal energy will reach the receiver data demodulator for reliable data detection. The task of achieving and maintaining code synchronization is usually delegated to the receiver [7-23].

The authors of [11; 12] describe an FH transceiver using a synchronization method based on a simple time division duplexing (TDD) frame structure. The latter consists of a pilot tone, a frame ID, and actual data, with synchronization being accomplished by means of energy detection and pattern matching. [16] proposes to use Bayesian techniques to address jointly the problem of frequency estimation and synchronization of frequency hopping signals in a FH system. To maintain synchronization in the presence of fading or narrowband interference, [18] propose a time division duplex packet algorithm based on slow FH system. By using the power sum definition, [22] proposes the cost function that has minimum at zero hop-timing error. However, the acquisition range is quite limited.

In general, synchronization are carried out by using a pilot signal or sync

bit which has the disadvantages of requiring additional time slots and bandwidth, reduces the data rate.

Alternatively, the use of a parameter estimation algorithm may be explored in the absence of pilot signals. Specifically, [7] proposes an algorithm that uses a time-frequency representation of the observed signal before estimating the parameters that characterize the time-frequency trajectory of the signal. Based on the trajectory estimated, the hopping transitions and frequencies can be found, even though as discussed in [7], the method suffers from an inevitable threshold effect. Similarly, [8] proposes a wavelet estimation technique that uses an instantaneous correlation function for the detection of frequency hopping signals. The ML-based algorithm proposed by [10] for frequency hop synchronization does not use any pilot signal. An iterative method is derived to estimate the hopping frequency and hop transition time at the same time.

1.2.4 Typical Types of Jamming Against FHSS

In FHSS systems, there are four main kinds of intentionally jamming sources. These are barrage noise, single tone, multi-tone and partial-band jammers. Among these types of jammers, the most popular one is the barrage

noise jammer which only transmits a band-limited white Gaussian noise whose power spectrum covers the entire frequency range of a target FHSS receiver. Consequently, a barrage noise jammer usually has the same effect as thermal noise, which enhances the noise level at a target FHSS receiver [77].

The second type of intentional jamming is single-tone jamming. A single-tone jammer simply transmits an un-modulated carrier signal at a certain frequency in the currently used FHSS signal bandwidth. As a result, this type of jamming induces a quite insignificant effect on FHSS systems since the instantaneous FHSS frequency bandwidth is small and changes continuously. For FHSS systems, a more effective tone jamming strategy is the use of multi-tone jamming which transmits various un-modulated carrier signals in the entire FHSS frequency bandwidth [1]. Multi-tone jamming is more efficient in interfering a fast FHSS system.

To obtain a more efficient jamming strategy in slow FHSS systems, partial-band jamming is usually employed [1]. This jamming scheme transmits all its available power to a certain portion of the entire FHSS signal bandwidth [78]. In fact, such jammers include extremely effective ones which are called follower partial-band jammers [79] (smart or repeater jammers). A follower partial band jammer is able to determine the currently used frequency band of a target FHSS receiver and injects its interfering signals to that frequency band.

1.2.5 Performance of FHSS Systems in a Jamming Environment

FHSS is known to be robust against intentional jammers. However, the performance will be severely degraded by the PBJN [24] or a multi-tone jammer (MTJ).

Conventionally, fast FH with noncoherent FSK modulation is used to protect the transmitting signals against a certain hostile jammer. The MTJ strategy causes more critical harm than the PBJN algorithm does, because the former possesses more effective power utilization.

The performance evaluation of fast FH/MFSK communication systems using various diversity-combining methods in the presence of MTJ and AWGN can be found in [24-46]. [25] derives an optimum structure of an ML receiver for a fast FHSS communication system with the interference of MTJ and AWGN. It shows that the side information of noise variance, signal tone amplitude, and multiple interfering tone amplitude at each hop, as well as the computation of nonlinear modified Bessel function are required to implement the optimum ML receiver. [28] further investigate the performance of the product-combining receiver and the clipper receiver against MTJ for an

FFH/MFSK system over AWGN channels. By employing a square law receiver, [26] analytically investigates the performance degradation to orthogonal noncoherent FFH MFSK due to multitone interference, where the channel for each hop band is modeled as a slowly fading Ricean process.

However, there is a penalty incurred in subdividing a signal into several FH elements. This is due to the fact that the energy from these separate elements has to be combined noncoherently. In addition, in FH systems, the transmitters and receivers contain clocks that must be synchronized. That is, the transmitters and receivers must hop at the same rate at the same time. The faster the hopping rate, the higher the jamming resistance, and the more accurate the clocks must be. This means that a highly accurate clock is required to allow a very fast hop rate for the purpose of defeating a follower jammer. Some systems may still have limitations that do not allow for fast hopping.

Investigations on slow FHSS systems in the presence of partial-band jamming have been carried out in [47-55] while studies on follower jamming mitigation have been well documented in [56-58]. Specifically, in [54], a countermeasure to a follower partial-band Gaussian noise jammer was proposed for FHSS communications. The proposed scheme makes use of randomized decisions by the transmitter and the receiver to lure the jammer so that system performance can be improved. Of course, this implies that both the

transmitter and receiver have to require a higher level of synchronization.

1.2.6 Anti-jamming Algorithms For FHSS Systems

An antenna array using the sample matrix inversion (SMI) algorithm is exploited to isolate the desired signal and the jamming signal for the purpose of suppressing the latter in [56]. This algorithm, however, assumes that the antennas have equal gains in the direction of the jammer, and will not function properly under a quasi-static flat fading channel.

The algorithm proposed in [58] has a better performance in a jamming dominant scenario. This, however, treats the received jamming signals as deterministic unknowns to be estimated, and so, the lower the jamming power (or the higher the signal to jamming ratio), the less accurate the jamming estimates. The increased inaccuracy in the jamming estimates leads in turn to a deterioration in performance. On the other hand, under the traditional ML algorithm, the received jamming components are considered as additional receiver noise. Thus, the higher the jamming power, the higher the amount of total noise, and the worse the performance.

1.3 Research Objective and Contributions

To investigate the FH synchronization problem, keeping in mind the discussions in Section 1.2.3, we further assume that hopping is an unknown parameter. Noting that this scenario is worse than even [10], Chapter 2 proposes and investigates an algorithm for estimating the hopping transition time, hopping period and frequencies in a frequency hopping system under the presence of flat fading. For optimality, the algorithm aims to minimize a ML-based objective function.

To combat jamming signal with FHSS system, [24-46] discussed the performance of fast FHSS under that attack of MTJ with various antenna types. Although [47-58] have investigations on the performance of slow FHSS systems in the presence of partial-band jamming, very few papers [56-58] consider Rayleigh flat fading channel.

The MLBB algorithm, which consists of a two-element array, first uses an ML-based approach to obtain an ML estimate of the ratio of the jamming fading gains. Based on this ML estimate, a simple beamforming structure is employed to place a null toward the follower jamming source, and symbol detection is then performed by the ML technique.

The principle of vector similarity has attracted a lot of interest recently in

applications such as searching [59-61], face authentication [62] and fuzzy set systems [63;64]. This principle may also be profitably employed in some digital wireless communication systems where multiple dimensional vector representations are frequently used in such systems for a variety of purposes such as symbol detection.

This dissertation also investigates how vector similarity can be formulated to lead to a novel area-based and volumetric-based vector similarity metric that can be used for carrying out symbol detection in the presence of jamming signals and white noise in FHSS communication systems.

Taking the effect of follower jamming and flat fading into account, two jamming rejection algorithms are proposed in this dissertation. Specifically, the proposed VSM algorithm uses a two-element array to reject single follower jamming signal interference and carry out symbol detection in slow FH/MFSK systems over quasi-static flat fading channels. In addition, in the presence of more than two jammers, the volumetric-based algorithm can be used to carry out symbol detection.

Simulation and analytical results show that the performances of the MLBB and VSM are better than the traditional ML approach, the SMI method and the algorithm proposed in [58], especially in jamming dominant scenarios. In addition, the performance of the volumetric-based algorithm is better than those

of the traditional ML approach and the SMI method in the presence of more than two jammers.

1.4 Structure of the Dissertation

CHAPTER 2 proposes an ML-based algorithm for estimating the hopping transition time, hopping period and frequencies in a frequency hopping system in the presence of flat fading.

The transmitted signal model with the jamming model is presented in CHAPTER 3. The proposed MLBB algorithm, which can eliminate one jammer with two receivers, is presented in CHAPTER 4.

In CHAPTER 5, the VSM algorithm is introduced. Based on the simulation results, we show that the VSM has the best performance among MLBB, ML, SMI and the algorithm proposed in [58].

To eliminate the effects caused by more than two jammers, the details of the volumetric-based algorithm, which can be used for carrying out symbol detection in the presence of jamming signals and white noise, is described in CHAPTER 6.

Finally, CHAPTER 7 concludes this dissertation and suggests some future

research work.

CHAPTER 2

SYNCHRONIZATION OF FREQUENCY HOPPING SYSTEMS

2.1 Introduction

Typically, the available channel bandwidth in an FHSS communication system is divided into a large number of contiguous frequency slots, with the carrier frequency pseudorandomly hopping from one value to another in consecutive signaling intervals or hopping periods. During synchronization or when no data is being transmitted, the receiver receives an unknown carrier tone that changes its frequency at regular hopping transitions. In the presence of flat fading, the tone will also be subjected to unknown amplitude and phase changes that depend on the frequency of the tone and the multipath environment. In this chapter, we are interested in investigating how the hopping frequency, hopping transitions and period can be estimated from the received signal. The estimation of these parameters will serve to synchronize the receiver to the FHSS transmitter.

2.1.1 Transmitted Signal Model

To jointly estimate the hopping transitions and period, at least 3 hops are needed. For the sake of simplicity, consider a three-hop frequency hopping (FH) signal model, which is shown in (2.1)

$$s(n)=\begin{cases} e^{2j\pi f_1 nT_s}, n=0,...,V-1 \\ e^{2j\pi f_2 (n-V)T_s}, n=V,...,2V-1 \\ e^{2j\pi f_3 (n-2V)T_s}, n=2V,...,3V-1 \end{cases}, \quad (2.1)$$

where f_1, f_2 and f_3 are the hopping frequencies in the three hops, T_s is the sampling period, V is the number of samples per hop, and VT_s is the hopping period. A total of L ($L>2V$) samples are taken, which spans the three hops.

2.1.2 Received Signal Model

In a flat fading environment, the phase and amplitude of the transmitted signal will be changed due to multipath fading, and the received signal in an interval of LT_s (or L samples) can be written as

$$r(n)=\begin{cases} \alpha_1 e^{2j\pi f_1 (V-K-1+n)T_s}+w(n), n=1,...,K \\ \alpha_2 e^{2j\pi f_2 (n-K-1)T_s}+w(n), n=K+1,...,K+V \\ \alpha_3 e^{2j\pi f_3 (n-V-K-1)T_s}+w(n), n=K+V+1,...,L \end{cases}. \quad (2.2)$$

The complex constant α_i, i=1,2,3 represents the phase shift and attenuation of the ith hop through the transmitting path, and $w(n)$ is AWGN with a mean of 0 and a variance of σ^2. Note that there are K samples in hop one, V samples in hop two and $L-V-K$ samples in hop three, with K

representing the uncertainty in hop timing between the transmitter and receiver in the first hop. The problem of finding out K and V in (2.2), together with the hopping frequencies, is thus equivalent to solving the synchronization problem. Fig. 2.1 illustrates how the timings of the signals at the transmitter and receiver are related.

Transmission: $3V$ samples in 3 hops

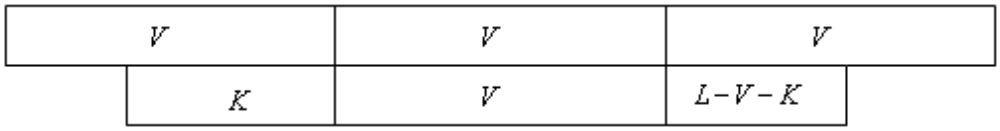

Reception: L samples spanning 3 hops

Fig. 2.1 Transmitted and received signal blocks

Defining the vectors

$$\mathbf{r} = [r(1), ..., r(L)]^T , \tag{2.3}$$

$$\mathbf{s} = [\alpha_1 e^{2j\pi f_1 (V-K)Ts}, ..., \alpha_1 e^{2j\pi f_1 (V-1)T_s}, \alpha_2, ..., \alpha_2 e^{2j\pi f_2 (V-1)T_s}, \alpha_3, ..., \alpha_3 e^{2j\pi f_3 (L-V-K-1)T_s}]^T \tag{2.4}$$

and

$$\mathbf{w} = [w(1), ..., w(L)]^T , \tag{2.5}$$

the received signal in vector form is given by

$$\mathbf{r} = \mathbf{s} + \mathbf{w} . \tag{2.6}$$

For analytical convenience, the received signal vector $\mathbf{r}$ can be partitioned into three parts, with each part corresponding to one hop of the signal, as follows:

$$\begin{bmatrix} \mathbf{r}_1 \\ \mathbf{r}_2 \\ \mathbf{r}_3 \end{bmatrix} = \begin{bmatrix} \alpha_1 \mathbf{s}_1 \\ \alpha_2 \mathbf{s}_2 \\ \alpha_3 \mathbf{s}_3 \end{bmatrix} + \begin{bmatrix} \mathbf{w}_1 \\ \mathbf{w}_2 \\ \mathbf{w}_3 \end{bmatrix} \tag{2.7}$$

where

$$\mathbf{r}_1 = \left[r(1), ..., r(K) \right]^T, \tag{2.8}$$

$$\mathbf{r}_2 = \left[r(K+1), ..., r(K+V) \right]^T, \tag{2.9}$$

$$\mathbf{r}_3 = \left[r(K+V+1), ..., r(L) \right]^T, \tag{2.10}$$

$$\mathbf{s}_1 = e^{2j\pi f_1 (V-K) T_s} \left[1, ..., e^{2j\pi f_1 (K-1) T_s} \right]^T, \tag{2.11}$$

$$\mathbf{s}_2 = \left[1, ..., e^{2j\pi f_2 (V-1) T_s} \right]^T, \tag{2.12}$$

$$\mathbf{s}_3 = \left[1, ..., e^{2j\pi f_3 (L-V-K-1) T_s} \right]^T, \tag{2.13}$$

$$\mathbf{w}_1 = \left[w(1), ..., w(K) \right]^T, \tag{2.14}$$

$$\mathbf{w}_2 = \left[w(K+1), ..., w(K+V) \right]^T \tag{2.15}$$

and

$$\mathbf{w}_3 = \left[w(K+V+1), ..., w(L) \right]^T. \tag{2.16}$$

With the model in (2.7), the synchronization problem of estimating V and K, together with three hopping frequencies f_1, f_2 and f_3, will now be addressed.

2.2 ML Estimation of Hopping Transition Time and Period

Based on the signal model in (2.7), the likelihood function of the received signal is

$$f(\alpha_1,\alpha_2,\alpha_3,f_1,f_2,f_3,K,V)=\frac{1}{\sqrt{(2\pi\sigma)^L}}e^{\frac{-1}{2\sigma^2}\|\mathbf{r}-\mathbf{s}\|^2}$$
$$=\frac{1}{\sqrt{(2\pi\sigma)^L}}e^{\frac{-1}{2\sigma^2}\left(\|\mathbf{r}_1-\alpha_1\mathbf{s}_1\|^2+\|\mathbf{r}_2-\alpha_2\mathbf{s}_2\|^2+\|\mathbf{r}_3-\alpha_3\mathbf{s}_3\|^2\right)}. \quad (2.17)$$

The ML estimates of the parameters f_1, f_2, f_3, K and V can be found by maximizing (2.17), which is equivalent to minimizing the objective function

$$\phi(\alpha_1,\alpha_2,\alpha_3,f_1,f_2,f_3,K,V)=\phi_1(\alpha_1,f_1,K,V)+\phi_2(\alpha_2,f_2,K,V)+\phi_3(\alpha_3,f_3,K,V), \quad (2.18)$$

where

$$\phi_1(\alpha_1,f_1,K,V)=\|\mathbf{r}_1-\alpha_1\mathbf{s}_1\|^2, \quad (2.19)$$

$$\phi_2(\alpha_2,f_2,K,V)=\|\mathbf{r}_2-\alpha_2\mathbf{s}_2\|^2 \quad (2.20)$$

and

$$\phi_3(\alpha_3,f_3,K,V)=\|\mathbf{r}_3-\alpha_3\mathbf{s}_3\|^2. \quad (2.21)$$

To minimize $\phi_1(\alpha_1,f_1,K,V)$, we can set $\frac{\partial\phi_1}{\partial\alpha_1}=0$ which results in

$$\hat{\alpha}_1=\frac{1}{K}\mathbf{s}_1^H\mathbf{r}_1. \quad (2.22)$$

Substituting (2.22) into(2.19), the objective function $\phi_1(\alpha_1,f_1,K,V)$

becomes

$$\phi_1(f_1,K,V)=\phi_1(\hat{\alpha}_1,\,f_1,K,V)=\left\|\left(I-\frac{1}{K}\mathbf{s}_1\mathbf{s}_1^H\right)\mathbf{r}_1\right\|^2. \qquad (2.23)$$

Based on (2.11) it is easily to obtain

$$\mathbf{s}_1^H\mathbf{s}_1=K. \qquad (2.24)$$

By substituting (2.24) into (2.23), we find

$$\phi_1(f_1,K,V)=\left\|\left(I-\frac{1}{K}\mathbf{s}_1\mathbf{s}_1^H\right)\mathbf{r}_1\right\|^2=\mathbf{r}_1^H\left(\mathbf{I}-\frac{1}{K}\mathbf{s}_1\mathbf{s}_1^H\right)\left(\mathbf{I}-\frac{1}{K}\mathbf{s}_1\mathbf{s}_1^H\right)\mathbf{r}_1=\mathbf{r}_1^H\left(\mathbf{I}-\frac{1}{K}\mathbf{s}_1\mathbf{s}_1^H\right)\mathbf{r}_1 \qquad (2.25)$$

Because only $\mathbf{s}_1$ depends on f_1, the differentiation of (2.25) with respect to f_1 is

$$\frac{\partial\phi_1}{\partial f_1}=\mathbf{r}_1^H\left[\frac{\partial\left(\mathbf{I}-\frac{1}{K}\mathbf{s}_1\mathbf{s}_1^H\right)}{\partial f_1}\right]\mathbf{r}_1 \qquad (2.26)$$

where

$$\frac{\partial\left(\mathbf{I}-\frac{1}{K}\mathbf{s}_1\mathbf{s}_1^H\right)}{\partial f_1}=-\frac{1}{K}\left[\frac{\partial\mathbf{s}_1}{\partial f_1}\mathbf{s}_1^H+\mathbf{s}_1\frac{\partial\mathbf{s}_1^H}{\partial f_1}\right]. \qquad (2.27)$$

Substituting (2.11) into(2.27), we obtain

$$\frac{\partial\mathbf{s}_1}{\partial f_1}=2j\pi T_s\mathbf{D}_1\mathbf{s}_1 \qquad (2.28)$$

and

$$\frac{\partial\mathbf{s}_1^H}{\partial f_1}=2j\pi T_s\mathbf{s}_1^H\mathbf{D}_1 \qquad (2.29)$$

where

$$\mathbf{D}_1=diag\left\{\left[(V-K),(V-K+1),\ldots,(V-1)\right]\right\}. \qquad (2.30)$$

With (2.28) and (2.29), (2.27) can be written as

$$\frac{\partial \phi_1}{\partial f_1} = \frac{4\pi T_s}{K} \mathrm{Im}\left[\mathbf{r}_1^H \mathbf{D}_1 \mathbf{s}_1 \mathbf{s}_1^H \mathbf{r}_1 \right]. \tag{2.31}$$

Thus, the ML estimation for f_1, corresponding to $\frac{\partial \phi_1}{\partial f_1} = 0$, is given by

$$\hat{f}_1 = \arg_{f_1} \left\{ \mathrm{Im}[\mathbf{r}_1^H \mathbf{D}_1 \mathbf{s}_1 \mathbf{s}_1^H \mathbf{r}_1] = 0 \right\}. \tag{2.32}$$

With the estimated $\hat{\alpha}_1$ and $\hat{f}_1$, the objective function of (2.19) becomes

$$\phi_1(K,V) = \phi_1(\hat{\alpha}_1, \hat{f}_1, K, V) = \left\| \left(I - \frac{1}{K} \hat{\mathbf{s}}_1 \hat{\mathbf{s}}_1^H \right) \mathbf{r}_1 \right\|^2 \tag{2.33}$$

where

$$\hat{\mathbf{s}}_1 = e^{2j\pi \hat{f}_1 (V-K) T_s} \left[1, \ldots, e^{2j\pi \hat{f}_1 (K-1) T_s} \right]^T. \tag{2.34}$$

By carrying out the same analysis, $\hat{\alpha}_2$ and $\hat{f}_2$ are given by

$$\hat{\alpha}_2 = \frac{1}{V} \mathbf{s}_2^H \mathbf{r}_2 \tag{2.35}$$

and

$$\hat{f}_2 = \arg_{f_2} \left\{ \mathrm{Im}[\mathbf{r}_2^H \mathbf{D}_2 \mathbf{s}_2 \mathbf{s}_2^H \mathbf{r}_2] = 0 \right\} \tag{2.36}$$

where

$$\mathbf{D}_2 = diag\left\{ \left[0, 1, \ldots, (V-1) \right] \right\}. \tag{2.37}$$

Likewise, with $\hat{\alpha}_2$ and $\hat{f}_2$, the objective function of (2.20) becomes

$$\phi_2(K,V) = \phi_2(\hat{\alpha}_2, \hat{f}_2, K, V) = \left\| \left(I - \frac{1}{V} \hat{\mathbf{s}}_2 \hat{\mathbf{s}}_2^H \right) \mathbf{r}_2 \right\|^2 \tag{2.38}$$

where

$$\hat{\mathbf{s}}_2 = \left[1, \ldots, e^{2j\pi \hat{f}_2 (V-1) T_s} \right]^T. \tag{2.39}$$

Similarly, $\hat{\alpha}_3$ and $\hat{f}_3$ are given by

$$\hat{\alpha}_3 = \frac{1}{L-K-V}\mathbf{s}_3^H \mathbf{r}_3 \tag{2.40}$$

and

$$\hat{f}_3 = \arg_{f_3}\left\{\mathrm{Im}[\mathbf{r}_3^H \mathbf{D}_3 \mathbf{s}_3 \mathbf{s}_3^H \mathbf{r}_3] = 0\right\} \tag{2.41}$$

where

$$\mathbf{D}_3 = diag\left\{\left[0,1,\ldots,\left(L-K-V-1\right)\right]\right\}. \tag{2.42}$$

In addition, with $\hat{\alpha}_3$ and $\hat{f}_3$, the objective function of (2.21) becomes

$$\phi_3(K,V) = \phi_3(\hat{\alpha}_3, \hat{f}_3, K, V) = \left\| \left(I - \frac{1}{L-K-V}\hat{\mathbf{s}}_3 \hat{\mathbf{s}}_3^H \right)\mathbf{r}_3 \right\|^2 \tag{2.43}$$

where

$$\hat{\mathbf{s}}_3 = \left[1,\ldots, e^{2j\pi \hat{f}_3 (L-K-V-1)T_s}\right]^T. \tag{2.44}$$

Combining these results, the objective function in (2.18) becomes

$$\phi(K,V) = \phi_1(K,V) + \phi_2(K,V) + \phi_3(K,V) \tag{2.45}$$

and the ML estimation of K and V can be found from

$$[\hat{K},\hat{V}] = \arg\min_{K,V}\left[\phi(K,V)\right]. \tag{2.46}$$

Summarizing, the ML-based algorithm for finding $\hat{K}$, $\hat{V}$, $\hat{f}_1$, $\hat{f}_2$ and $\hat{f}_3$ can be implemented as shown in Table 2.1.

Table 2.1: ML estimation of $\hat{K}$ and $\hat{V}$

Step 1	Let $v = \lceil L/3 \rceil$, where $\lceil q \rceil$ is the smallest integer greater than q.
Step 2	Let $k = 1$.
Step 3	Calculate $\hat{f}_1(k,v)$ from (2.32), $\hat{f}_2(k,v)$ from (2.36) and $\hat{f}_3(k,v)$ from (2.41).
Step 4	Calculate $\phi_1(k,v)$ from (2.33), $\phi_2(k,v)$ from (2.38) and $\phi_3(k,v)$ from (2.43).
Step 5	If $k = v-1$, go to Step 6. Otherwise, set $k = k+1$ and go to Step 3.
Step 6	If $v = \lfloor L/2 \rfloor + 1$, go to Step 7. Otherwise, set $v = v+1$ and go to Step 2. $\lfloor q \rfloor$ is the largest integer smaller than q.
Step 7	Compute the objective function $\phi(k,v)$ from (2.45) and determine the estimate $\hat{K}$ and $\hat{V}$ from (2.46).
Step 8	Using the estimate $\hat{K}$ and $\hat{V}$, the estimated frequency is given by $\hat{f}_1(\hat{K},\hat{V})$, $\hat{f}_2(\hat{K},\hat{V})$ and $\hat{f}_3(\hat{K},\hat{V})$.

2.3 A Recursive Algorithm for Solving the ML Equations

As detailed in Table 2.1, the ML estimates $\hat{K}$ and $\hat{V}$ depending on $\phi(K,V)$, which in turns depends on $\hat{f}_1(K,V)$, $\hat{f}_2(K,V)$ and $\hat{f}_3(K,V)$ in Step 3. Because this is a time consuming process, we will now formulate a recursive algorithm for the ML estimation of $\hat{f}_1(K,V)$, $\hat{f}_2(K,V)$ and $\hat{f}_3(K,V)$.

First consider $\hat{f}_1(K,V)$, which can be obtained from (2.32). Expanding the right hand side of this equation, we find

$$\mathrm{Im}\left[\mathbf{r}_1^H \mathbf{D}_1 \mathbf{s}_1 \mathbf{s}_1^H \mathbf{r}_1\right] = \mathrm{Im}\left[\sum_{n=1}^{K}\sum_{m=1}^{K}(V-K+n-1)r^*(n)r(m)e^{2j\pi f_1(n-m)T_s}\right]. \quad (2.47)$$

Substituting (2.47) into (2.32), we have

$$\hat{f}_1(K,V) = \arg_{f_1}\left\{\mathrm{Im}\left[\sum_{n=1}^{K}\sum_{m=1}^{K}(V-K+n-1)r^*(n)r(m)e^{2j\pi f_1(n-m)T_s}\right]=0\right\}. \quad (2.48)$$

Using (2.48), $\hat{f}_1(K+1,V)$ and $\hat{f}_1(K,V+1)$ are given by

$$\hat{f}_1(K+1,V) = \arg_{f_1}\left\{\mathrm{Im}\left[\sum_{n=1}^{K+1}\sum_{m=1}^{K+1}(V-K+n-2)r^*(n)r(m)e^{2j\pi f_1(n-m)T_s}\right]=0\right\} \quad (2.49)$$

and

$$\hat{f}_1(K,V+1)=\arg_{f_1}\left\{\mathrm{Im}\left[\sum_{n=1}^{K}\sum_{m=1}^{K}\left(V-K+n\right)r^*\left(n\right)r\left(m\right)e^{2j\pi f_1(n-m)T_s}\right]=0\right\}. \tag{2.50}$$

Denoting the difference between $\hat{f}_1(K+1,V)$ and $\hat{f}_1(K,V)$ as $\Delta\hat{f}_1(K,V)$ and the difference between $\hat{f}_1(K,V+1)$ and $\hat{f}_1(K,V)$ as $\delta\hat{f}_1(K,V)$, we have

$$\hat{f}_1(K+1,V)=\hat{f}_1(K,V)+\Delta\hat{f}_1(K,V) \tag{2.51}$$

and

$$\hat{f}_1(K,V+1)=\hat{f}_1(K,V)+\delta\hat{f}_1(K,V). \tag{2.52}$$

Noting that (2.48), (2.49) and (2.50) for determining $\hat{f}_1(K,V)$, $\hat{f}_1(K+1,V)$ and $\hat{f}_1(K,V+1)$ are almost the same, $\Delta\hat{f}_1(K,V)$ and $\delta\hat{f}_1(K,V)$ will in general be small. Thus, using the first-order Taylor expansion for $e^{2j\pi f_1(K+1,V)(n-m)T_s}$ and $e^{2j\pi f_1(K,V+1)(n-m)T_s}$, we have

$$e^{2j\pi f_1(K+1,V)(n-m)T_s}=e^{2j\pi\left(f_1(K,V)+\Delta f_1(K,V)\right)(n-m)T_s}=e^{2j\pi f_1(K,V)(n-m)T_s}\left[1+2j\pi\Delta f_1\left(K,V\right)(n-m)T_s\right] \tag{2.53}$$

and

$$e^{2j\pi f_1(K,V+1)(n-m)T_s}=e^{2j\pi\left(f_1(K,V)+\delta f_1(K,V)\right)(n-m)T_s}=e^{2j\pi f_1(K,V)(n-m)T_s}\left[1+2j\pi\delta f_1\left(K,V\right)(n-m)T_s\right]. \tag{2.54}$$

Using (2.48), (2.49), (2.51) and (2.53), $\Delta\hat{f}_1(K,V)$ can then be shown to be

$$\Delta\hat{f}_1(K,V)=\frac{\mathrm{Im}\left\{a(K,V)\right\}}{-T_s\,\mathrm{Re}\left\{\sum_{n=1}^{K+1}\sum_{m=1}^{K+1}\left(V-K+n-2\right)\left(n-m\right)r^*\left(n\right)r\left(m\right)e^{2j\pi f_1(K,V)(n-m)T_s}\right\}} \tag{2.55}$$

where

$$a(K,V)=\sum_{n=1}^{K+1}(V-K+n-1)r^{*}(n)r(K+1)e^{2j\pi f_1(K,V)(n-K-1)T_s}$$
$$+\sum_{m=1}^{K}Vr^{*}(K+1)r(m)e^{2j\pi f_1(K,V)(K+1-m)T_s}-\sum_{n=1}^{K+1}\sum_{m=1}^{K+1}r^{*}(n)r(m)e^{2j\pi f_1(K,V)(n-m)T_s}. \tag{2.56}$$

Similarly, using (2.48), (2.50), (2.52) and (2.54), $\delta\hat{f}_1(K,V)$ is given by

$$\delta\hat{f}_1(K,V)=\frac{\mathrm{Im}\left\{\sum_{n=1}^{K}\sum_{m=1}^{K}r^{*}(n)r(m)e^{2j\pi f_1(K,V)(n-m)T_s}\right\}}{-T_s\,\mathrm{Re}\left\{\sum_{n=1}^{K+1}\sum_{m=1}^{K+1}(V-K+n)(n-m)r^{*}(n)r(m)e^{2j\pi f_1(K,V)(n-m)T_s}\right\}}. \tag{2.57}$$

As derived, $\hat{f}_1(K,V)$ can be refined by either

$$\hat{f}_1(K,V)=\hat{f}_1(K-1,V)+\Delta\hat{f}_1(K-1,V) \tag{2.58}$$

or

$$\hat{f}_1(K,V)=\hat{f}_1(K,V-1)+\delta\hat{f}_1(K,V-1). \tag{2.59}$$

The most appropriate refinement is such that the appropriate objective function $\phi_1(K,V)$ is minimized:

$$\hat{f}_1(K,V)=\arg\min_{\hat{f}_1(K,V)}\left\{\phi_1(K,V)\,|_{\hat{f}_1(K,V)=\hat{f}_1(K-1,V)+\Delta\hat{f}_1(K-1,V),\,\hat{f}_1(K,V-1)+\delta\hat{f}_1(K,V-1)}\right\}. \tag{2.60}$$

The above method to refine the estimate $\hat{f}_1(K,V)$ can be adapted to $\hat{f}_2(K,V)$ and $\hat{f}_3(K,V)$ as well, and the entire algorithm formulated is basically recursive and will result in ML estimates. Specifically, $\hat{f}_2(K,V)$ and $\hat{f}_3(K,V)$ can be refined by using

$$\hat{f}_2(K,M)=\arg\min_{\hat{f}_2(K,V)}\left\{\phi_2(K,V)\big|_{\hat{f}_2(K,V)=v_2(K-1,V)+\Delta\hat{f}_2(K-1,V),\,\hat{f}_2(K,V-1)+\delta\hat{f}_2(K,V-1)}\right\} \tag{2.61}$$

and

$$\hat{f}_3(K,V)=\arg\min_{\hat{f}_3(K,V)}\left\{\phi_3(K,V)\big|_{\hat{f}_3(K,V)=\hat{f}_3(K-1,V)+\Delta\hat{f}_3(K-1,V),\,\hat{f}_3(K,V-1)+\delta\hat{f}_3(K,V-1)}\right\} \tag{2.62}$$

where

$$\Delta\hat{f}_2(K,V)=\frac{\mathrm{Im}\{b(K,V)\}}{-T_s\,\mathrm{Re}\left\{\sum_{n=1}^{V}\sum_{m=1}^{V}(n-1)(n-m)r^*(K+n+1)r(K+m+1)e^{2j\pi f_2(K,V)(n-m)T_s}\right\}}, \tag{2.63}$$

$$\delta\hat{f}_2(K,V)=\frac{\mathrm{Im}\{b'(K,V)\}}{-T_s\,\mathrm{Re}\left\{\sum_{n=1}^{V+1}\sum_{m=1}^{V+1}(n-1)(n-m)r^*(K+n)r(K+m)e^{2j\pi f_2(K,V)(n-m)T_s}\right\}}, \tag{2.64}$$

$$\Delta\hat{f}_3(K,V)=\delta\hat{f}_3(K,V)=\frac{\mathrm{Im}\{c(K,V)\}}{-T_s\,\mathrm{Re}\{c'(K,V)\}}, \tag{2.65}$$

$$\begin{aligned}b(K,V)=&\sum_{n=1}^{V+1}(n-1)r^*(K+n)r(K+V+1)e^{2j\pi f_2(K,V)(n-V-1)T_s}\\&+\sum_{m=1}^{V}Vr^*(K+V+1)r(K+m)e^{2j\pi f_2(K,V)(V+1-m)T_s}\\&-\sum_{n=2}^{V+1}\sum_{m=2}^{V+1}r^*(K+n)r(K+m)e^{2j\pi f_2(K,V)(n-m)T_s}\\&-\sum_{n=2}^{V+1}(n-1)r^*(K+n)r(K+1)e^{2j\pi f_2(K,V)(n-1)T_s}\end{aligned}, \tag{2.66}$$

$$\begin{aligned}b'(K,V)=&\sum_{n=1}^{V+1}(n-1)r^*(K+n)r(K+V+1)e^{2j\pi f_2(K,V)(n-V-1)T_s}\\&+\sum_{m=1}^{V}Vr^*(K+V+1)r(K+m)e^{2j\pi f_2(K,V)(V+1-m)T_s}\end{aligned}, \tag{2.67}$$

$$c(K,V) = -\sum_{n=2}^{L-K-V}(n-1)r^*(K+V+n)r(K+V+1)e^{2j\pi f_3(K,V)(n-1)T_s} - \sum_{n=2}^{L-K-V}\sum_{m=2}^{L-K-V} r^*(K+V+n)r(K+V+m)e^{2j\pi f_3(K,V)(n-m)T_s} \quad (2.68)$$

and

$$c'(K,V) = \sum_{n=1}^{L-K-V-1}\sum_{m=1}^{L-K-V-1}(n-1)(n-m)r^*(K+V+n+1)r(K+V+m+1)e^{2j\pi f_3(K,V)(n-m)T_s}. \quad (2.69)$$

As given by Table 2.1, the computational complexity of the proposed algorithm is associated mainly with the calculation of the frequency estimates and the objective function. Table 2.2 gives a rough estimation of the computational complexity of the various important steps in this process as a function of the hopping period *V*. As can be seen from the last row of the table, the proposed algorithm requires roughly $O(V^3)$ complex multiplications.

Table 2.2: Computational complexity of the proposed ML- based algorithm

	# Addition	# Multiplication
$\Delta\hat{f}_1(K,V)$	$2V^3+\frac{13}{2}V^2-\frac{5}{2}V-15$	$\frac{10}{3}V^3+10V^2+\frac{11}{3}V-17$
$\delta\hat{f}_1(K,V)$	$\frac{5}{3}V^3+\frac{3}{2}V^2+\frac{5}{6}V-4$	$\frac{10}{3}V^3+V^2+\frac{11}{3}V-8$
$\phi_1(K,V)$	$\frac{4}{3}V^3-6V^2-\frac{5}{3}V$	$3V^3-3V^2+V$
$\Delta\hat{f}_2(K,V)$	$4V^3+3V^2-V-6$	$10V^3+5V^2-8V-7$
$\delta\hat{f}_2(K,V)$	$3V^3+8V^2-4V-7$	$6V^3+16V^2-9V-13$
$\phi_2(K,V)$	$4V^3-6V^2+2V$	$6V^3-6V^2$
$\Delta\hat{f}_3(K,V)$ $=\delta\hat{f}_3(K,V)$	$\frac{28}{3}V^3-(12L+9)V^2+$ $\left(4L^2+6L+\frac{8}{3}\right)V-$ $(4L^2-6L+3)$	$\frac{70}{3}V^3-\left(30L+\frac{45}{2}\right)V^2+$ $\left(10L^2+15L+\frac{37}{6}\right)V-$ $(10L^2-15L+7)$
$\phi_3(K,V)$	$\frac{28}{3}V^3-(12L+7)V^2+$ $\left(4L^2+10L+\frac{5}{3}\right)V-$ $(4L^2-2L+4)$	$14V^3-(18L+15)V^2+$ $(6L^2+18L+1)V-6L^2$
Total	$\frac{104}{3}V^3-(24L+9)V^2+$ $(8L^2+16L-2)V$ $+(8L^2-8L+39)$	$69V^3-\left(28L+\frac{29}{2}\right)V^2+$ $\left(16L^2+33L-\frac{3}{2}\right)V-$ $(16L^2-15L+52)$

2.4 Numerical Results and Discussions

Some simulation results will now be presented to better illustrate the performance of the proposed algorithm and also to compare it with the technique based on time-frequency distribution (TFD) [65]. A brief discussion of TFD is given in Appendix A.

In the scenario being simulated, the frequencies in the three hops are f_1=18kHz, f_2=29kHz, and f_3=37kHz, and the sampling frequency is 1MHz. The values of α_1, α_2 and α_3, which account for the overall effects of phase shift and fading, are 0.8+0.3*j*, 0.6+0.5 *j* and 0.4+0.8*j*, respectively. The hopping period is V=128, and the hop transition is at K=56. The estimation is carried out using a total of *L*=300 samples and the SNR is 10dB.

Fig. 2.2, Fig. 2.3 and Fig. 2.4 show the frequency estimates $\hat{f}_1(K,V)$, $\hat{f}_2(K,V)$ and $\hat{f}_3(K,V)$ calculated recursively by using (2.60), (2.61) and (2.62) as a function of *K* and *V*. While this may be difficult to observe from the 3D plot, note that at the correct value of V=128 and K=56, the frequency estimates will be very close to their actual values. They will not of course be equal to the actual values exactly due to the effect of noise.

From the data for Fig. 2.2, Fig. 2.3 and Fig. 2.4, using (2.45) with (2.33), (2.38) and (2.43), the objective functions $\phi_1(K,V)$, $\phi_2(K,V)$, $\phi_3(K,V)$ and $\phi(K,V)$ can be calculated. These functions are plotted against K and V in Fig. 2.5, Fig. 2.6, Fig. 2.7 and Fig. 2.8, respectively. Note that at the actual values of K=56 and V=128, the objective function $\phi(K,V)$ has its

minimum value.

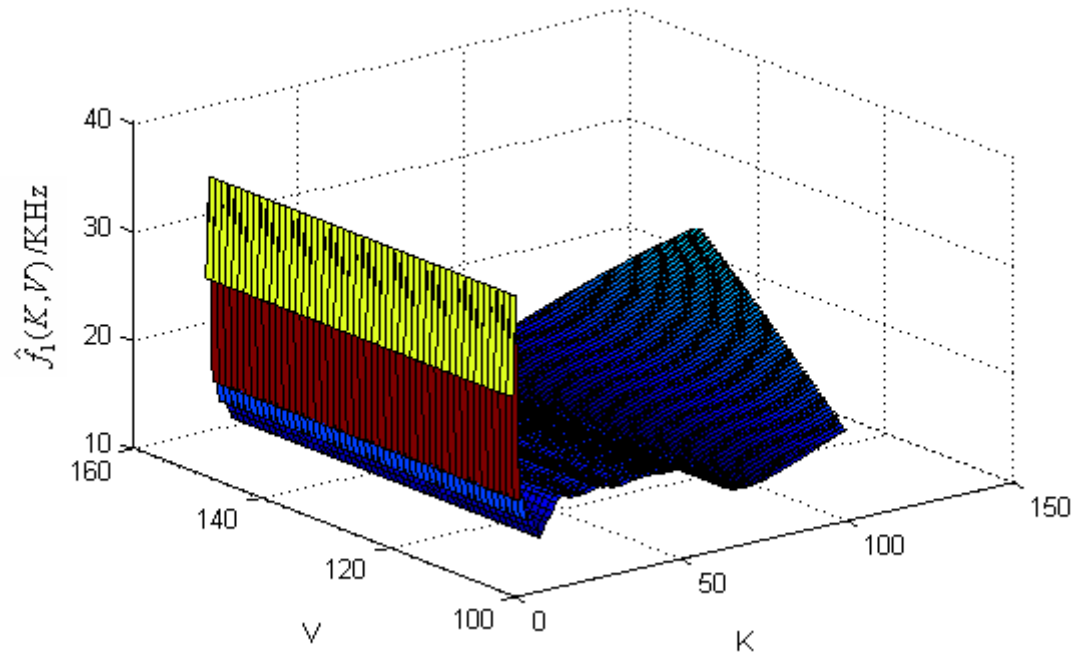

Fig. 2.2 Variation of $\hat{f}_1(K,V)$ from (2.60)

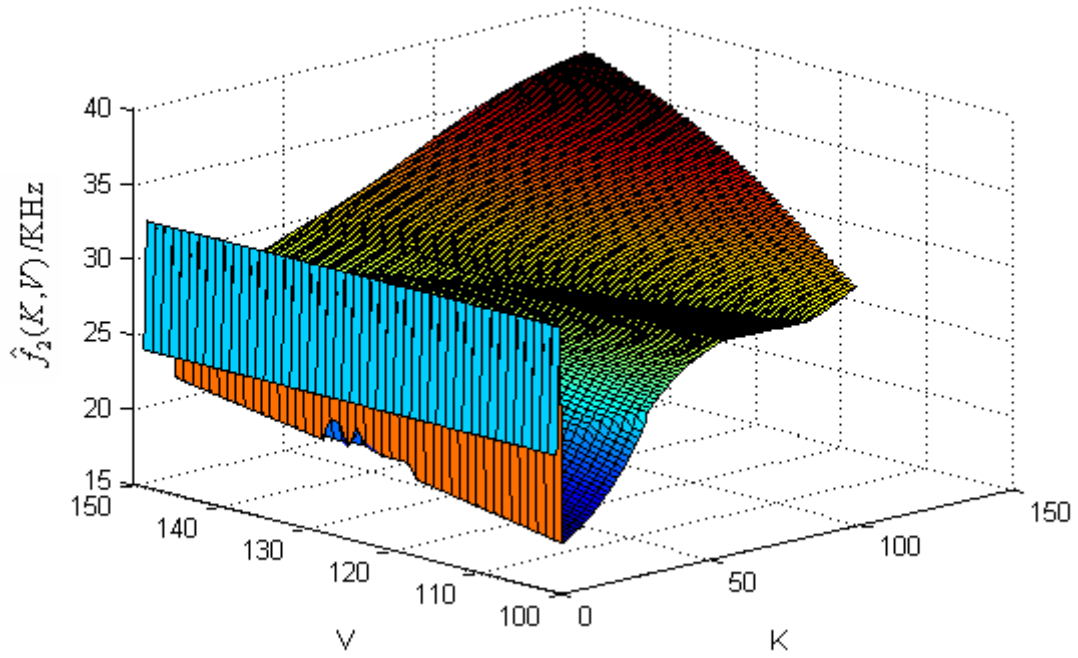

Fig. 2.3 Variation of $\hat{f}_2(K,V)$ from (2.61)

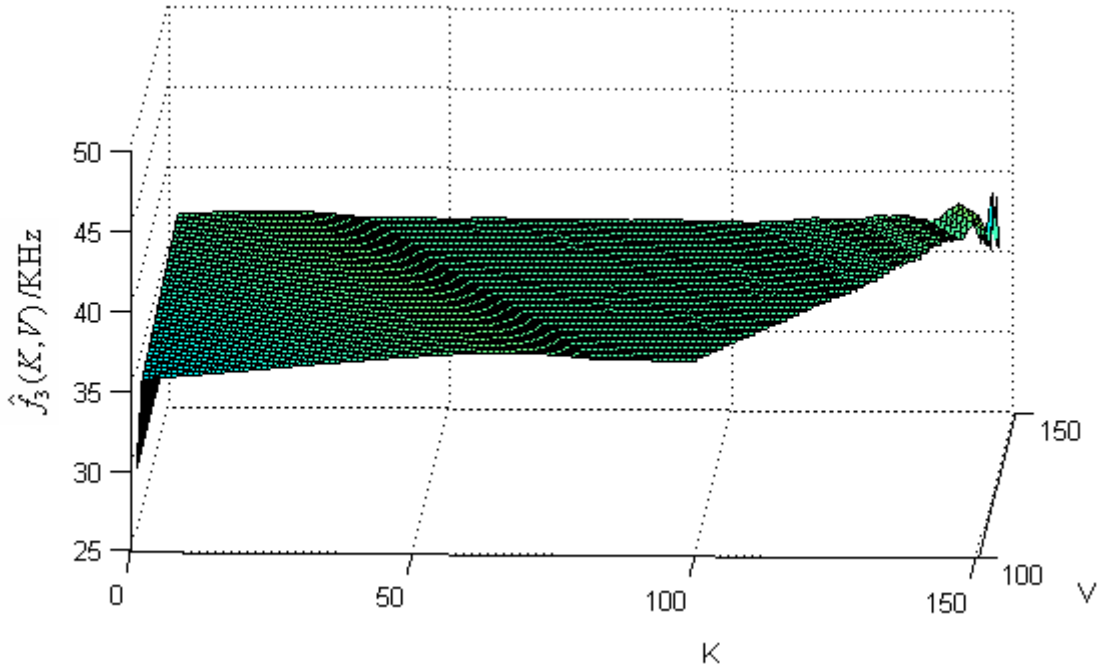

Fig. 2.4 Variation of $\hat{f}_3(K,V)$ from (2.62)

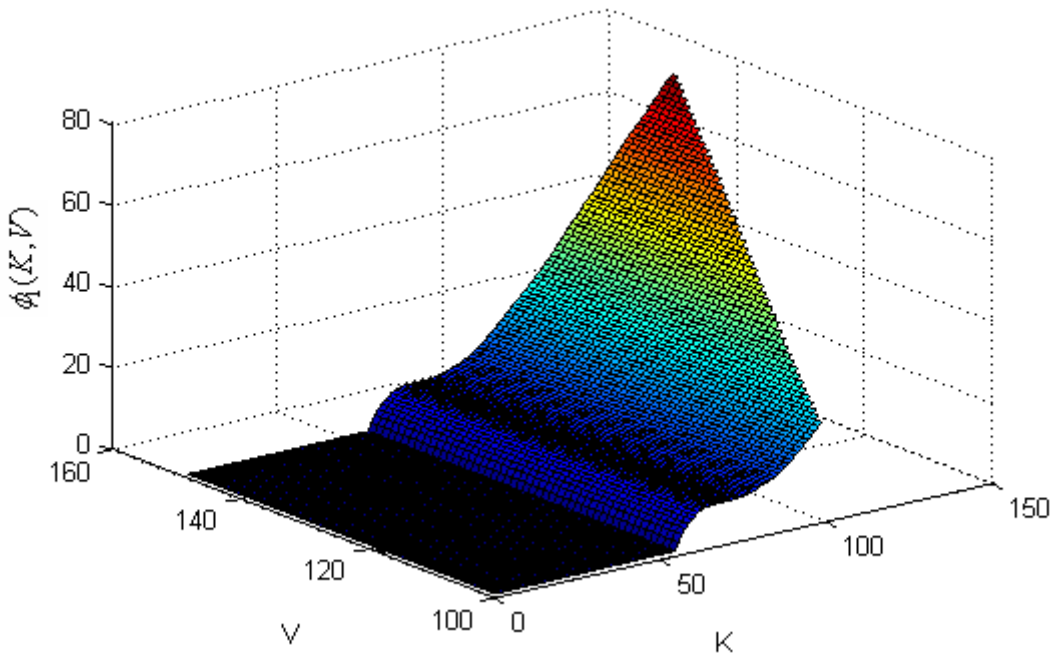

Fig. 2.5 Variation of $\phi_1(K,V)$ from (2.33)

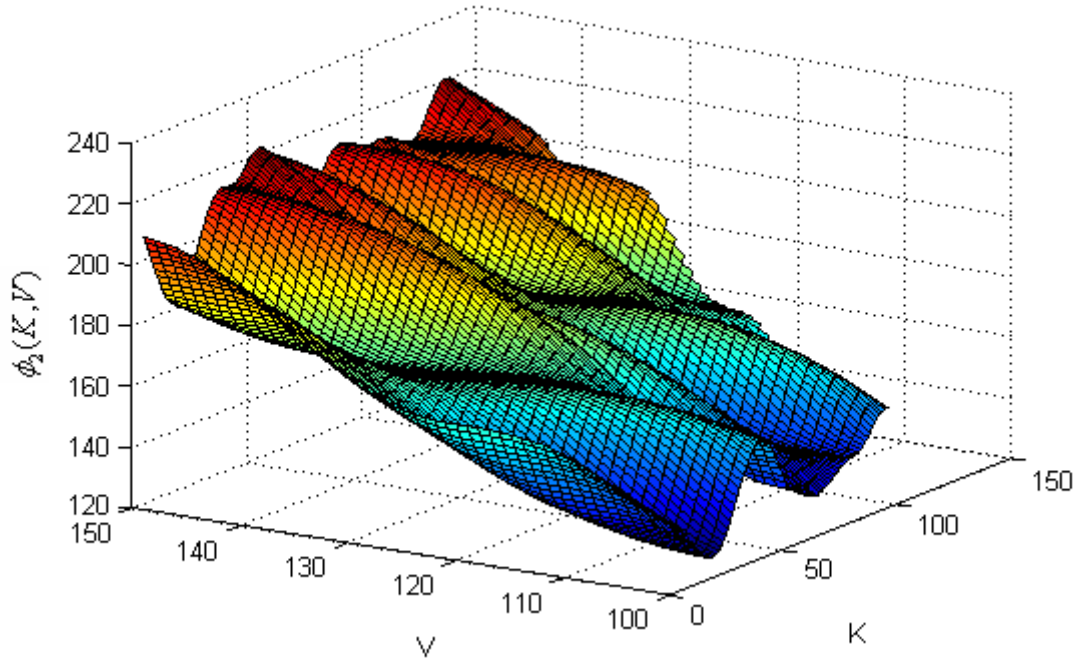

Fig. 2.6 Variation of $\phi_2(K,V)$ from (2.38)

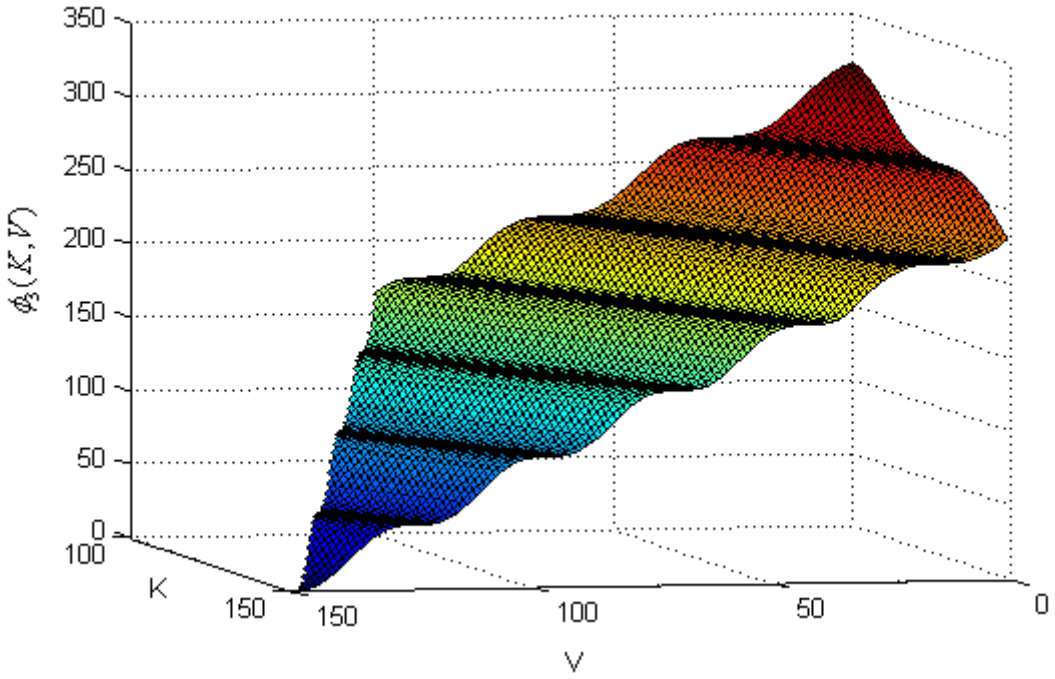

Fig. 2.7 Variation of $\phi_3(K,V)$ from (2.43)

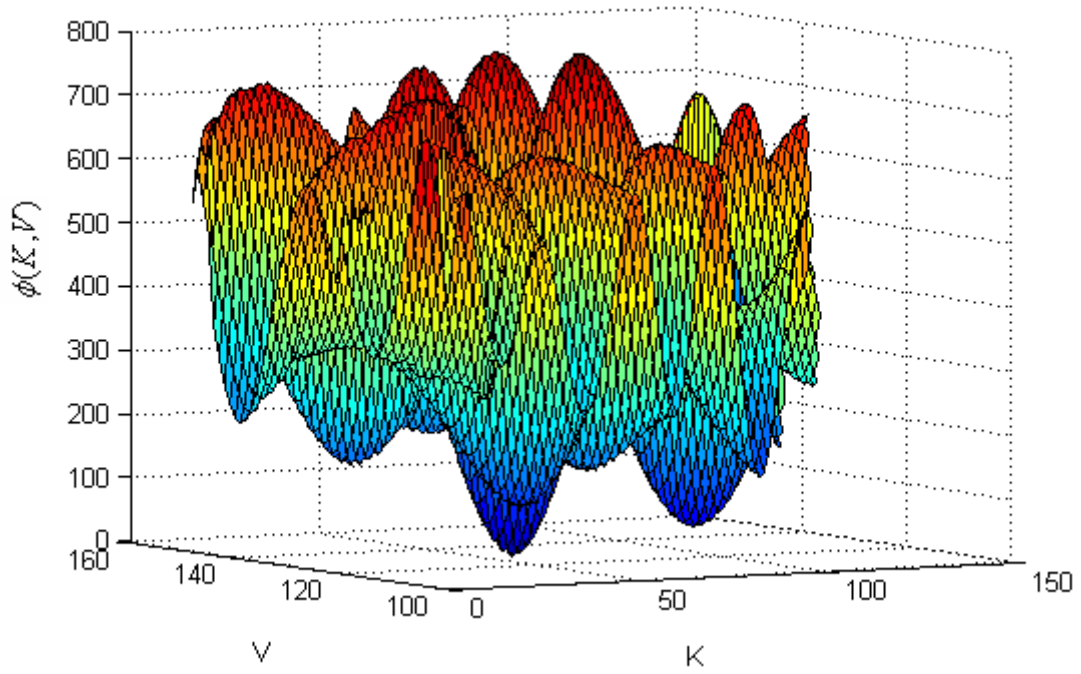

Fig. 2.8 $\phi(K,V)$ versus K and V

Then, using these values of K and V, the corresponding frequency estimates can be found from Fig. 2.2, Fig. 2.3 and Fig. 2.4 to be $\hat{f}_1(56,128)$ =17.86kHz, $\hat{f}_2(56,128)$ =29.04kHz and $\hat{f}_3(56,128)$ =37.01kHz, respectively.

Following the above process, we carried out another 500 Monte Carlo experiments under different SNR for the purpose of finding the probability of error in estimating K. The results are presented in Fig. 2.9. Meanwhile, the error bar of the estimation is shown in Fig. 2.9. For comparison, the results obtained by TFD are also shown. The Wigner distribution given by $W_x(t,f)=\int_{-\infty}^{\infty} r^*(t-0.5\tau)r(t+0.5\tau)e^{-j2\pi f\tau}d\tau$ is employed in the simulation, and the instantaneous frequency is obtained by $\hat{f}(t)=\arg\max_f\left[|W_x(t,f)|\right]$. The transition time is then estimated by finding the position at which maximum change in successive instantaneous frequency estimations occurs. From Fig. 2.9,

we can see that the proposed ML-based algorithm has a lower estimation error probability than the TFD based method. Based on the finite number of simulation results obtained, the probability of error decreases to zero for the proposed ML algorithm at an SNR greater than 4dB. For the TFD based method, however, the SNR has to be at least 11dB for the error probability to be zero.

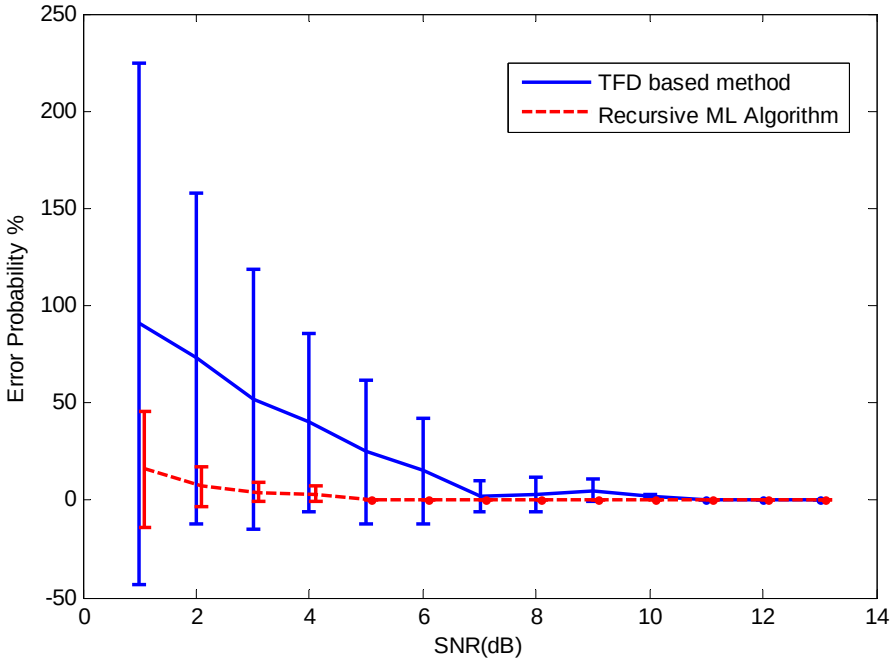

Fig. 2.9 Error bar in estimating K

2.5 Summary

In this chapter, an ML-based recursive algorithm for estimating the hopping transition time, hopping period and frequencies in a frequency hopping system is proposed and investigated. Without using any pilot or sync bit, the

proposed ML-based algorithm is formulated to work in the presence of unknown flat fading. It makes use of an efficient recursive technique formulated for estimating the hopping frequencies in various hops of the received signal. The estimated hopping frequencies are used in an integrated optimization procedure where the hopping transitions and period are adjusted together with refinements to the hopping frequencies to minimize the overall ML objective function. Compared with the other algorithm, the proposed algorithm has been found to have a better performance in terms of estimation errors.

CHAPTER 3

FH/MFSK SYSTEM WITH JAMMING IN THE PRESENCE OF FADING

3.1 System Model

Consider an MFSK modulated slow FHSS system. To suppress the detrimental effects of a follower partial band jammer, we explore the use of a simple multi-element receiving array, where the signal from each element is down converted and sampled at N times the symbol rate [56;79;80]. The samples collected from the antenna array elements over one symbol duration will be used to estimate the desired information symbol by using MLBB, area-based VSM, and the volumetric-based algorithm, which will be described in more detail in CHAPTER 4, CHAPTER 5 and CHAPTER 6, respectively. Note that to eliminate X jammers, at least X+1 receiver antennas must be employed.

3.1.1 Signal Model

Without loss of generality, consider the detection of the symbol in a hop over the interval $0 < t < T_y$, where T_y is the symbol duration. The complex envelop of the transmitted signal can be expressed by

$$s(t) = \exp\left[j2\pi \left(f_i + d_0 f_d \right) t \right], \tag{3.1}$$

where f_i is the hopping frequency, $d_0 \in [0,1,\ldots,M-1]$ represents the information symbol, and f_d stands for the frequency spacing between two adjacent MFSK tones. Unlike the conventional MFSK system, the proposed algorithm does not require the MFSK tones to be orthogonal.

3.1.2 Partial Band Jamming Model

As described in [66], a follower partial band jammer first measures the hopping frequency and the spectrum of the desired hop and then directs the available transmitting power discriminately to the currently used frequency slot. Without perfect knowledge of the desired signal but knowing the hopping frequency of the desired signal, such a jammer will most likely transmit a signal that is different, perhaps noise like, than the desired signal and will cover the entire band of the latter. The complex envelop of a follower partial-band

jamming signal can thus be represented as

$$J(t) = n_j(t)\exp\left[j2\pi\left(f_i + B_J / 2\right)t \right], \tag{3.2}$$

where $n_j(t)$ is a baseband equivalent band-limited signal with bandwidth B_J and can be modeled as a zero-mean band-limited Gaussian random process. The exponential term in (3.2) indicates that this baseband signal is then up converted to covering the frequency slot occupied by the desired signal. Note that a follower jammer will not send any jamming signal before the hopping frequency and spectrum of the desired signal are determined.

3.2 Received Signal Model

Assuming that the desired signal and the follower jamming signal experience a quasi-static flat fading channel, the received baseband signal at the *p*-th antenna element will be given by

$$r_p(t) = \alpha_p s(t) + \sum_{k=1}^{X} \beta_{kp} J_k\left(t\right) + w_p(t) \tag{3.3}$$

where X is the number of jamming signals, $w_p(t)$ is the complex white Gaussian receiver noise, and the complex coefficients α_p and β_{kp} account for the overall effects of phase shifts, fading and antenna response for the desired signal and the jamming signals at the *p*-th antenna element, respectively [57;58]. Note that, following [67] and [68] in slow frequency hopping systems,

the fading gains are taken to be frequency nonselective and remain unchanged within a certain processing interval, for example, a hop duration.

At the *p*-th antenna element, the received signal is sampled at *N* times the symbol rate. Using (3.1), (3.2) and (3.3), the received sample is thus

$$r_{p,n} = \alpha_p \exp\left(j\omega_n \left(d_0 \right) \right) + \sum_{k=1}^{X} \beta_{kp} J_{k,n} + w_{p,n} \tag{3.4}$$

where

$$r_{p,n} = r_p \left(\left(\frac{1}{2N} + \frac{n}{N} \right) T_s \right),$$

$$\omega_n \left(d_0 \right) = 2\pi \left(f_i + d_0 f_d \right) \left(\frac{1}{2N} + \frac{n}{N} \right) T_s,$$

$$J_{k,n} = J_k \left(\left(\frac{1}{2N} + \frac{n}{N} \right) T_s \right)$$

and

$$w_{p,n} = w_p \left(\left(\frac{1}{2N} + \frac{n}{N} \right) T_s \right), \text{for } n = 0, 1, \ldots, N\text{-}1.$$

Based on (3.4), the signal-to-jamming power ratio (SJR) and the signal-to-noise power ratio (SNR) are $\text{SJR}_k = p_s / p_{J_k}$, $k = 1, 2, \cdots, X$, and $\text{SNR} = p_s / p_w$, respectively, with $p_w = E\left(\left| w_{p,n} \right|^2 \right)$, $p_s = E\left(\left| \alpha_p \exp\left[j\omega_n \left(d_0 \right) \right] \right|^2 \right) = E\left(\left| \alpha_p \right|^2 \right)$ and $p_{J_k} = E\left(\left| \beta_p \right|^2 \right) E\left(\left| J_{kn} \right|^2 \right)$.

For convenience, equation (3.4) can be written in vector form for the *N* samples from the sensors as follows:

$$\mathbf{r}_p = \alpha_p \mathbf{s}\left(d_0 \right) + \mathbf{v}_p + \mathbf{w}_p \tag{3.5}$$

where

$$\mathbf{r}_p = \left[r_{p,0}, r_{p,1}, \cdots, r_{p,N-1}\right]^T, \tag{3.6}$$

$$\mathbf{s}(d_0) = \left[\exp\left(j\omega_0(d_0)\right), \exp\left(j\omega_1(d_0)\right), \cdots \exp\left(j\omega_{N-1}(d_0)\right)\right]^T, \tag{3.7}$$

$$\mathbf{v}_p = \sum_{k=1}^{X} \beta_{kp} \mathbf{J}_k, \tag{3.8}$$

$$\mathbf{J}_p = \left[J_{k,0}, J_{k,1}, \cdots, J_{k,N-1}\right]^T, k=1, 2, \cdots, X \tag{3.9}$$

and

$$\mathbf{w}_p = \left[w_{p,0}, w_{p,1}, \cdots, w_{p,N-1}\right]^T, p = 1, 2, \cdots, X+1. \tag{3.10}$$

Because the hopping frequency and spectrum of the desired signal need to be found, a follower jammer will not transmit any jamming signal during the initial measurement phase, and will be activated only after some delay following the beginning of each frequency hop [56]. Note that by exploiting the unjammed interval at the beginning of each hop duration, the channel gains α_p (p = 1, 2, $\cdots$, X+1) of the desired signal can in practice be blindly estimated by an ML procedure as shown below.

In the unjammed portion of the hop, a joint ML estimation of d_0, α_p can be obtained from

$$\hat{\alpha}_p, \hat{d}_0 = \underset{\alpha_p, d_0 = \{0,1,\cdots,M-1\}}{\arg\min} \left\{ \sum_{p=1}^{X+1} \left\| \mathbf{r}_p - \alpha_p \mathbf{s}(d_0) \right\|^2 \right\} \tag{3.11}$$

Differentiating $\sum_{p=1}^{X+1} \left\| \mathbf{r}_p - \alpha_p \mathbf{s}(d_0) \right\|^2$ with respect to α_p and setting the results to zero, the ML estimates of α_p are given by

$$\hat{\alpha}_p = \mathbf{s}^H\left(\hat{d}_0\right)\mathbf{r}_p \Big/ \left\|\mathbf{s}\left(\hat{d}_0\right)\right\|^2, p = 1, 2, \cdots X+1 \tag{3.12}$$

with

$$\hat{d}_0 = \underset{d_0=0,1,2,\cdots,M-1}{\arg\min} \left\{ \sum_{p=1}^{X+1} \left\| \mathbf{r}_p - \frac{\mathbf{s}^H\left(d_0\right)\mathbf{r}_p\mathbf{s}\left(d_0\right)}{\left|\mathbf{s}\left(d_0\right)\right|^2} \right\|^2 \right\}. \tag{3.13}$$

3.3 Summary

The signal model introduced by this chapter serves as a basis for the subsequent chapters. First, we propose MLBB which is based on [58]. After estimating the ratio of jamming gains, MLBB further utilizes the beamforming technique to get a better BER performance than [58]. VSM and volumetric-based algorithms utilize the spatial correlation of the jamming signals and have the best performance when compared with the other algorithms in most scenarios.

We will introduce MLBB, VSM and volumetric-based algorithms in the following chapters, respectively. Also, theoretical performance will be presented, and the performance of the three proposed algorithms will be compared based on theoretical BER values.

CHAPTER 4

MAXIMUM LIKELIHOOD-BASED BEAMFORMING ALGORITHM

4.1 Introduction of Maximum Likelihood-based Beamforming Algorithm

In this chapter, an MLBB algorithm that uses a two-element array is proposed to reject one follower jamming signal and carry out symbol detection in slow FH/MFSK system over quasi-static flat fading channels. Deploying a received signal model that takes care of flat fading, the proposed algorithm first uses an ML-based approach to obtain an ML estimate of the ratio of jamming fading gains. Based on this ML estimate, a simple beamforming structure is employed to place a null toward the follower jamming source and the symbol detection is then performed by the ML technique.

4.1.1 ML-based Estimation of the Ratio of Jamming Fading Gains

Based on (3.5), for each element, the received signal in vector form is

$$\mathbf{r}_1 = \alpha_1 \mathbf{s}(d_0) + \mathbf{v} + \mathbf{w}_1 \tag{4.1}$$

and

$$\mathbf{r}_2 = \alpha_2 \mathbf{s}(d_0) + \eta \mathbf{v} + \mathbf{w}_2 \tag{4.2}$$

where

$$\mathbf{v} = \beta_{11} \left[J_0, J_1, \cdots J_{(N-1)} \right]^T \tag{4.3}$$

and

$$\eta = \beta_{12} / \beta_{11}. \tag{4.4}$$

Consider the detection for each symbol in one hop. Because MFSK signaling is employed, the desired symbol d_0 only takes on values from the alphabet {0, 1, ⋯, M–1}. A joint ML estimation of η and $\mathbf{v}$ can thus be expressed as

$$\hat{\eta}(d) = \arg \min_{\eta, \mathbf{v}} \left\{ \left\| \mathbf{r}_1 - \alpha_1 \mathbf{s}(d) - \mathbf{v} \right\|^2 + \left\| \mathbf{r}_2 - \alpha_2 \mathbf{s}(d) - \eta \mathbf{v} \right\|^2 \right\} \tag{4.5}$$

where the candidate symbol value $d \in \{0, 1, \cdots M-1\}$.

For convenience, let us define

$$\mathbf{z}_p(d) = \mathbf{r}_p - \alpha_p \mathbf{s}(d), \quad \text{for} \quad p = 1, 2. \tag{4.6}$$

The cost function in (4.5) then becomes

$$\Gamma(d) = \left\|\mathbf{z}_1(d) - \mathbf{v}\right\|^2 + \left\|\mathbf{z}_2(d) - \eta\mathbf{v}\right\|^2 . \tag{4.7}$$

Differentiating the cost function $\Gamma(d)$ with respect to η and $\mathbf{v}$, respectively, and setting the results to zero, we obtain

$$\mathbf{v} = \frac{\mathbf{z}_1(d) + \eta^* \mathbf{z}_2(d)}{1 + \left|\eta\right|^2} \tag{4.8}$$

and

$$\eta = \frac{\mathbf{v}^H \mathbf{z}_2(d)}{\left\|\mathbf{v}\right\|^2} . \tag{4.9}$$

Substituting (4.8) into (4.7) yields

$$\Gamma(d) = \frac{\left\|\mathbf{z}_2(d) - \eta\mathbf{z}_1(d)\right\|^2}{1 + \left|\eta\right|^2} . \tag{4.10}$$

By substituting (4.8) into (4.9), we find

$$a(d)\eta^2 + b(d)\eta - a^*(d) = 0 , \tag{4.11}$$

where

$$a(d) = \mathbf{z}_2^H(d)\mathbf{z}_1(d) \tag{4.12}$$

and

$$b(d) = \left\|\mathbf{z}_1(d)\right\|^2 - \left\|\mathbf{z}_2(d)\right\|^2 . \tag{4.13}$$

Details of the above derivations are shown in Appendix B.

As a result, the closed-form expressions for the ML estimates of $\hat{\eta}$ which are the solutions to (4.11) can be determined by

$$\hat{\eta}_1(d) = \frac{-b(d) - \sqrt{b^2(d) + 4\left|a(d)\right|^2}}{2a(d)} \tag{4.14}$$

and

$$\hat{\eta}_2(d) = \frac{-b(d) + \sqrt{b^2(d) + 4\left|a(d)\right|^2}}{2a(d)}. \qquad (4.15)$$

From (4.10), (4.14) and (4.15), we can find

$$\Gamma_p(d) = \frac{\left\|\mathbf{z}_2(d) - \hat{\eta}_p(d)\mathbf{z}_1(d)\right\|^2}{1 + \left|\hat{\eta}_p(d)\right|^2}, \text{ for } p = 1, 2. \qquad (4.16)$$

Equations (4.14) and (4.15) show that two possible value of $\hat{\eta}(d)$ for a fixed value of *d* exist. Consequently, from (4.16), we have to calculate the two cost functions $\Gamma_1(d)$ and $\Gamma_2(d)$ corresponding to a fixed *d* for the purpose of estimating the ratio of jamming fading gains. However, as shown below, $\Gamma_2(d)$ is always smaller than $\Gamma_1(d)$ for a fixed value of *d*. Therefore, it is sufficient to compute only $\hat{\eta}_2(d)$ in (4.15).

Substituting (4.12) and (4.13) into (4.14) and (4.15) yields

$$\eta_1(d) = \frac{\left\|\mathbf{z}_2(d)\right\|^2 - \left\|\mathbf{z}_1(d)\right\|^2 - \sqrt{\left(\left\|\mathbf{z}_2(d)\right\|^2 - \left\|\mathbf{z}_1(d)\right\|^2\right)^2 + 4\left|\mathbf{z}_2^H(d)\mathbf{z}_1(d)\right|^2}}{2\mathbf{z}_2^H(d)\mathbf{z}_1(d)} \qquad (4.17)$$

and

$$\eta_2(d) = \frac{\left\|\mathbf{z}_2(d)\right\|^2 - \left\|\mathbf{z}_1(d)\right\|^2 + \sqrt{\left(\left\|\mathbf{z}_2(d)\right\|^2 - \left\|\mathbf{z}_1(d)\right\|^2\right)^2 + 4\left|\mathbf{z}_2^H(d)\mathbf{z}_1(d)\right|^2}}{2\mathbf{z}_2^H(d)\mathbf{z}_1(d)}. \qquad (4.18)$$

Substituting (4.17) and (4.18) into (4.16), respectively, we deduce

$$\Gamma_1(d) = \left\|\mathbf{z}_1(d)\right\|^2 + \frac{\sqrt{\left(\left\|\mathbf{z}_2(d)\right\|^2 - \left\|\mathbf{z}_1(d)\right\|^2\right)^2 + 4\left|\mathbf{z}_2^H(d)\mathbf{z}_1(d)\right|^2}}{1 + \left|\eta_1(d)\right|^2} \qquad (4.19)$$

and

$$\Gamma_2(d) = \left\|\mathbf{z}_1(d)\right\|^2 - \frac{\sqrt{\left(\left\|\mathbf{z}_2(d)\right\|^2 - \left\|\mathbf{z}_1(d)\right\|^2\right)^2 + 4\left|\mathbf{z}_2^H(d)\mathbf{z}_1(d)\right|^2}}{1+\left|\eta_2(d)\right|^2}. \qquad (4.20)$$

From (4.19) and (4.20) we can see that $\Gamma_2(d)$ is always smaller than $\Gamma_1(d)$.

4.1.2 Beamforming Algorithm of Jamming Rejection

Based on the ML estimate of the jamming fading gains, a simple beamforming structure can be employed to place a null toward the follower jammer. Specifically, to cancel a jammer completely with the fading gains estimated, the weighting vector of the beamforming structure should be

$$\mathbf{h} = [\hat{\eta}, -1]^T . \qquad (4.21)$$

This will give rise to a resulting output signal of

$$\mathbf{h}^T\mathbf{r} = (\hat{\eta}\alpha_1 - \alpha_2)\mathbf{s}(d_0) + (\hat{\eta} - \eta)\mathbf{v} + \tilde{\mathbf{w}} \qquad (4.22)$$

where

$$\mathbf{r} = [\mathbf{r}_1, \mathbf{r}_2]^T$$

and

$$\tilde{\mathbf{w}} = \hat{\eta}\mathbf{w}_1 - \mathbf{w}_2 .$$

As a result, the transmitted symbol can be estimated by

$$d_0 = \arg \min_{d} \{||\tilde{\mathbf{s}}(d)\text{-}\mathbf{s}(d)||^2; d = 0,1,\cdots,M-1\} \quad (4.23)$$

where

$$\tilde{\mathbf{s}}(d) = \frac{\hat{\eta}(d)\mathbf{r}_1 - \mathbf{r}_2}{\hat{\eta}(d)\alpha_1 - \alpha_2}. \quad (4.24)$$

The detailed procedure for the proposed MLBB jamming rejection and symbol detection algorithm is shown in Table 4.1. Table 4.2 presents the computational complexity of the MLBB algorithm. Note that the computational complexity is due to steps 1, 2, 4 and 5 in Table 1 because these steps involve vector operations. As can be seen, the computational complexity of the algorithm is roughly equal to $8NM + NM$ multiplications.

Table 4.1: Details of the MLBB algorithm

Step	Calculation
1	Calculate $\mathbf{z}_1(d)$ and $\mathbf{z}_2(d)$, $d = 0,\cdots,M-1$, using (4.6)
2	Calculate both $a(d)$ and $b(d)$, $d = 0,\cdots,M-1$, using (4.12) and (4.13)
3	Calculate $\hat{\eta}(d)$, $d = 0,\cdots,M-1$, using (4.15)
4	Calculate $\tilde{\mathbf{s}}(d)$, $d = 0,\cdots,M-1$, based on (4.24)
5	Calculate $\|\tilde{\mathbf{s}}(\mathrm{d})\text{-}(\hat{\eta}(d)\alpha_1 - \alpha_2)\mathbf{s}(\mathrm{d})\|^2, d = 0,\cdots,M-1$
6	Obtain the ML estimate of the transmitted symbol $\hat{d}_0$ based on (4.23)

Table 4.2: Computational complexity of the proposed MLBB algorithm per symbol

Step	# addition	# multiplication
1	$2NM$	$2NM$
2	$3NM-3NM$	$3NM$
4	NM	NM
5	$2NM$	$2NM+M$
Total	$8NM-3NM$	$8NM+NM$

4.2 Performance of MLBB Algorithm

Numerical simulations were conducted to validate the performance of the proposed MLBB algorithm for slow FH systems with various MFSK modulations. In this simulation study, each hop has 8 MFSK symbols, the symbol rate is 200000 symbols per second, and the hop rate is 25000 hops per second.

Fig. 4.1 shows the performance of the MLBB, SMI, the algorithm proposed in [58], and the traditional ML algorithm plotted against SJR. The

SNR is 30dB, and the number of samples per symbol is 4. As observed, the proposed MLBB algorithm is more robust against the SJR than the other algorithms and its performance only differs slightly over various SJR values. However, in high SJR scenarios, ML and SMI out performs MLBB scheme.

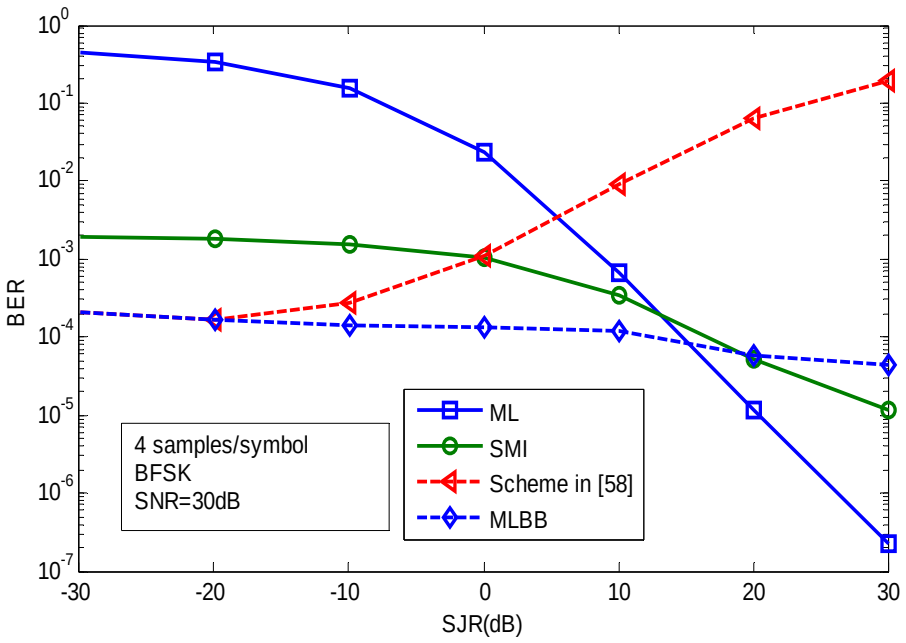

Fig. 4.1: Performance of the traditional ML algorithm, SMI algorithm, algorithm proposed in [58], and proposed MLBB algorithm versus SJR with SNR=30dB

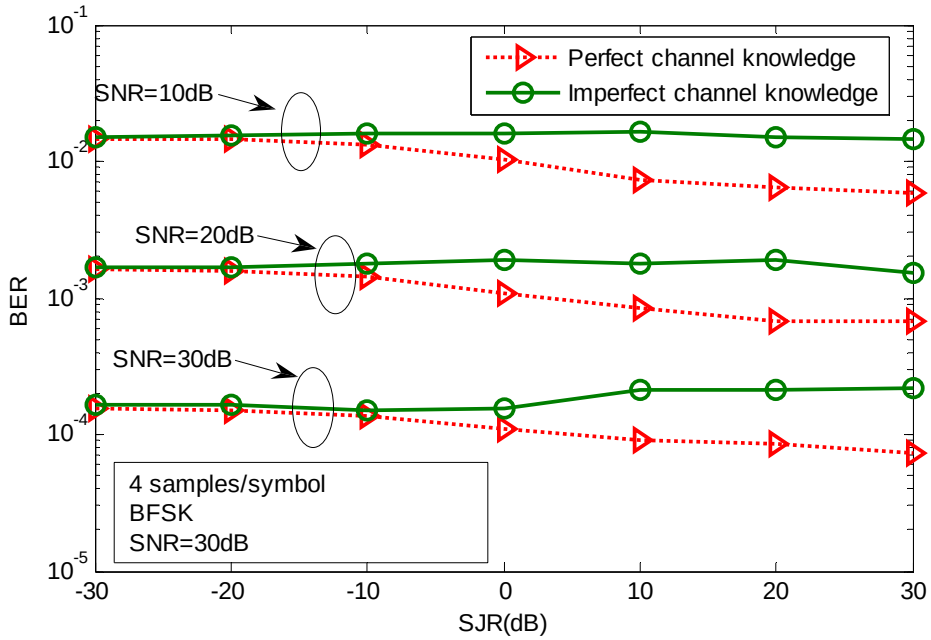

Fig. 4.2: Performance of the proposed MLBB algorithm with perfect and imperfect channel knowledge for various SJR and SNR values with BFSK and 4 samples per symbol

To investigate the effect of imperfect channel estimation, Fig. 4.2 shows the BER performance of the proposed MLBB algorithm with the channel gains of the desired signal estimated by using a standard ML procedure in the unjammed portion of the hop. Obviously, by using samples in just one symbol duration to estimate the channel gains, the performance of the MLBB algorithm degrades slightly compared to the case where the channel knowledge is perfect.

For comparison with the SMI and traditional ML algorithms, the performance of the proposed MLBB algorithm versus SNR is plotted in Fig.

4.3. It can be seen that, unlike traditional ML algorithm, both the SMI and MLBB algorithms have lower BER when SNR increases and the MLBB algorithm has the best performance.

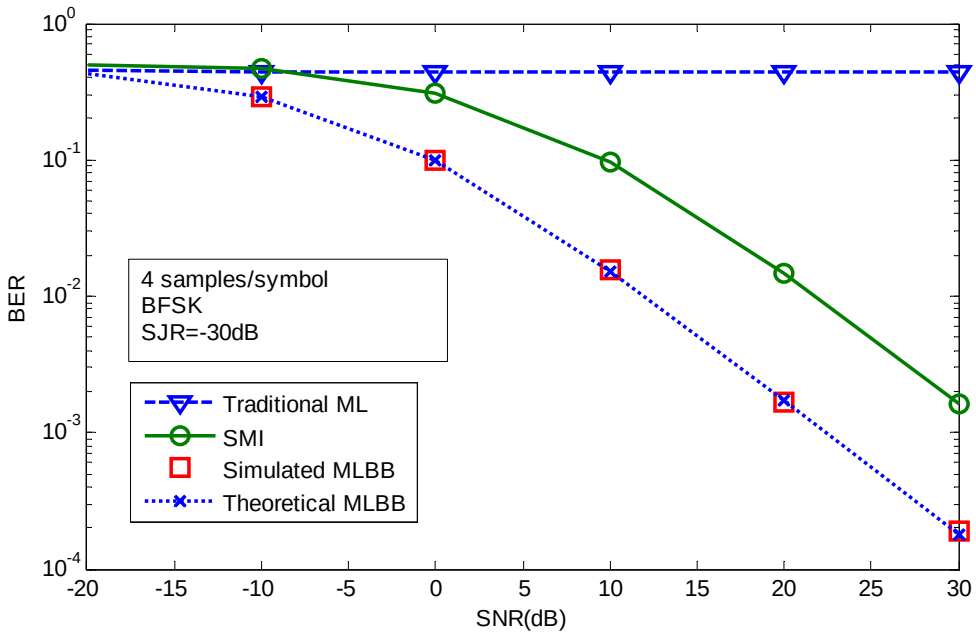

Fig. 4.3: Performance of the traditional ML algorithm, the SMI algorithm and the MLBB algorithm versus SNR with SJR=-30dB

Fig. 4.4 shows the effect of the number of samples per symbol in the MLBB algorithm when SNR is 20dB and the modulation system is BFSK. As the number of samples per symbol increases, the performance of the MLBB algorithm becomes much better. However, the resulting computational complexity also increases.

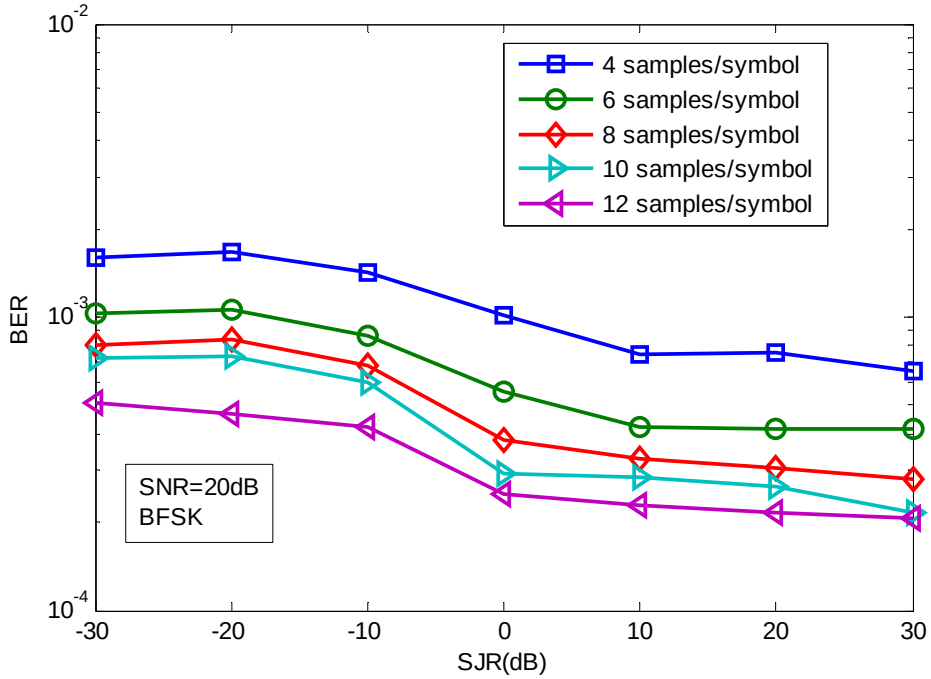

Fig. 4.4: Performance of the MLBB algorithm for various numbers of samples per symbol

Fig. 4.5 shows the performance of the MLBB algorithm under various MFSK signaling. The number of samples per symbol is 4 and the SNR is 20dB. Clearly, the MLBB algorithm with BFSK signaling attains the lowest BER values.

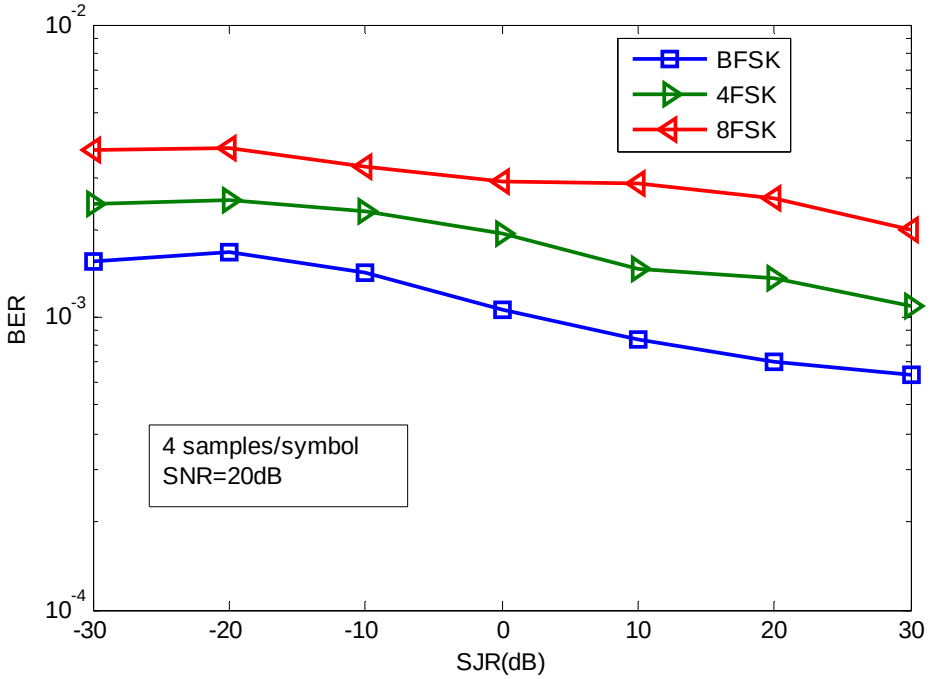

Fig. 4.5: Performance of the MLBB algorithm for various MFSK modulations

4.3 Theoretical Analysis of MLBB Algorithm

4.3.1 General BER Expression of MLBB Algorithm

In this section, we will derive a theoretical expression for the BER of the proposed MLBB jamming rejection and symbol detection algorithm. For the sake of simplicity, we consider only BFSK signaling and a jamming dominant

channel, noting that the case for M-ary signaling can be similarly analyzed. In addition, taking the two possible BFSK symbols to be equally probable, using the decision rule of (4.23), and assuming, without loss of generality, that the transmitted symbol value is $d_0 = 0$, the BER of the MLBB algorithm can be easily shown to be

$$P_e = \Pr\{ f(0) > f(1) \}, \tag{4.25}$$

where the two conditional cost functions $f(0)$ and $f(1)$ are given by

$$f(m) = \|\tilde{\mathbf{s}}(\mathrm{m})\text{-}\mathbf{s}(\mathrm{m})\|^2 \Big|_{d_0=0}, m = 0,1. \tag{4.26}$$

Similarly, the input signal vectors now become

$$\mathbf{r}_1 = \alpha_1 \mathbf{s}(0) + \mathbf{v} + \mathbf{w}_1 \tag{4.27}$$

and

$$\mathbf{r}_2 = \alpha_2 \mathbf{s}(0) + \eta \mathbf{v} + \mathbf{w}_2 . \tag{4.28}$$

Substituting (4.6), (4.18), (4.23), (4.24), (4.27) and (4.28) into (4.26) yields the conditional cost functions $f(0)$ and $f(1)$ as follows

$$f(0) = \left\| \frac{\hat{\eta}(0)\mathbf{b} - \mathbf{a}}{\hat{\eta}(0)\alpha_1 - \alpha_2} \right\|^2 \tag{4.29}$$

and

$$f(1) = \left\| \frac{\hat{\eta}(1)\hat{\mathbf{b}} - \hat{\mathbf{a}}}{\hat{\eta}(1)\alpha_1 - \alpha_2} \right\|^2 \tag{4.30}$$

where

$$\mathbf{a} = \eta \mathbf{v} + \mathbf{w}_2 , \tag{4.31}$$

$$\mathbf{b} = \mathbf{v} + \mathbf{w}_1, \tag{4.32}$$

$$\hat{\mathbf{a}} = \mathbf{s}_2 + \eta\mathbf{v} + \mathbf{w}_2, \tag{4.33}$$

$$\hat{\mathbf{b}} = \mathbf{s}_1 + \mathbf{v} + \mathbf{w}_1, \tag{4.34}$$

$$\mathbf{s}_1 = \alpha_1(\mathbf{s}(0) - \mathbf{s}(1)), \tag{4.35}$$

$$\mathbf{s}_2 = \alpha_2(\mathbf{s}(0) - \mathbf{s}(1)), \tag{4.36}$$

$$\hat{\eta}(0) = \frac{\|\mathbf{a}\|^2 - \|\mathbf{b}\|^2 + \sqrt{(\|\mathbf{a}\|^2 - \|\mathbf{b}\|^2)^2 + 4|\mathbf{a}^H\mathbf{b}|^2}}{2\mathbf{a}^H\mathbf{b}}, \tag{4.37}$$

and

$$\hat{\eta}(1) = \frac{\|\hat{\mathbf{a}}\|^2 - \|\hat{\mathbf{b}}\|^2 + \sqrt{(\|\hat{\mathbf{a}}\|^2 - \|\hat{\mathbf{b}}\|^2)^2 + 4|\hat{\mathbf{a}}^H\hat{\mathbf{b}}|^2}}{2\hat{\mathbf{a}}^H\hat{\mathbf{b}}}. \tag{4.38}$$

Details of the above derivations are shown in Appendix C.

Substituting (4.29) and (4.30) into (4.25), the theoretical BER of the MLBB algorithm is thus given by

$$P_e = \Pr\{\Delta > 0\} \tag{4.39}$$

where

$$\Delta = \left\| \frac{\hat{\eta}(0)\mathbf{b} - \mathbf{a}}{\hat{\eta}(0) - \lambda} \right\|^2 - \left\| \frac{\hat{\eta}(1)\hat{\mathbf{b}} - \hat{\mathbf{a}}}{\hat{\eta}(1) - \lambda} \right\|^2$$

and

$$\lambda = \frac{\alpha_2}{\alpha_1}.$$

4.3.2 Approximate BER Expression in the Jamming Dominant Scenario

Under a "worst case" heavily jammed scenario, where the power of the jammer is much larger than that of receiver noise $\mathbf{w}_p$ (p = 1, 2), the high order terms with respect to receiver noise $\mathbf{w}_p$ (p = 1, 2) can be omitted in a power series expansion of Δ. As a result, Δ can be approximated by using just the zeroth and first order terms of $\mathbf{w}_1$ and $\mathbf{w}_2$. The conditional cost function Δ can therefore be approximated by

$$\Delta = h_1 m_1 + h_2 m_2 \tag{4.40}$$

where

$$h_1 = -\|\mathbf{s}_2 + \eta\mathbf{v}\|^2 - \|\mathbf{s}_1 + \mathbf{v}\|^2 + \sqrt{c} + \mathrm{Re}\left\{\mathbf{w}_2^H\left(\frac{\mathbf{q}_2}{2\sqrt{c}} - 2\eta\mathbf{v} - 2\mathbf{s}_2\right)\right\} + \mathrm{Re}\left\{\mathbf{w}_1^H\left(\frac{\mathbf{q}_1}{2\sqrt{c}} - 2\mathbf{v} - 2\mathbf{s}_1\right)\right\},$$

$$h_2 = \|\mathbf{s}_1\|^2 + \|\mathbf{s}_2\|^2 + 2\,\mathrm{Re}\{\mathbf{s}_1^H\mathbf{v}\} + 2\,\mathrm{Re}\{\eta\mathbf{s}_2^H\mathbf{v}\} + \left(1 + |\eta|^2\right)\|\mathbf{v}\|^2 - \sqrt{c},$$

$$m_1 = \frac{\left|k + \dfrac{\|\mathbf{s}_2 + \eta\mathbf{v}\|^2 - \|\mathbf{s}_1 + \mathbf{v}\|^2 + \sqrt{c}}{2(\mathbf{s}_2 + \eta\mathbf{v})^H(\mathbf{s}_1 + \mathbf{v})}\right|^2}{1 + \left|\dfrac{\|\mathbf{s}_2 + \eta\mathbf{v}\|^2 - \|\mathbf{s}_1 + \mathbf{v}\|^2 + \sqrt{c}}{2(\mathbf{s}_2 + \eta\mathbf{v})^H(\mathbf{s}_1 + \mathbf{v})}\right|^2},$$

$$m_2 = \frac{|k|^2 - 1 - 2\,\mathrm{Re}\left\{k^* \dfrac{\|\mathbf{s}_2 + \eta\mathbf{v}\|^2 - \|\mathbf{s}_1 + \mathbf{v}\|^2 + \sqrt{c}}{2(\mathbf{s}_2 + \eta\mathbf{v})^H (\mathbf{s}_1 + \mathbf{v})}\right\}}{1 + \left|\dfrac{\|\mathbf{s}_2 + \eta\mathbf{v}\|^2 - \|\mathbf{s}_1 + \mathbf{v}\|^2 + \sqrt{c}}{2(\mathbf{s}_2 + \eta\mathbf{v})^H (\mathbf{s}_1 + \mathbf{v})}\right|^2} - \frac{|k|^2 - 1 - 2\,\mathrm{Re}\{k^* \eta\}}{1 + |\eta|^2},$$

$$c = \left(\|\mathbf{s}_2 + \eta\mathbf{v}\|^2 - \|\mathbf{s}_1 + \mathbf{v}\|^2\right)^2 + 4\left|(\mathbf{s}_2 + \eta\mathbf{v})^H (\mathbf{s}_1 + \mathbf{v})\right|^2,$$

$$\mathbf{q}_1 = 4(\mathbf{s}_1 + \mathbf{v})\left(\|\mathbf{s}_1 + \mathbf{v}\|^2 - \|\mathbf{s}_2 + \eta\mathbf{v}\|^2\right) + 8(\mathbf{s}_2 + \eta\mathbf{v})^H (\mathbf{s}_1 + \mathbf{v})(\mathbf{s}_2 + \eta\mathbf{v})$$

and

$$\mathbf{q}_2 = 4(\mathbf{s}_2 + \eta\mathbf{v})\left(\|\mathbf{s}_2 + \eta\mathbf{v}\|^2 - \|\mathbf{s}_1 + \mathbf{v}\|^2\right) + 8(\mathbf{s}_1 + \mathbf{v})^H (\mathbf{s}_2 + \eta\mathbf{v})(\mathbf{s}_1 + \mathbf{v}).$$

Note that within a certain symbol, h_2, m_1 and m_2 are constants independent of noise. However, the parameter h_1 is random and is a linear combination of the real and imaginary parts of the independent zero-mean Gaussian receiver noise samples $w_{p,n}$. As a result, h_1 will be Gaussian distributed. The mean μ_{err} and the variance σ_{err}^2 of h_1 can therefore be computed by using

$$\mu_{err} = -\|\mathbf{s}_2\|^2 - \|\mathbf{s}_1\|^2 - 2\,\mathrm{Re}\left\{\left(\mathbf{s}_1 + \eta^*\mathbf{s}_2\right)^H \mathbf{v}\right\} + \sqrt{c} - \left(1 + |\eta|^2\right)\|\mathbf{v}\|^2 \qquad (4.41)$$

and

$$\sigma_{err}^2 = \sigma^2\left(\left\|\frac{\mathbf{q}_2}{2\sqrt{c}} - 2\eta\mathbf{v} - 2\mathbf{s}_2\right\|^2 + \left\|\frac{\mathbf{q}_1}{2\sqrt{c}} - 2\mathbf{v} - 2\mathbf{s}_1\right\|^2\right) \qquad (4.42)$$

where σ^2 is the variance of the real and imaginary parts of the zero-mean Gaussian receiver noise samples $w_{p,n}$.

Based on (4.40), (4.41) and (4.42), the theoretical BER of the MLBB

algorithm can be approximately determined by

$$P_e = Q\left(-\mu_\Delta \Big/ \sqrt{\sigma_\Delta^2}\right), \tag{4.43}$$

where

$$\mu_\Delta = \mu_{err} m_1 + h_2 m_2, \tag{4.44}$$

$$\sigma_\Delta^2 = \sigma_{err}^2 m_1^2 \tag{4.45}$$

and

$$Q(x) = \int_x^{+\infty} \exp\left(-y^2/2\right) \Big/ \left(2\pi\right) dy\,. \tag{4.46}$$

The validity of the performance analysis and the tightness of the analytical BER values of MLBB algorithm derived for BFSK signaling are demonstrated in Fig. 4.6. Three different SNR values are used to show the tightness between the simulated and analytical BER values. It is observed that the simulation results are very close to the theoretical ones derived by (4.43).

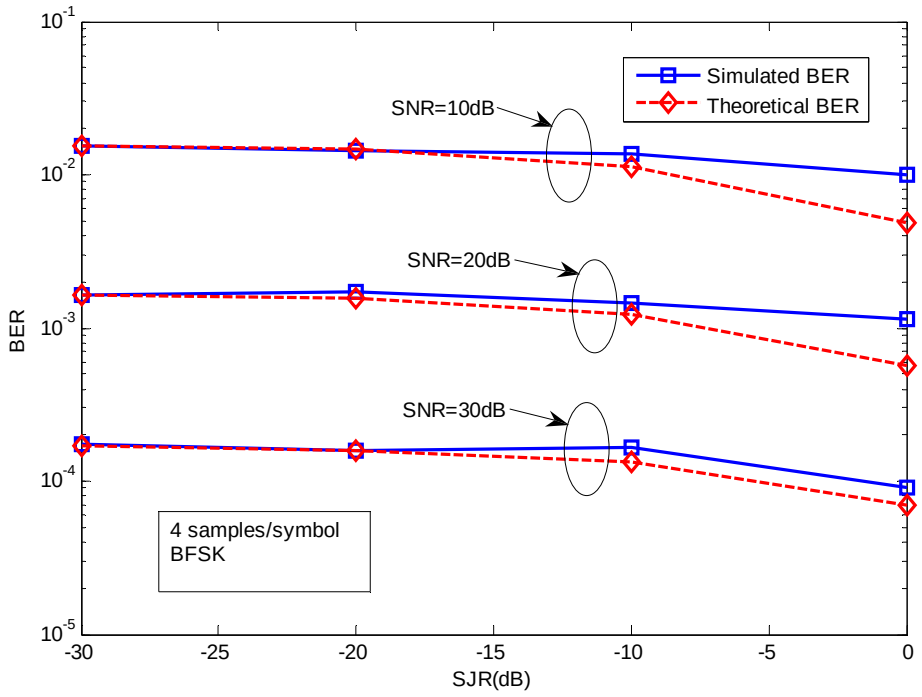

Fig. 4.6: Theoretical (4.43) and simulated BER values of the MLBB algorithm for various SJR and SNR values

4.4 Summary

In this chapter, the MLBB algorithm was proposed for slow FH/MFSK systems in the presence of a follower partial-band jammer over quasi-static flat fading channels. The proposed algorithm first uses the ML technique to estimate the ratio of jamming fading gains and then places a null toward the follower jamming source. By regarding the received jamming components as

deterministic quantities to be estimated instead of receiver noise, the MLBB algorithm avoids the degradation of either the SMI algorithm or the traditional ML one in jamming dominant channels. As a result, the performance of the MLBB algorithm outperforms these two existing algorithms. In addition, an analytical BER expression for the proposed MLBB algorithm was derived in the jamming dominant scenarios. Finally, the proposed MLBB algorithm can be integrated with any coded FH/MFSK transmission to further enhance the receiver performance.

CHAPTER 5

AREA-BASED VECTOR SIMILARITY METRIC ALGORITHM

5.1 Introduction of Area-based VSM Algorithm

In this chapter, we also assume that the number of jammers is one and that the receiver has two antenna elements. The received signal can be represented as

$$\mathbf{r}_1 = \alpha_1 \mathbf{s}(d_0) + \mathbf{v}_1 + \mathbf{w}_1 \tag{5.1}$$

and

$$\mathbf{r}_2 = \alpha_2 \mathbf{s}(d_0) + \mathbf{v}_2 + \mathbf{w}_2 \tag{5.2}$$

where

$$\mathbf{v}_p = \beta_{1p}[J_0, J_1, \cdots J_{N-1}]^T, \; p = 1, 2. \tag{5.3}$$

We will make use of the fact that because the jamming components $\mathbf{v}_1$ and $\mathbf{v}_2$ are spatially correlated or parallel in the complex space, the area in the triangle defined by these vectors will be zero. More specifically, based on (5.1) and (5.2) with $\alpha_p \mathbf{s}(d)$ being the transmitted symbol vector and $\mathbf{r}_p$ being the received signal vector, the noisy received jamming component at the two array elements are

$$\mathbf{z}_p(d) = \mathbf{r}_p - \alpha_p \mathbf{s}(d),\ p = 1, 2\,. \tag{5.4}$$

The area defined by $\mathbf{z}_1(d)$ and $\mathbf{z}_2(d)$ are then given by

$$\Gamma(d) = \|\mathbf{z}_1(d)\|\|\mathbf{z}_2(d)\|\sin\theta, \tag{5.5}$$

where

$$\theta = \cos^{-1}\left[\frac{\left|\mathbf{z}_1^H(d)\mathbf{z}_2(d)\right|}{\|\mathbf{z}_1(d)\|\|\mathbf{z}_2(d)\|}\right] \tag{5.6}$$

is the Hermitian angle [69] between $\mathbf{z}_1(d)$ and $\mathbf{z}_2(d)$.

Because the area given by (5.5) will be zero in the absence of white noise, (5.5) can be used as an objective function for the purpose of symbol detection and jamming removal. Specifically, with this area-based VSM objective function or metric, the transmitted symbol can be detected by using

$$\hat{d}_0 = \arg\ \min_{\mathrm{d}}\left\{\Gamma(d); d = 0,1,\cdots,M-1\right\}. \tag{5.7}$$

Table 5.1 gives the detailed processing steps for the proposed VSM jamming rejection and symbol detection algorithm, while Table 5.2 presents the computational complexity of the algorithm. Note that the computational complexity is due mainly to steps 1 and 2 in Table 5.1 because these steps involve vector operations. As can be seen, the computational complexity of the algorithm is roughly equal to $5NM + 4M$ multiplications.

Table 5.1: Details of the proposed VSM algorithm

Step	Calculation
1	Calculate $\mathbf{z}_1(d)$ and $\mathbf{z}_2(d)$, $d = 0,\cdots,M-1$, using (5.4)
2	Calculate $\Gamma(d)$, $d = 0,\cdots,M-1$, using (5.5)
3	Obtain the VSM estimate of the transmitted symbol $\hat{d}_0$ using (5.7).

Table 5.2: Computational complexity of the proposed VSM algorithm per symbol

Step	# addition	# multiplication	# sqrt
1	$2NM$	$2NM$	0
2	$3NM-2M$	$3NM+4M$	$2M$
Total	$5NM-2M$	$5NM+4M$	$2M$

5.2 Performance of Area-based VSM Algorithm

Numerical simulations were conducted to validate the performance of the proposed VSM algorithms for slow FH systems with various MFSK

modulations. In the simulation study, each hop has 8 MFSK symbols, the symbol rate is 200000 symbols per second, and the hop rate is 25000 hops per second. A total of 20 million symbols are used for each simulation run. In the simulation, the fading coefficients are modeled as independent identically distributed (i.i.d) complex Gaussian random variables with zero-mean and a variance of 0.5 per dimension.

Fig. 5.1 compares the BER performance of the proposed VSM algorithm, the SMI algorithm, the traditional ML algorithm, the MLBB algorithm and the algorithm proposed in [58]. In this figure, the BER performance is plotted versus SJR, with SNR fixed at 30dB and the number of samples per symbol at $N = 4$. The VSM algorithm outperforms other algorithms for SJR<25dB. Over a channel with SJR>25dB where the jamming signal is negligible, the traditional ML algorithm has a slightly better performance than the VSM algorithm, even though both the traditional ML and the VSM algorithms attain highly reliable bit detection with BER values of about 10^{-6}. The ML algorithm has a better performance because it makes use of a signal model which assumes that there is no jamming and therefore has fewer parameters to be estimated. As jamming becomes negligible, this model becomes perfect. Then, with the smallest number of parameters to be estimated, better estimation accuracy can be obtained, leading to a better performance.

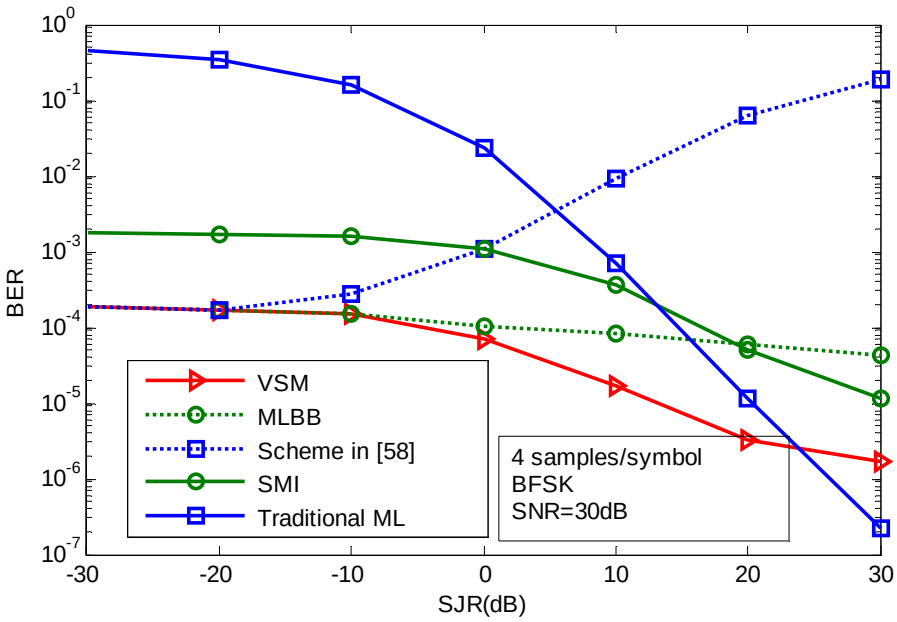

Fig. 5.1: Performance of various algorithms versus SJR with 30dB SNR, BFSK and 4 samples per symbol

Fig. 5.2 and Fig. 5.3 show the BER performance of the proposed VSM algorithm, the SMI-based algorithm, the traditional ML algorithm, the MLBB algorithm and the algorithm proposed in [58] under 8-FSK (with 4 samples per symbol) and 16-FSK (with 8 samples per symbol) modulations, respectively. As can be observed, the VSM algorithm outperforms the other algorithms.

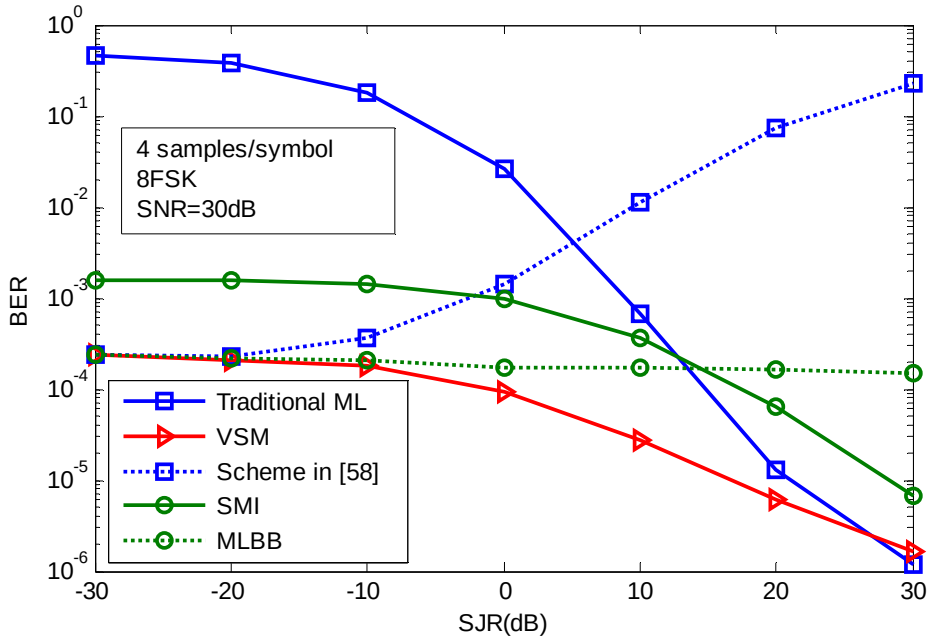

Fig. 5.2: Performance of various algorithms versus SJR with 30dB SNR, 8-FSK and 4 samples per symbol

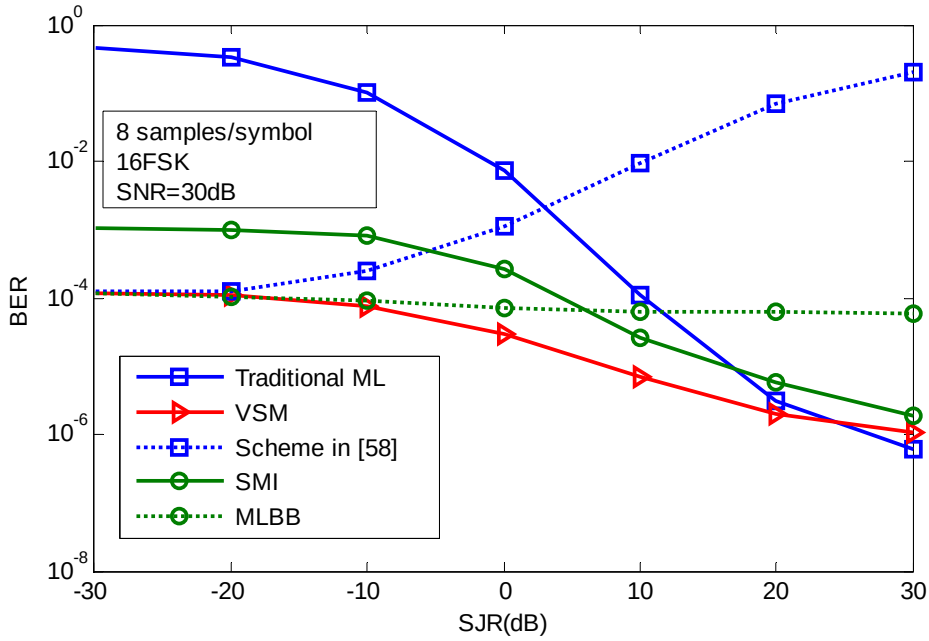

Fig. 5.3: Performance of various algorithms versus SJR with 30dB SNR, 16-FSK and 8 samples per symbol

With SJR fixed at 0dB, Fig. 5.4 compares the performance of the VSM algorithm with the other algorithms for various SNR conditions. The number of samples per symbol is $N = 4$. Over a channel with comparable jamming and signal power (SJR=0dB), treating the jamming signal as receiver noise gives rise to an error floor in the BER performance when the traditional ML algorithm is used.

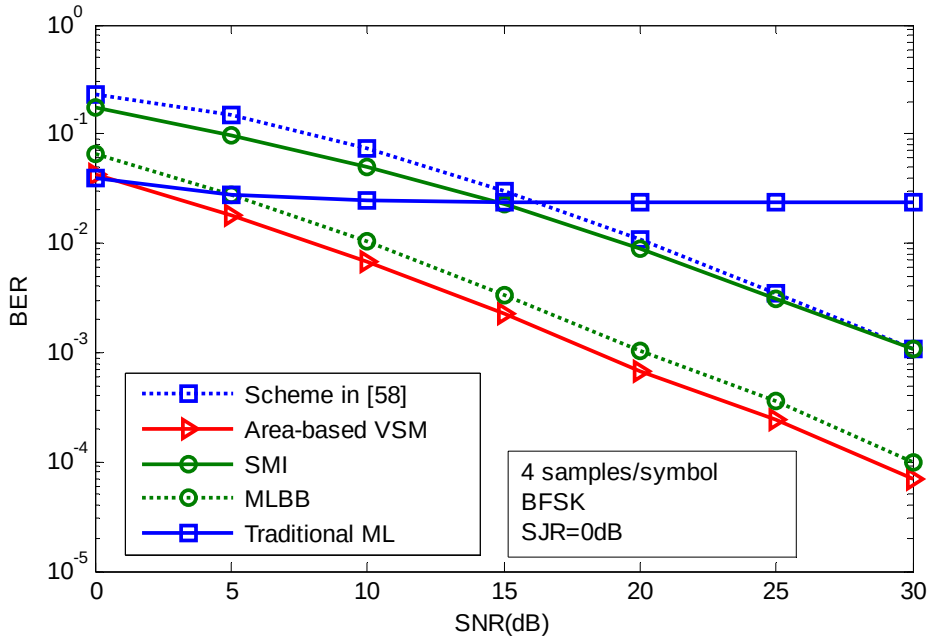

Fig. 5.4: Performance of various algorithms versus SNR with 0dB SJR, BFSK and 4 samples per symbol

Fig. 5.5 and Fig 5.6 show the effect of changing the number of samples per symbol for the area-based VSM algorithm with SNR = 30dB and BFSK/16-FSK modulations. As can be seen, increasing the number of samples per symbol N leads to a better BER performance at the cost of higher

computational complexity (as shown in Table 5.2).

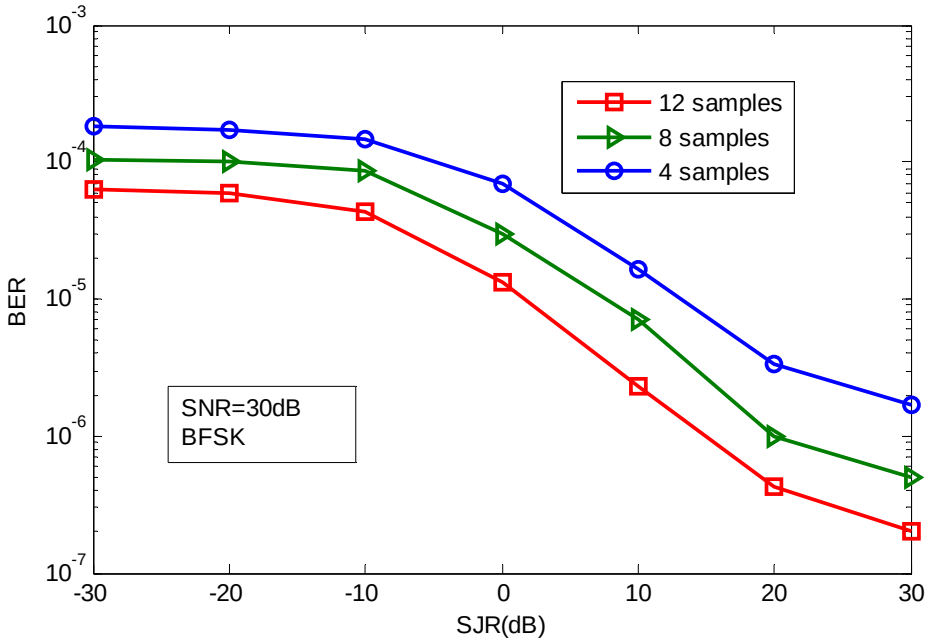

Fig. 5.5: Performance of the VSM algorithm for various numbers of samples per symbol with 30dB SNR and BFSK

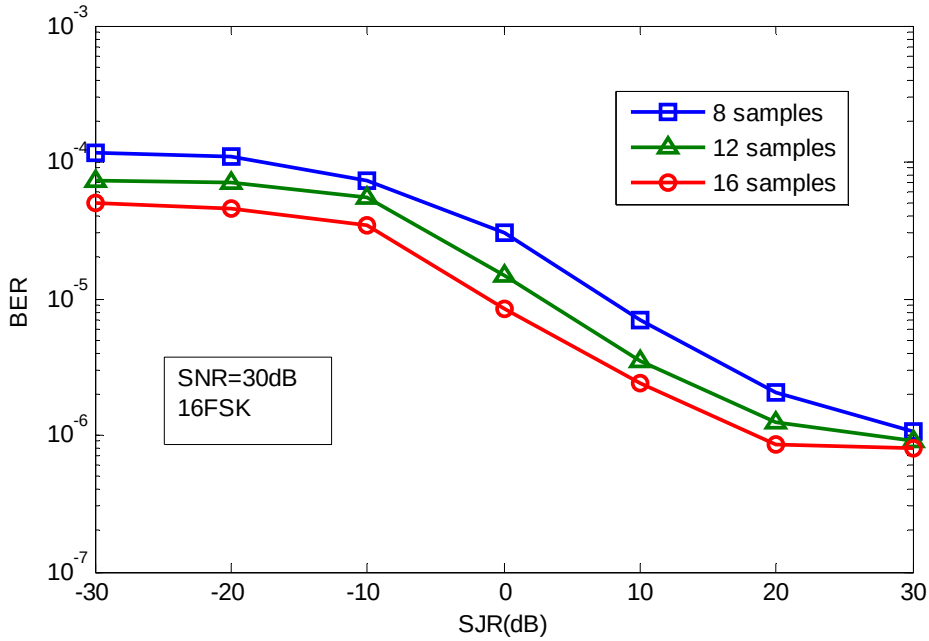

Fig. 5.6: Performance of the VSM algorithm for various numbers of samples per symbol with 30dB SNR and 16-FSK

To investigate the robustness of the VSM algorithm against imperfect channel knowledge, Fig. 5.7 shows the BER performance of the VSM algorithm with the channel gains of the desired signal estimated blindly by using a standard ML procedure in the unjammed portion of each hop as described in CHAPTER 3. In the simulation, the ratio of unjammed interval to hop duration is set to be 0.25. With imperfect channel knowledge, the performance of the VSM algorithm degrades slightly as compared with the case when perfect channel knowledge is available at the receiver.

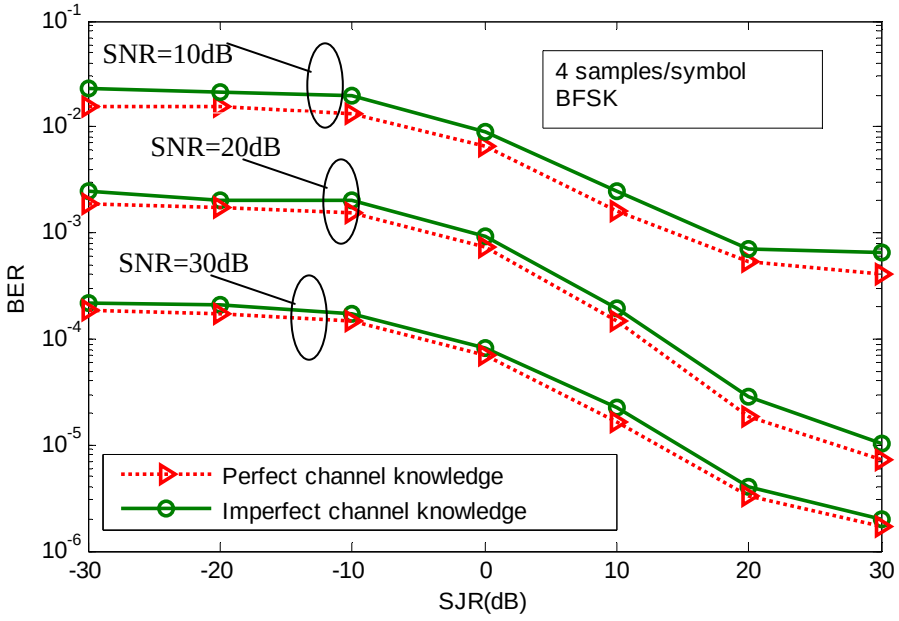

Fig. 5.7: Performance of the VSM algorithm with perfect and imperfect channel knowledge for various SJR and SNR values with BFSK and 4 samples per symbol

5.3 Theoretical Analysis of Area-based VSM Algorithm

5.3.1 General BER Expression of Area-based VSM Algorithm

In this section, we will derive a theoretical BER expression for the proposed area-based VSM jamming rejection and symbol detection algorithm. For the sake of simplicity, we consider BFSK signaling only, and note that the case for *M*-ary signaling can be similarly analyzed. In addition, we take the two possible BFSK symbols to be equally probable, and assume, without loss of generality, that the transmitted symbol value is $d_0 = 0$. Using (5.1) and (5.2), the vectors of the received samples from two receive antennas will then become

$$\mathbf{r}_1 = \alpha_1 \mathbf{s}(0) + \mathbf{v}_1 + \mathbf{w}_1 \tag{5.8}$$

and

$$\mathbf{r}_2 = \alpha_2 \mathbf{s}(0) + \mathbf{v}_2 + \mathbf{w}_2. \tag{5.9}$$

Using (5.8), (5.9) and (5.5) for the objective function (5.7), the BER of the area-based VSM algorithm can readily be shown to be

$$P_e = \Pr\{\Gamma(0) > \Gamma(1) \mid d_0 = 0\}, \tag{5.10}$$

where $\Gamma(0)$ and $\Gamma(1)$, as given below, are the objective functions for a correct and an incorrect decision, respectively:

$$\Gamma(0) = \|\mathbf{v}_1 + \mathbf{w}_1\|\|\mathbf{v}_2 + \mathbf{w}_2\|\sin\theta_1, \tag{5.11}$$

$$\Gamma(1) = \|\mathbf{k}_1 + \mathbf{w}_1\|\|\mathbf{k}_2 + \mathbf{w}_2\|\sin\theta_2, \tag{5.12}$$

$$\theta_1 = \cos^{-1}\left[\frac{\left|(\mathbf{v}_1 + \mathbf{w}_1)^H(\mathbf{v}_2 + \mathbf{w}_2)\right|}{\|\mathbf{v}_1 + \mathbf{w}_1\|\|\mathbf{v}_2 + \mathbf{w}_2\|}\right], \tag{5.13}$$

$$\theta_2 = \cos^{-1}\left[\frac{\left|(\mathbf{k}_1 + \mathbf{w}_1)^H(\mathbf{k}_2 + \mathbf{w}_2)\right|}{\|\mathbf{k}_1 + \mathbf{w}_1\|\|\mathbf{k}_2 + \mathbf{w}_2\|}\right], \tag{5.14}$$

$$\mathbf{k}_1 = \alpha_1(\mathbf{s}(0) - \mathbf{s}(1)) + \mathbf{v}_1, \tag{5.15}$$

and

$$\mathbf{k}_2 = \alpha_2(\mathbf{s}(0) - \mathbf{s}(1)) + \mathbf{v}_2. \tag{5.16}$$

By substituting (5.13) and (5.14) into (5.11) and (5.12), squaring and expanding the resulting expressions, (5.10) can be expressed in terms of the noise $\mathbf{w}_p$ (p=1, 2) and the jamming components $\mathbf{v}_p$ (p=1, 2) as follows:

$$P_e = \Pr\{g(0) - g(1) > 0 \mid d_0 = 0\}, \tag{5.17}$$

where

$$g(0) = \|\mathbf{v}_1 + \mathbf{w}_1\|^2\|\mathbf{v}_2 + \mathbf{w}_2\|^2 - \left|(\mathbf{v}_1 + \mathbf{w}_1)^H(\mathbf{v}_2 + \mathbf{w}_2)\right|^2 \tag{5.18}$$

and

$$g(1) = \|\mathbf{k}_1 + \mathbf{w}_1\|^2\|\mathbf{k}_2 + \mathbf{w}_2\|^2 - \left|(\mathbf{k}_1 + \mathbf{w}_1)^H(\mathbf{k}_2 + \mathbf{w}_2)\right|^2. \tag{5.19}$$

5.3.2 Approximate BER Expression in the Jamming Dominant Scenario

Because it is mathematically intractable to obtain an explicit expression for the BER from (5.17) in general, we will now attempt to derive an approximate BER expression under the scenario where the power of jamming signal is higher than that of desired signal and noise (a jamming dominant scenario), or when $p_w << p_J$ and $p_S << p_J$.

After expanding the various squares and modulus square terms in (5.17), $g(0)-g(1)$ becomes

$$g(0)-g(1)=\|\mathbf{k}_1\|^2\|\mathbf{k}_2\|^2-\left|\mathbf{k}_1^H\mathbf{k}_2\right|^2+2\,\mathrm{Re}\left\{\mathbf{h}_1^H\mathbf{w}_1\right\}+2\,\mathrm{Re}\left\{\mathbf{h}_2^H\mathbf{w}_2\right\}+o \quad (5.20)$$

where

$$o=\begin{bmatrix}\|\mathbf{v}_1\|^2\|\mathbf{w}_2\|^2+\|\mathbf{w}_1\|^2\|\mathbf{v}_2\|^2-\left|\mathbf{v}_1^H\mathbf{w}_2\right|^2-\left|\mathbf{w}_1^H\mathbf{v}_2\right|^2\\ +2\left(\mathrm{Re}\left\{\mathbf{v}_2^H\mathbf{w}_2\right\}+\|\mathbf{w}_2\|^2\right)\mathrm{Re}\left\{\mathbf{v}_1^H\mathbf{w}_1\right\}+2\left(\mathrm{Re}\left\{\mathbf{v}_1^H\mathbf{w}_1\right\}+\|\mathbf{w}_1\|^2\right)\mathrm{Re}\left\{\mathbf{v}_2^H\mathbf{w}_2\right\}\\ +2\,\mathrm{Re}\left\{\left(\mathbf{v}_1^H\mathbf{v}_2+\mathbf{v}_1^H\mathbf{w}_2+\mathbf{w}_1^H\mathbf{v}_2\right)^H\mathbf{w}_1^H\mathbf{w}_2+\left(\mathbf{v}_1^H\mathbf{w}_2\right)^H\mathbf{w}_1^H\mathbf{v}_2\right\}\end{bmatrix}$$

$$-\begin{bmatrix}\|\mathbf{k}_1\|^2\|\mathbf{w}_2\|^2+\|\mathbf{w}_1\|^2\|\mathbf{k}_2\|^2-\left|\mathbf{k}_1^H\mathbf{w}_2\right|^2-\left|\mathbf{w}_1^H\mathbf{k}_2\right|^2\\ +2\left(\mathrm{Re}\left\{\mathbf{k}_2^H\mathbf{w}_2\right\}+\|\mathbf{w}_2\|^2\right)\mathrm{Re}\left\{\mathbf{k}_1^H\mathbf{w}_1\right\}+2\left(\mathrm{Re}\left\{\mathbf{k}_1^H\mathbf{w}_1\right\}+\|\mathbf{w}_1\|^2\right)\mathrm{Re}\left\{\mathbf{k}_2^H\mathbf{w}_2\right\}\\ +2\,\mathrm{Re}\left\{\left(\mathbf{k}_1^H\mathbf{k}_2+\mathbf{k}_1^H\mathbf{w}_2+\mathbf{w}_1^H\mathbf{k}_2\right)^H\mathbf{w}_1^H\mathbf{w}_2+\left(\mathbf{k}_1^H\mathbf{w}_2\right)^H\mathbf{w}_1^H\mathbf{k}_2\right\}\end{bmatrix} \quad (5.21)$$

$$\mathbf{h}_1^H=\|\mathbf{k}_2\|^2\mathbf{k}_1^H-\mathbf{k}_1^H\mathbf{k}_2\mathbf{k}_2^H \quad (5.22)$$

and

$$\mathbf{h}_2^H = \|\mathbf{k}_1\|^2 \mathbf{k}_2^H - \mathbf{k}_2^H \mathbf{k}_1 \mathbf{k}_1^H . \tag{5.23}$$

Note that in a jamming dominant channel where $\mathbf{k}_1 \approx \mathbf{v}_1$ and $\mathbf{k}_2 \approx \mathbf{v}_2$, the term o in (5.20) will be close to zero and can be neglected, leading to

$$g(0) - g(1) = \|\mathbf{k}_1\|^2 \|\mathbf{k}_2\|^2 - \left|\mathbf{k}_1^H \mathbf{k}_2\right|^2 + 2\,\mathrm{Re}\left\{\mathbf{h}_1^H \mathbf{w}_1\right\} + 2\,\mathrm{Re}\left\{\mathbf{h}_2^H \mathbf{w}_2\right\}. \tag{5.24}$$

Using (5.24), the condition given by (5.17) is equivalent to

$$h_0 + 2\,\mathrm{Re}\left\{\mathbf{h}_1^H \mathbf{w}_1\right\} + 2\,\mathrm{Re}\left\{\mathbf{h}_2^H \mathbf{w}_2\right\} > 0 \tag{5.25}$$

where

$$h_0 = \left|\mathbf{k}_1^H \mathbf{k}_2\right|^2 - \|\mathbf{k}_1\|^2 \|\mathbf{k}_2\|^2 . \tag{5.26}$$

It is noted that h_0, $\mathbf{h}_1$ and $\mathbf{h}_2$ are constants and independent of noise. Specifically, the left hand side of (5.25) consists of a constant and a linear combination of Gaussian-distributed receiver noise components. Hence, it is also Gaussian distributed with a mean of h_0 and a variance of

$$\sigma_J^2 = 4\sigma^2 \left(\|\mathbf{h}_1\|^2 + \|\mathbf{h}_2\|^2\right) \tag{5.27}$$

where σ^2 is the variance of the real and imaginary parts of the zero-mean Gaussian receiver noise samples $w_{p,n}$.

Based on (5.17), (5.25) and (5.27), the approximate BER expression of the area-based VSM algorithm in a jamming dominant channel is given by

$$P_{eJ} = Q\left(-h_0 / \sqrt{\sigma_J^2}\right) \tag{5.28}$$

where

$$Q(x)=\frac{1}{\sqrt{2\pi}}\int_{x}^{+\infty}\exp\left(-\frac{y^2}{2}\right)dy\,.$$

The validity of the performance analysis and the tightness of the analytical BER values of the VSM algorithm derived for BFSK signaling are demonstrated in Fig. 5.8. As mentioned, the BER expressions are derived under a jamming dominant channel approximation. As a result, the theoretical BER curves match the simulated ones well in the low SJR regime (high jamming power), but mismatch appears in the high SJR region (low jamming power).

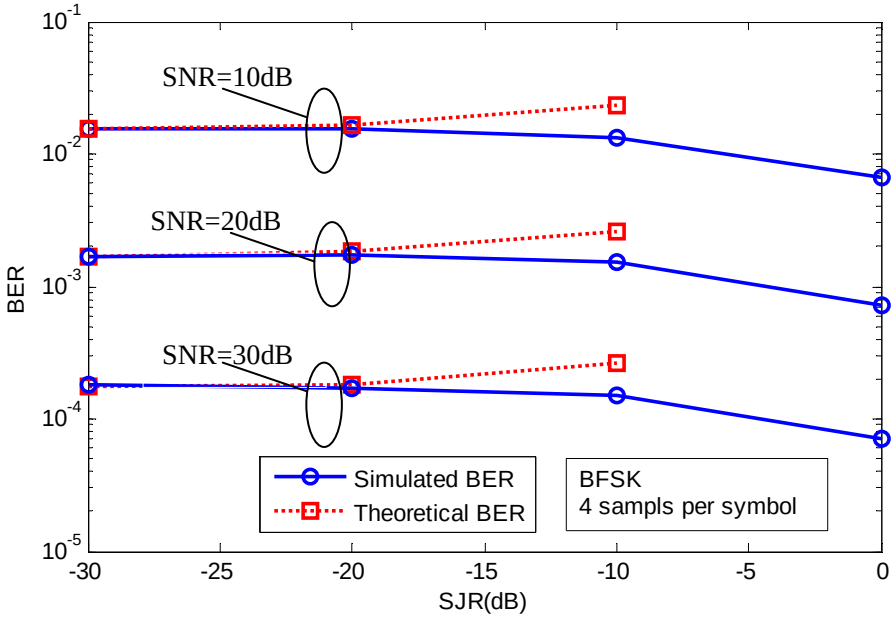

Fig. 5.8: Theoretical (5.28) and simulated BER of the VSM algorithm in jamming dominant channels for various SJR and SNR values with BFSK and 4 samples per symbol

5.4 Summary

In this chapter, an area-based vector similarity metric is proposed for symbol detection in slow FH/MFSK systems in the presence of a follower partial-band jammer over quasi-static flat fading channels. By exploiting the unknown spatial correlation of the received jamming components, the proposed algorithm is able to reject jamming and overcome the performance degradation of the SMI algorithm or the traditional ML algorithm used in jamming dominant channels. Analytical BER expression for the VSM algorithm has also been derived in jamming dominant channels and shown to agree well with simulation results.

CHAPTER 6

VOLUMETRIC-BASED DETECTION ALGORITHM

6.1 Introduction of the Volumetric-based Algorithm

We have introduced two algorithms that can eliminate only one follower partial band jammer in CHAPTER 4 and CHAPTER 5. In this chapter, we will introduce the volumetric-based algorithm that can deal with more jammers.

We will make use of the fact that, because the jamming components $\mathbf{v}_p$ (p=1, 2, ⋯, X+1) are spatially correlated, $\mathbf{v}_p$ will be equal to a linear combination of $\mathbf{J}_1, \mathbf{J}_2, \cdots, \mathbf{J}_X$. Thus, the "volume" defined by the vectors $\mathbf{v}_1, \mathbf{v}_2, \cdots, \mathbf{v}_{X+1}$ in a linear space with X+1 dimensions will be zero, which is of course a direct result of the fact that this set of X+1 vectors are not linearly independent and that these vectors have a span of only X. More specifically, based on (3.5) with $\alpha_p \mathbf{s}(d)$ being the transmitted symbol vector and $\mathbf{r}_p$ being the received signal vector, the noisy received jamming components at the

array elements are

$$\mathbf{z}_p(d) = \mathbf{r}_p - \alpha_p \mathbf{s}(d),\ p = 1, 2, \cdots, X+1. \tag{6.1}$$

For the sake of simplicity, we will derive the cost function for X=2 jammers with 3 receiver elements first. Then we will show how this can be extended to a more general case of X jammers.

Given three vectors $\mathbf{z}_1(d), \mathbf{z}_2(d)$ and $\mathbf{z}_3(d)$ obtained from (6.1), the volume defined can be found from first calculating the base area $S(d)$ defined by 2 of the vectors, and then calculating the distance from the remaining vector to the base. Without loss of generally, assume that the base is defined by $\mathbf{z}_1(d)$ and $\mathbf{z}_2(d)$, and the remaining vector is $\mathbf{z}_3(d)$. The volume defined by $\mathbf{z}_1(d), \mathbf{z}_2(d)$ and $\mathbf{z}_3(d)$ is then

$$\Gamma_2(d) = \frac{1}{3} S(d) \|\mathbf{h}(d)\| \tag{6.2}$$

where $\mathbf{h}(d)$ is the vector that corresponds to the height from $\mathbf{z}_3(d)$ to the base defined by $\mathbf{z}_1(d)$ and $\mathbf{z}_2(d)$, and is orthogonal to $\mathbf{z}_1(d)$ and $\mathbf{z}_2(d)$.

From [70], the area defined by $\mathbf{z}_1(d)$ and $\mathbf{z}_2(d)$ is given by

$$S(d) = \|\mathbf{z}_1(d)\| \|\mathbf{z}_2(d)\| \sin\theta \tag{6.3}$$

where

$$\theta = \cos^{-1}\left[\frac{\left|\mathbf{z}_1^H(d)\mathbf{z}_2(d)\right|}{\|\mathbf{z}_1(d)\| \|\mathbf{z}_2(d)\|} \right]$$

is the Hermitian angle between $\mathbf{z}_1(d)$ and $\mathbf{z}_2(d)$. The vector $\mathbf{h}(d)$ is

$$\mathbf{h}(d) = \mathbf{z}_3(d) - [a(d)\mathbf{z}_1(d) + b(d)\mathbf{z}_2(d)] \tag{6.4}$$

where $a(d)\mathbf{z}_1(d)+b(d)\mathbf{z}_2(d)$ is the projection of $\mathbf{z}_3(d)$ on the subspace defined by $\mathbf{z}_1(d)$ and $\mathbf{z}_2(d)$.

Because $\mathbf{h}(d)$ is orthogonal to $\mathbf{z}_1(d)$ and $\mathbf{z}_2(d)$, we have

$$\frac{\left|\mathbf{h}^H(d)\mathbf{z}_1(d)\right|}{\left\|\mathbf{h}(d)\right\|\left\|\mathbf{z}_1(d)\right\|}=0 \tag{6.5}$$

and

$$\frac{\left|\mathbf{h}^H(d)\mathbf{z}_2(d)\right|}{\left\|\mathbf{h}(d)\right\|\left\|\mathbf{z}_2(d)\right\|}=0. \tag{6.6}$$

Substituting (6.4) into (6.5) and (6.6), we get

$$\left[\mathbf{z}_3(d)-a(d)\mathbf{z}_1(d)-b(d)\mathbf{z}_2(d)\right]^H\mathbf{z}_1(d)=0 \tag{6.7}$$

and

$$\left[\mathbf{z}_3(d)-a(d)\mathbf{z}_1(d)-b(d)\mathbf{z}_2(d)\right]^H\mathbf{z}_2(d)=0\,. \tag{6.8}$$

From (6.7) and (6.8), it can be shown that

$$a(d)=\frac{\left\|\mathbf{z}_2(d)\right\|^2\mathbf{z}_1^H(d)\mathbf{z}_3(d)-\mathbf{z}_1^H(d)\mathbf{z}_2(d)\mathbf{z}_2^H(d)\mathbf{z}_3(d)}{\left\|\mathbf{z}_1(d)\right\|^2\left\|\mathbf{z}_2(d)\right\|^2-\left|\mathbf{z}_1^H(d)\mathbf{z}_2(d)\right|^2} \tag{6.9}$$

and

$$b(d)=\frac{\left\|\mathbf{z}_1(d)\right\|^2\mathbf{z}_2^H(d)\mathbf{z}_3(d)-\mathbf{z}_2^H(d)\mathbf{z}_1(d)\mathbf{z}_1^H(d)\mathbf{z}_3(d)}{\left\|\mathbf{z}_1(d)\right\|^2\left\|\mathbf{z}_2(d)\right\|^2-\left|\mathbf{z}_1^H(d)\mathbf{z}_2(d)\right|^2}. \tag{6.10}$$

Thus, by substituting (6.9), (6.10), (6.3) and (6.4) into (6.2), the volume defined by $\mathbf{z}_1(d),\mathbf{z}_2(d)$ and $\mathbf{z}_3(d)$ is

$$\Gamma_2(d)=\frac{1}{3}\left\|\mathbf{z}_3(d)-a(d)\mathbf{z}_1(d)-b(d)\mathbf{z}_2(d)\right\|\left\|\mathbf{z}_1(d)\right\|\left\|\mathbf{z}_2(d)\right\|\sin\theta\,. \tag{6.11}$$

Because the volume given by (6.11) will be zero in the absence of white

noise, (6.11) can be used as an objective function for the purpose of symbol detection and jamming removal. Specifically, with this volumetric-based objective function, the transmitted symbol can be detected by using

$$\hat{d}_0 = \arg \min_{d} \{\Gamma_2(d); d = 0,1,\cdots,M-1\}. \qquad (6.12)$$

Table 6.1 gives the detailed processing steps for the new volumetric-based jamming rejection and symbol detection algorithm, while Table 6.2 presents the computational complexity of the algorithm. Note that the computational complexity is mainly due to steps 1 and 2 in Table 6.1, as these steps involve vector operations. As can be seen, the computational complexity of the algorithm is roughly equal to $19NM + 12M$ multiplications.

Table 6.1: Details of the proposed volumetric-based algorithm

Step	Calculation
1	Calculate $\mathbf{z}_1(d)$, $\mathbf{z}_2(d)$ and $\mathbf{z}_3(d)$, $d = 0,\cdots,M-1$, using (6.1)
2	Calculate $\Gamma_2(d)$, $d = 0,\cdots,M-1$, using (6.11)
3	Obtain the volumetric-based estimation of the transmitted symbol $\hat{d}_0$ using (6.12).

Table 6.2: Computational complexity of the volumetric-based algorithm per symbol

Step	# addition	# multiplication	# sqrt
1	$3NM$	$3NM$	0
2	$16NM-10M$	$16NM+12M$	$3M$
Total	$19NM-10M$	$19NM+12M$	$3M$

To see how this "volumetric-based" algorithm can be extended to deal with a larger array with more jammers, we note that the volume defined by 3 vectors is calculated from first finding the area defined by 2 of the vectors, and then multiplying this area with the height when the remaining vector is projected onto this area. Thus, in a more general case when we have x+1 vectors, the "volume" can also be calculated by first finding the "area" defined by x of the vectors, and then multiplying this "area" with the height obtained when the remaining vector is projected onto this "area". Of course, in an x+1 dimensional space, the "area" defined by x vectors is actually the "volume" defined by these same set of vectors in an x dimensional space.

With the above consideration, now assume that $\Gamma_x(d)$ is the cost function for the scenario with x jammers and x+1 receiving antennas. Because this cost function corresponds to the "volume" with x jammers, it can be taken as the

"area" when there is 1 more jammer. The "volume", $\Gamma_{x+1}(d)$, for the x+1 jammers and x+2 receiving antennas case can thus be calculated based on

$$\Gamma_{x+1}(d) = \mu\Gamma_x(d)\left\|\mathbf{h}_{x+1}(d)\right\| \tag{6.13}$$

where μ is a positive real number, and $\left\|\mathbf{h}_{x+1}(d)\right\|$ is the distance from $\mathbf{z}_{x+2}(d)$ to the subspace formed by $\mathbf{z}_1(d)$, $\mathbf{z}_2(d)$, $\cdots$, $\mathbf{z}_{x+1}(d)$. $\mathbf{h}_{x+1}(d)$ is given by

$$\mathbf{h}_{x+1}(d) = \mathbf{z}_{x+2}(d) - \sum_{k=1}^{x+1} c_k(d)\mathbf{z}_k(d) \tag{6.14}$$

where $\sum_{k=1}^{x+1} c_k(d)\mathbf{z}_k(d)$ is the projection of $\mathbf{z}_{x+2}(d)$ on the subspace spanned by $\mathbf{z}_1(d)$, $\mathbf{z}_2(d)$, $\cdots$, $\mathbf{z}_{x+1}(d)$.

To find the constant $c_k(d)$ in (6.14), note that $\mathbf{h}_{x+1}(d)$ is orthogonal to $\mathbf{z}_1(d)$, $\mathbf{z}_2(d)$, $\cdots$, $\mathbf{z}_{x+1}(d)$, or

$$\frac{\left|\mathbf{h}_{x+1}^H(d)\mathbf{z}_k(d)\right|}{\left\|\mathbf{h}_{x+1}(d)\right\|\left\|\mathbf{z}_k(d)\right\|} = 0\,,\ k=1,\ 2,\ \cdots,\ x+1. \tag{6.15}$$

By substituting (6.14) into (6.15), $c_k(d)$ has to satisfy and can be found by using

$$\left[\mathbf{z}_{x+2}(d) - \sum_{k=1}^{x+1} c_k(d)\mathbf{z}_k(d)\right]^H \mathbf{z}_p(d) = 0\,,\ p=1,\ 2,\ \cdots,\ x+1. \tag{6.16}$$

In the same way as has been described earlier for the two jammers case, $\Gamma_{x+1}(d)$ can be easily calculated by (6.13) after using the set of linear equations in (6.16) to solve for $c_k(d)$. Then, eventually, the transmitted symbol can be

detected by using

$$\tilde{d}_0 = \arg\min_d \{\Gamma_{x+1}(d); d = 0,1,\cdots M-1\} \quad (6.17)$$

6.2 Performance of the Volumetric-based Algorithm

Numerical simulations were conducted to validate the performance of the proposed volumetric-based algorithm for slow FH systems with various MFSK modulations. In the simulation study, each hop has 8 MFSK symbols, the symbol rate is 200000 symbols per second, and the hop rate is 25000 hops per second. A total of 20 million symbols are used for each simulation run. In the simulation, the fading coefficients are modeled as i.i.d complex Gaussian random variables with zero-mean and a variance of 0.5 per dimension.

Figs. 6.1, 6.2 and 6.3 compare the BER performance of the proposed volumetric-based algorithm, the SMI algorithm, and the traditional ML algorithm for the case when there are 2 jammers and a 3-element array. The BER performance is plotted versus the signal to the first jamming ratio (SJR_1), with the signal to white noise ratio (SNR) fixed at 30dB, and the signal to the second jamming ratio (SJR_2) fixed at -30dB, 0dB and 30dB for Figs. 6.1, 6.2 and 6.3 respectively. The number of samples per symbol is given by $N = 4$. As can be seen, the proposed volumetric-based algorithm outperforms other

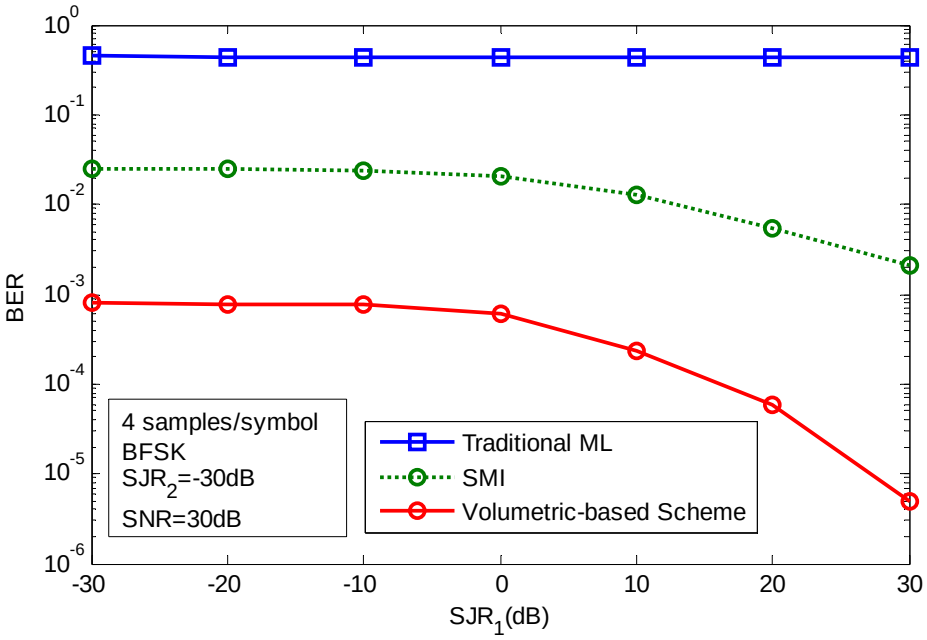

Fig. 6.1: Performance of various algorithms versus SJR_1 with 30dB SNR, -30dB SJR_2, BFSK and 4 samples per symbol

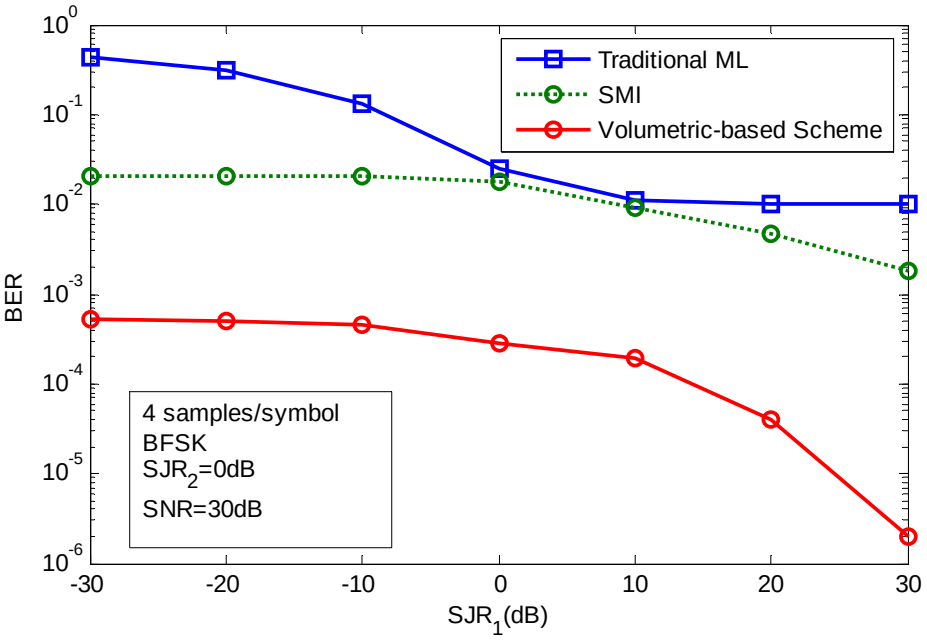

Fig. 6.2: Performance of various algorithms versus SJR_1 with 30dB SNR, 0dB SJR_2, BFSK and 4 samples per symbol

algorithms. As can be seen from Fig. 6.3, when the both power of jamming is small, using ML gives the best performance.

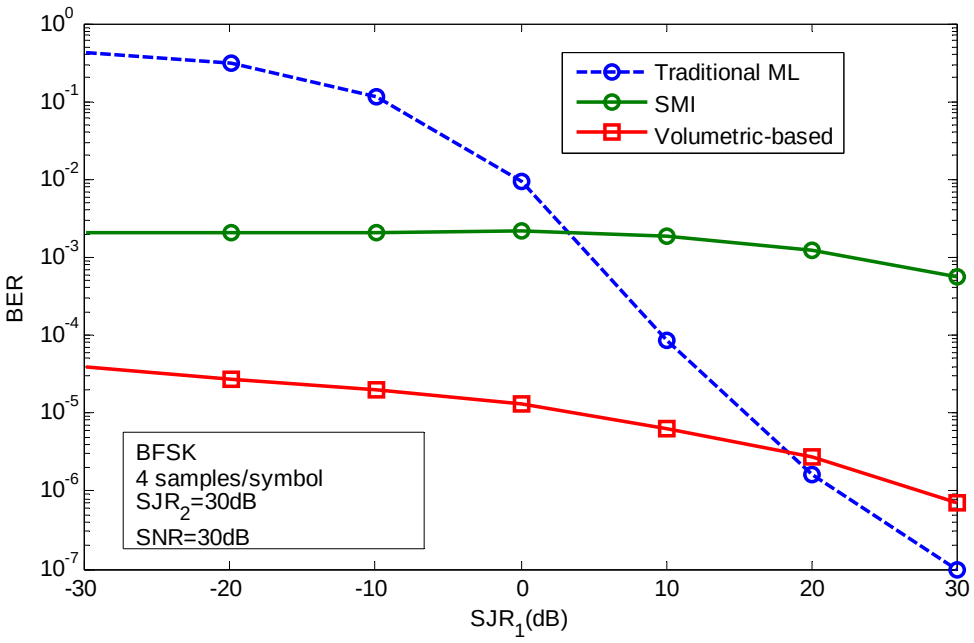

Fig. 6.3: Performance of various algorithms versus SJR_1 with 30dB SNR, 30dB SJR_2, BFSK and 4 samples per symbol

In the same format as Figs. 6.1, 6.2 and 6.3, Fig. 6.4 compares performance of the three algorithms when there are 3 jammers and 4 antennas. The signal to white noise ratio (SNR) is 30dB, the signal to the second jamming ratio (SJR_2) is -30dB, and the signal to the third jamming ratio (SJR_3) is also -30dB. Again, the proposed volumetric-based algorithm outperforms other algorithms.

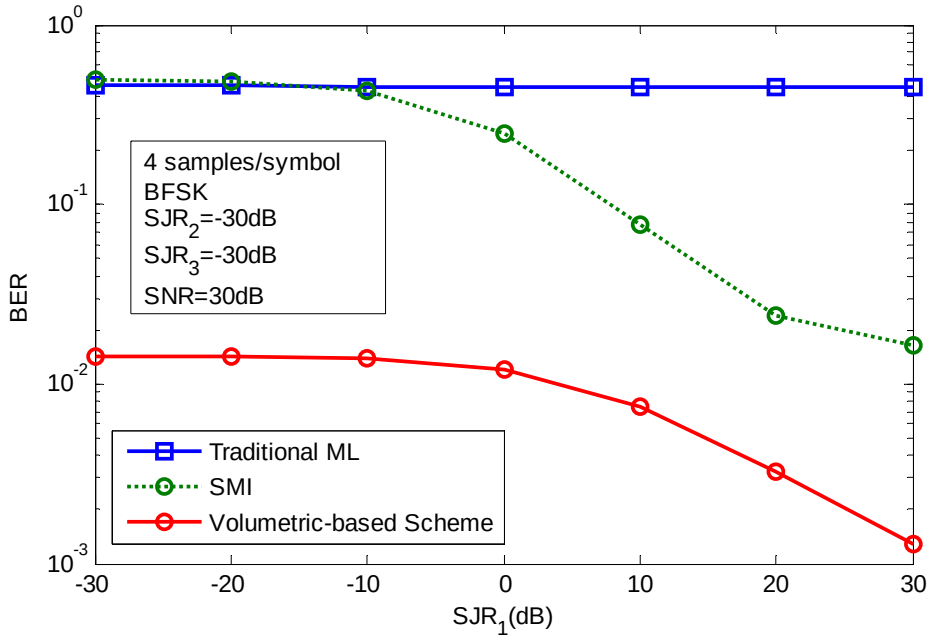

Fig. 6.4: Performance of various algorithms versus SJR_1 with 30dB SNR, -30dB SJR_2, -30dB SJR_3, BFSK and 4 samples per symbol

Figs. 6.5 and 6.6 show the BER performance of the three algorithms under 8-FSK (with 8 samples per symbol) modulation when there are 2 jammers and 3 antennas. The SNR is 30dB, and the SJR_2 is equal to -30dB and 0dB for Figs. 6.5 and 6.6, respectively. Once again, the volumetric-based algorithm has a better performance than other algorithms.

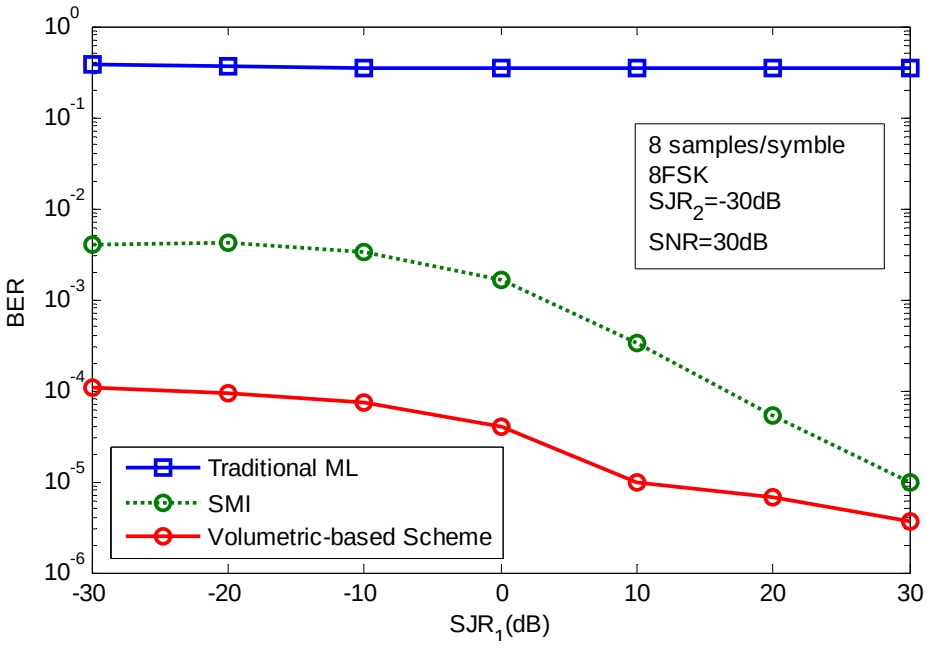

Fig. 6.5: Performance of various algorithms versus SJR_1 with 30dB SNR, -30dB SJR_2, 8-FSK and 8 samples per symbol

Fig. 6.7 shows the effect of changing the number of samples per symbol for the volumetric-based algorithm with SNR = 30dB, SJR_2=-30dB and BFSK modulations. Increasing the number of samples per symbol N leads to a better BER performance at the cost of higher complexity (as shown in Table 6.2).

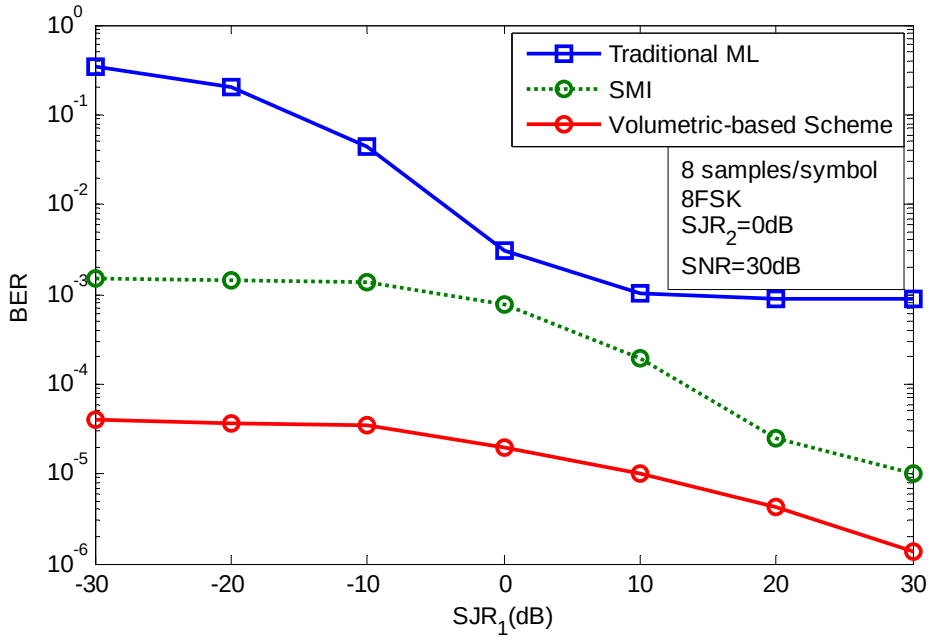

Fig. 6.6: Performance of various algorithms versus SJR_1 with 30dB SNR, 0dB SJR_2, 8-FSK and 8 samples per symbol

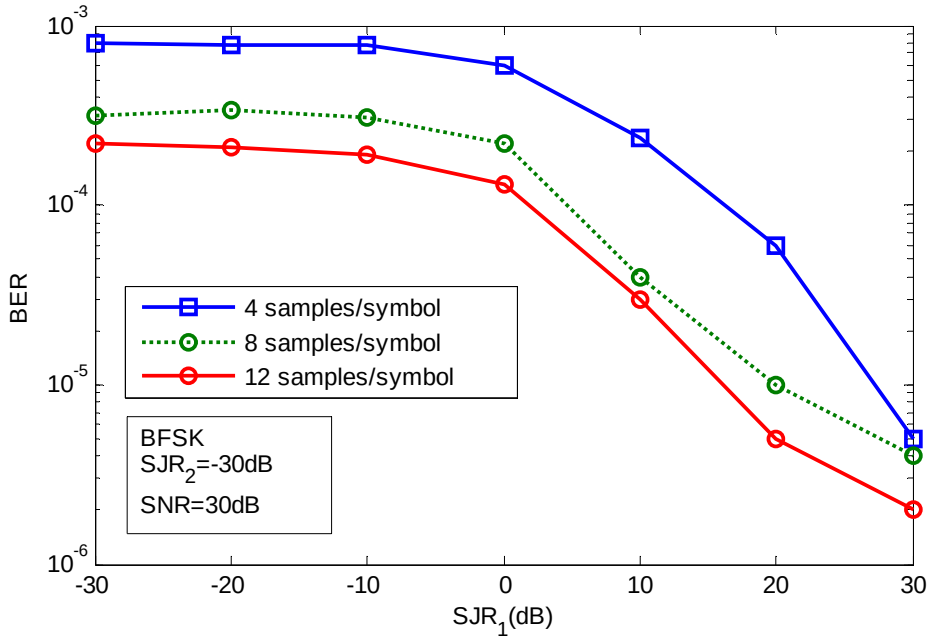

Fig. 6.7: Performance of the proposed volumetric-based algorithm for various numbers of samples per symbol with 30dB SNR, -30dB SJR_2 and BFSK

With SJR_1 and SJR_2 both fixed at -30dB, Fig. 6.8 compares the performance of the volumetric-based algorithm with the other algorithms under various SNR conditions. The number of samples per symbol is $N = 4$. Clearly, over a channel in a jamming dominant scenario, treating the jamming signal as receiver noise gives rise to an error floor in the BER performance when the traditional ML algorithm is used.

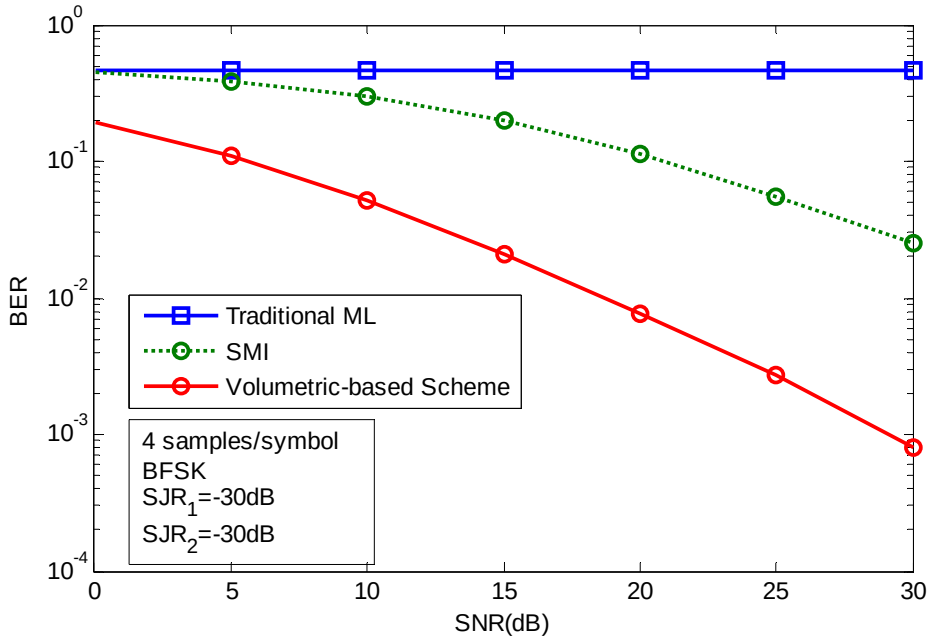

Fig. 6.8: Performance of various algorithms versus SNR with -30dB SJR_1, -30dB SJR_2, BFSK and 4 samples per symbol

To investigate the robustness of the volumetric-based algorithm against imperfect channel knowledge, Fig. 6.9 shows the BER performance of the volumetric-based algorithm with the channel gains of the desired signal

estimated blindly by using a standard ML procedure in the unjammed portion of each hop as described in CHAPTER 3. In the simulation, the ratio of unjammed interval to hop duration is set to be 0.25. With imperfect channel knowledge, the performance of the volumetric-based algorithm degrades slightly when compared with the case of having perfect channel knowledge.

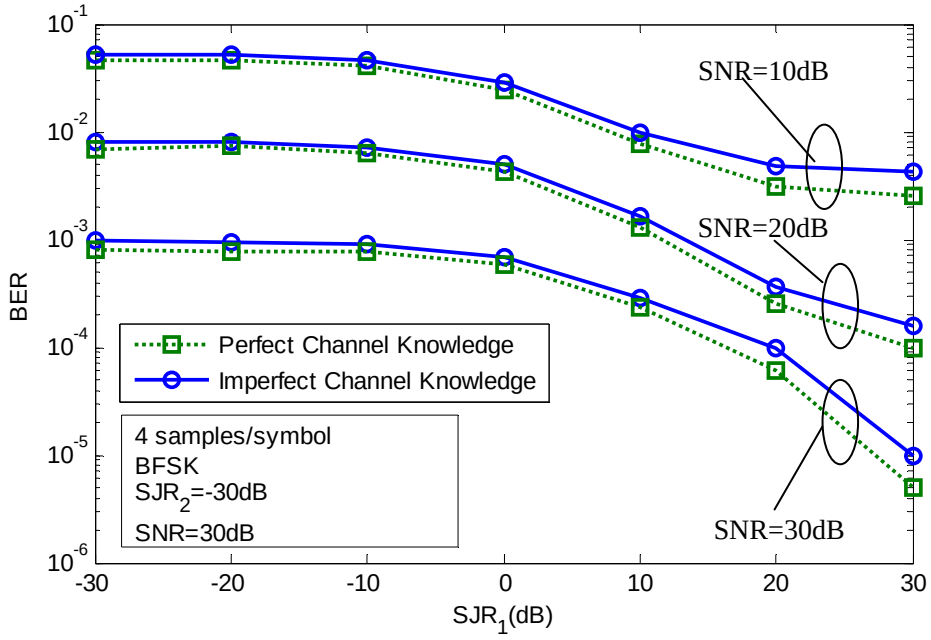

Fig. 6.9: Performance of hthe proposed algorithm with perfect and imperfect channel knowledge for various SJR_1 and SNR values with BFSK, -30dB SJR_2 and 4 samples per symbol

Fig. 6.10 compares the BER performance of the proposed volumetric-based algorithm, the SMI algorithm, the traditional ML algorithm and the VSM algorithm for the case when there is only one jammer and a

3-element array. For the area-based VSM algorithm, only two antennas are employed. The BER performance is plotted versus SJR, with SNR fixed at 30dB. The number of samples per symbol is given by $N = 4$. The proposed volumetric-based algorithm outperforms the other algorithms.

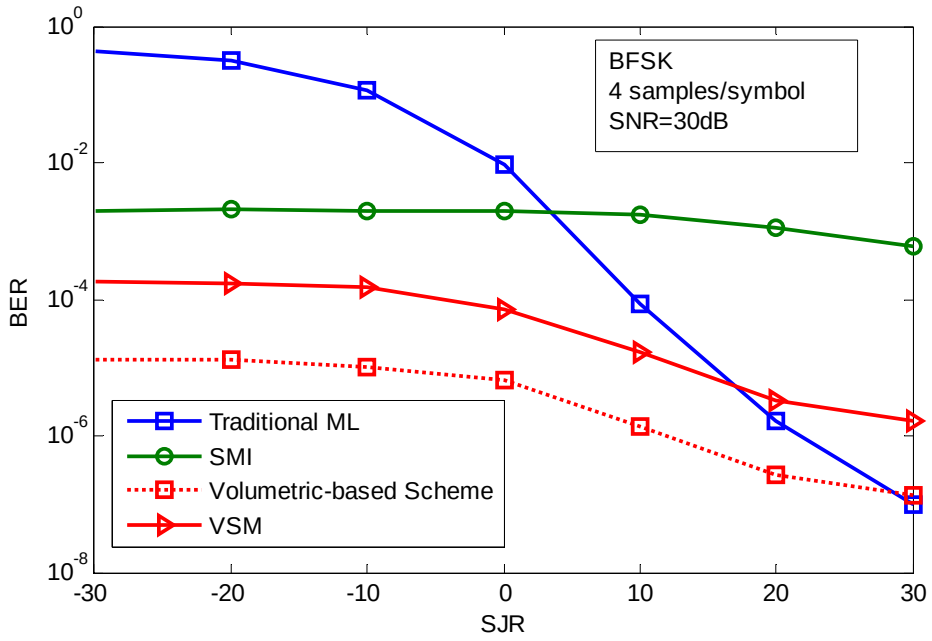

Fig. 6.10: Performance of various algorithms versus SJR with 30dB SNR, BFSK and 4 samples per symbol

6.3 Theoretical Analysis of the Volumetric-based Algorithm

6.3.1 General BER Expression of the Volumetric-based Algorithm

In this section, we will derive a theoretical BER expression for the proposed volumetric-based jamming rejection and symbol detection algorithm with two jammers and three antennas. We take the *M* possible MFSK symbols to be equally probable and assume, without loss of generality, that the transmitted symbol value is $d_0 = 0$. Using (3.5), the vectors of the received samples from the receive antennas are

$$\mathbf{r}_1 = \alpha_1 \mathbf{s}(0) + \mathbf{v}_1 + \mathbf{w}_1, \tag{6.18}$$

$$\mathbf{r}_2 = \alpha_2 \mathbf{s}(0) + \mathbf{v}_2 + \mathbf{w}_2, \tag{6.19}$$

and

$$\mathbf{r}_3 = \alpha_3 \mathbf{s}(0) + \mathbf{v}_3 + \mathbf{w}_3. \tag{6.20}$$

Using (6.18), (6.19), (6.20) and (6.11) for the objective function (6.12), the BER of the proposed volumetric-based algorithm can readily be shown to be

$$P_e = 1 - \prod_{d=1}^{M-1} \Pr\{\Gamma(0) < \Gamma(d) \mid d_0 = 0\} \tag{6.21}$$

where $\Gamma(0)$ and $\Gamma(d)$, as given below, are the objective functions for a correct and an incorrect decision, respectively:

$$\Gamma(0)=\frac{1}{3}\left\|(\mathbf{v}_3+\mathbf{w}_3)-a(0)(\mathbf{v}_1+\mathbf{w}_1)-b(0)(\mathbf{v}_2+\mathbf{w}_2)\right\|\left\|\mathbf{v}_1+\mathbf{w}_1\right\|\left\|\mathbf{v}_2+\mathbf{w}_2\right\|\sin\theta(0),$$

(6.22)

$$\Gamma(d)=\frac{1}{3}\left\|(\mathbf{k}_3(d)+\mathbf{w}_3)-a(d)(\mathbf{k}_1(d)+\mathbf{w}_1)-b(d)(\mathbf{k}_2(d)+\mathbf{w}_2)\right\| \left\|\mathbf{k}_1(d)+\mathbf{w}_1\right\|\left\|\mathbf{k}_2(d)+\mathbf{w}_2\right\|\sin\theta(d), \quad (6.23)$$

$$\sin\theta(0)=\cos^{-1}\left[\frac{\left|(\mathbf{v}_1+\mathbf{w}_1)^H(\mathbf{v}_2+\mathbf{w}_2)\right|}{\left\|\mathbf{v}_1+\mathbf{w}_1\right\|\left\|\mathbf{v}_2+\mathbf{w}_2\right\|}\right], \quad (6.24)$$

$$\sin\theta(d)=\cos^{-1}\left[\frac{\left|(\mathbf{k}_1(d)+\mathbf{w}_1)^H(\mathbf{k}_2(d)+\mathbf{w}_2)\right|}{\left\|\mathbf{k}_1(d)+\mathbf{w}_1\right\|\left\|\mathbf{k}_2(d)+\mathbf{w}_2\right\|}\right], \quad (6.25)$$

$$a(0)=\frac{\left\|\mathbf{v}_2+\mathbf{w}_2\right\|^2(\mathbf{v}_1+\mathbf{w}_1)^H(\mathbf{v}_3+\mathbf{w}_3)-(\mathbf{v}_1+\mathbf{w}_1)^H(\mathbf{v}_2+\mathbf{w}_2)(\mathbf{v}_2+\mathbf{w}_2)^H(\mathbf{v}_3+\mathbf{w}_3)}{\left\|\mathbf{v}_1+\mathbf{w}_1\right\|^2\left\|\mathbf{v}_2+\mathbf{w}_2\right\|^2-\left|(\mathbf{v}_1+\mathbf{w}_1)^H(\mathbf{v}_2+\mathbf{w}_2)\right|^2},$$

(6.26)

$$b(0)=\frac{\left\|\mathbf{v}_1+\mathbf{w}_1\right\|^2(\mathbf{v}_2+\mathbf{w}_2)^H(\mathbf{v}_3+\mathbf{w}_3)-(\mathbf{v}_2+\mathbf{w}_2)^H(\mathbf{v}_1+\mathbf{w}_1)(\mathbf{v}_1+\mathbf{w}_1)^H(\mathbf{v}_3+\mathbf{w}_3)}{\left\|\mathbf{v}_1+\mathbf{w}_1\right\|^2\left\|\mathbf{v}_2+\mathbf{w}_2\right\|^2-\left|(\mathbf{v}_1+\mathbf{w}_1)^H(\mathbf{v}_2+\mathbf{w}_2)\right|^2},$$

(6.27)

$$a(d)=\frac{\left\|\mathbf{k}_2(d)+\mathbf{w}_2\right\|^2(\mathbf{k}_1(d)+\mathbf{w}_1)^H(\mathbf{k}_3(d)+\mathbf{w}_3)- (\mathbf{k}_1(d)+\mathbf{w}_1)^H(\mathbf{k}_2(d)+\mathbf{w}_2)(\mathbf{k}_2(d)+\mathbf{w}_2)^H(\mathbf{k}_3(d)+\mathbf{w}_3)}{\left\|\mathbf{k}_1(d)+\mathbf{w}_1\right\|^2\left\|\mathbf{k}_2(d)+\mathbf{w}_2\right\|^2-\left|(\mathbf{k}_1(d)+\mathbf{w}_1)^H(\mathbf{k}_2(d)+\mathbf{w}_2)\right|^2},$$

(6.28)

$$b(d)=\frac{\left\|\mathbf{k}_1(d)+\mathbf{w}_1\right\|^2(\mathbf{k}_2(d)+\mathbf{w}_2)^H(\mathbf{k}_3(d)+\mathbf{w}_3)- (\mathbf{k}_2(d)+\mathbf{w}_2)^H(\mathbf{k}_1(d)+\mathbf{w}_1)(\mathbf{k}_1(d)+\mathbf{w}_1)^H(\mathbf{k}_3(d)+\mathbf{w}_3)}{\left\|\mathbf{k}_1(d)+\mathbf{w}_1\right\|^2\left\|\mathbf{k}_2(d)+\mathbf{w}_2\right\|^2-\left|(\mathbf{k}_1(d)+\mathbf{w}_1)^H(\mathbf{k}_2(d)+\mathbf{w}_2)\right|^2},$$

(6.29)

$$\mathbf{k}_1(d) = \alpha_1(\mathbf{s}(0) - \mathbf{s}(d)) + \mathbf{v}_1, \tag{6.30}$$

$$\mathbf{k}_2(d) = \alpha_2(\mathbf{s}(0) - \mathbf{s}(d)) + \mathbf{v}_2, \tag{6.31}$$

and

$$\mathbf{k}_3(d) = \alpha_3(\mathbf{s}(0) - \mathbf{s}(d)) + \mathbf{v}_3. \tag{6.32}$$

By substituting (6.22) and (6.23) into (6.21), squaring and expanding the resulting expressions, (6.21) can be expressed in terms of the noise $\mathbf{w}_p$ (p=1, 2, 3) and the jamming components $\mathbf{v}_p$ (p=1, 2, 3) as follows:

$$P_e = 1 - \prod_{d=1}^{M-1} \Pr\{g(0) < g(d) \mid d_0 = 0\} \tag{6.33}$$

where

$$\begin{aligned} g(0) = & \left\| (\mathbf{v}_3 + \mathbf{w}_3) - a(0)(\mathbf{v}_1 + \mathbf{w}_1) - b(0)(\mathbf{v}_2 + \mathbf{w}_2) \right\|^2 \\ & \left[\left\| \mathbf{v}_1 + \mathbf{w}_1 \right\|^2 \left\| \mathbf{v}_2 + \mathbf{w}_2 \right\|^2 - \left| (\mathbf{v}_1 + \mathbf{w}_1)^H (\mathbf{v}_2 + \mathbf{w}_2) \right|^2 \right] \end{aligned} \tag{6.34}$$

and

$$\begin{aligned} g(d) = & \left\| (\mathbf{k}_3(d) + \mathbf{w}_3) - a(d)(\mathbf{k}_1(d) + \mathbf{w}_1) - b(d)(\mathbf{k}_2(d) + \mathbf{w}_2) \right\|^2 \\ & \left[\left\| \mathbf{k}_1(d) + \mathbf{w}_1 \right\|^2 \left\| \mathbf{k}_2(d) + \mathbf{w}_2 \right\|^2 - \left| (\mathbf{k}_1(d) + \mathbf{w}_1)^H (\mathbf{k}_2(d) + \mathbf{w}_2) \right|^2 \right]. \end{aligned} \tag{6.35}$$

6.3.2 Approximate BER Expression in the Jamming Dominant Scenario

Because it is mathematically intractable to obtain an explicit expression

for the BER from (6.33) in general, we will now attempt to derive an approximate BER expression under the scenario where the power of jamming signal is higher than that of the desired signal and noise (a jamming dominant scenario) or when $p_w << p_{J_1}, p_{J_2}$ and $p_s << p_{J_1}, p_{J_2}$.

After expanding the various squares and modulus square terms in (6.33) and omitting the higher order terms involving $\mathbf{w}_p$ (p=1, 2, 3), $g(0)-g(d)$ becomes

$$g(0)-g(d)=h_0(d)+2\,\mathrm{Re}\left\{\mathbf{h}_1^H(d)\mathbf{w}_1\right\}+2\,\mathrm{Re}\left\{\mathbf{h}_2^H(d)\mathbf{w}_2\right\}+2\,\mathrm{Re}\left\{\mathbf{h}_3^H(d)\mathbf{w}_3\right\}, \tag{6.36}$$

where

$$h_0(d)=\|\mathbf{q}\|^2\left[\|\mathbf{v}_1\|^2\|\mathbf{v}_2\|^2-\left|(\mathbf{v}_1)^H(\mathbf{v}_2)\right|^2\right], \tag{6.37}$$

$$\mathbf{h}_1(d)=\mathbf{q}^H\left[\|\mathbf{k}_2(d)\|^2\mathbf{k}_1^H(d)\mathbf{k}_3(d)-\mathbf{k}_2^H(d)\mathbf{k}_1(d)\mathbf{k}_1^H(d)\mathbf{k}_3(d)\right], \tag{6.38}$$

$$\mathbf{h}_2(d)=\mathbf{q}^H\left[\|\mathbf{k}_1(d)\|^2\mathbf{k}_2^H(d)\mathbf{k}_3(d)-\mathbf{k}_1^H(d)\mathbf{k}_2(d)\mathbf{k}_2^H(d)\mathbf{k}_3(d)\right], \tag{6.39}$$

$$\mathbf{h}_3(d)=\mathbf{q}^H\left[\|\mathbf{v}_1\|^2\|\mathbf{v}_2\|^2-\left|\mathbf{v}_1^H\mathbf{v}_2\right|^2\right] \tag{6.40}$$

and

$$\mathbf{q}=\begin{bmatrix}\left(\|\mathbf{k}_1(d)\|^2\|\mathbf{k}_2(d)\|^2-\left|\mathbf{k}_1^H(d)\mathbf{k}_2(d)\right|^2\right)\mathbf{k}_3(d)\\ -\left(\|\mathbf{k}_2(d)\|^2\mathbf{k}_1^H(d)\mathbf{k}_3(d)-\mathbf{k}_1^H(d)\mathbf{k}_2(d)\mathbf{k}_2^H(d)\mathbf{k}_3(d)\right)\mathbf{k}_1(d)\\ -\left(\|\mathbf{k}_1(d)\|^2\mathbf{k}_2^H(d)\mathbf{k}_3(d)-\mathbf{k}_2^H(d)\mathbf{k}_1(d)\mathbf{k}_1^H(d)\mathbf{k}_3(d)\right)\mathbf{k}_2(d)\end{bmatrix}. \tag{6.41}$$

Using (6.36), the condition given by $\Pr\{g(0)<g(d)\,|\,d_0=0\}$ is

equivalent to

$$h_0(d) + 2\,\mathrm{Re}\left\{\mathbf{h}_1^H(d)\mathbf{w}_1\right\} + 2\,\mathrm{Re}\left\{\mathbf{h}_2^H(d)\mathbf{w}_2\right\} + 2\,\mathrm{Re}\left\{\mathbf{h}_3^H(d)\mathbf{w}_3\right\} < 0 \quad (6.42)$$

It is noted that $h_0(d)$, $\mathbf{h}_1(d)$, $\mathbf{h}_2(d)$ and $\mathbf{h}_3(d)$ are constants and independent of noise. Specifically, the left hand side of (6.42) consists of a constant and a linear combination of Gaussian-distributed receiver noise components. Hence, it is also Gaussian with a mean of $h_0(d)$ and a variance of

$$\sigma_J^2(d) = 4\sigma^2\left(\left\|\mathbf{h}_1(d)\right\|^2 + \left\|\mathbf{h}_2(d)\right\|^2 + \left\|\mathbf{h}_3(d)\right\|^2\right) \quad (6.43)$$

where σ^2 is the variance of the real and imaginary parts of the zero-mean Gaussian receiver noise samples $w_{p,n}$.

Based on (6.21), (6.33)and (6.43), an approximation to $\Pr\left\{g(0) < g(d) \mid d_0 = 0\right\}$ is

$$P_J(d) = Q\left(h_0(d)/\sqrt{\sigma_J^2(d)}\right). \quad (6.44)$$

Then, by substituting (6.44) into (6.33), the approximate BER expression for the jamming dominant scenario is

$$P_{eJ} = 1 - \prod_{d=1}^{M-1} P_J(d). \quad (6.45)$$

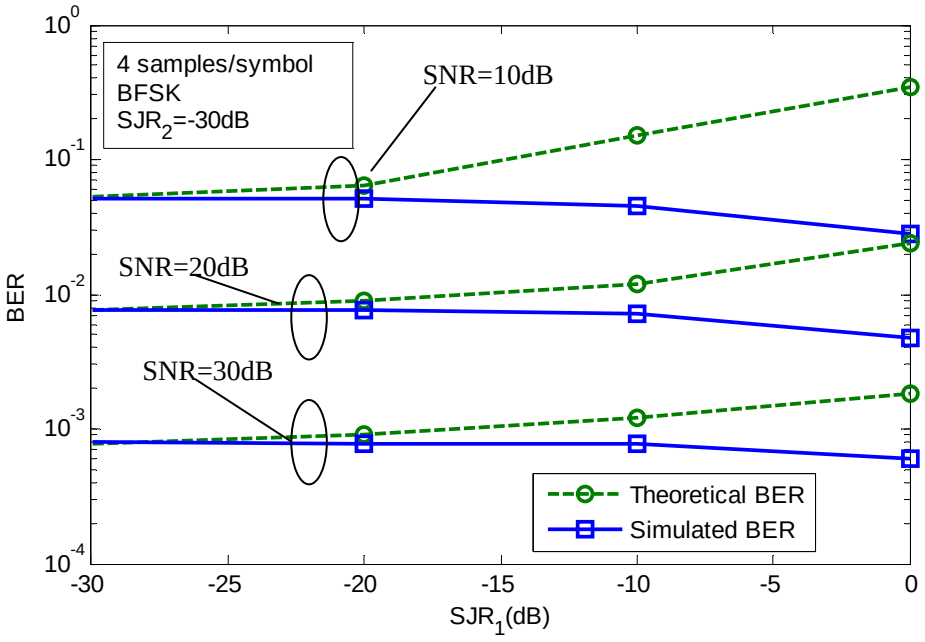

Fig. 6.11: Theoretical (6.45) and simulated BER of the proposed volumetric-based algorithm in jamming dominant channels with BFSK, -30dB SJR_2 and 4 samples per symbol

The validity of the performance analysis and the tightness of the analytical BER values derived for MFSK signaling are demonstrated in Fig. 6.11. As mentioned before, the BER expressions are derived under a jamming dominant channel. As a result, the theoretical BER curves match the simulated ones well in the very low SJR regime (high jamming power) and the very high SJR regime (high signal power).

6.4 Summary

In this chapter, a volumetric-based algorithm is proposed for symbol detection in slow FH/MFSK systems in the presence of multiple independent follower partial-band jammers over quasi-static flat fading channels. By exploiting the unknown spatial correlation of the received jamming components, the proposed algorithm is able to reject jamming and overcome the performance degradation of the SMI or the traditional ML algorithms. Analytical BER expression for the volumetric-based algorithm has also been derived in a jamming dominant channel. The theoretical BER results have been shown to agree well with simulation results.

CHAPTER 7

CONCLUSIONS AND PROPOSALS FOR FUTURE RESEARCH

7.1 Conclusions

In this dissertation, three anti-jamming algorithms (MLBB, VSM, and volumetric-based) are proposed and theoretically analyzed.

With the presence of a single jammer, the MLBB and VSM algorithms both have very good performance compared with ML, SMI and the scheme proposed in [58]. The computational complexity of these algorithms is given in Table 7.1.

The MLBB algorithm first uses the ML technique to estimate the ratio of jamming fading gains, and then places a null toward the follower jamming source. By regarding the received jamming components as deterministic quantities to be estimated instead of receiver noise, the MLBB algorithm avoids the degradation of both the SMI algorithm and the traditional ML technique in

Table 7.1: Computational complexity of various algorithms

Traditional ML	$2NM$
SMI	$4NM + M$
Algorithm in [58]	$6NM + 8M$
MLBB	$8NM$
VSM	$5NM + 4M$

jamming dominant channels. As a result, the performance of the MLBB algorithm outperforms these two existing algorithms when SJR<15dB. When SJR>15dB, ML and SMI give a better performance since the estimation of the ratio of jamming fading gains become less accurate than under low SJR regime. In addition, an analytical BER expression for the proposed MLBB algorithm has been derived in the jamming dominant scenarios. From table 7.1, we can see that MLBB has the highest computational complexity.

The second anti-jamming algorithm is the area-based VSM algorithm. By exploiting the unknown spatial correlation of the received jamming components, the VSM algorithm is able to reject jamming and overcome the performance of MLBB and thus is better than traditional ML and SMI in most scenarios. However, when SJR is too high (>25dB), ML becomes the best choice with the best performance and lowest computation complexity.

Analytical BER expression for the proposed area-based VSM algorithm has also been derived in a low receiver noise scenario and shown to agree well with simulation results. The computational complexity of VSM stands in the middle among these algorithms.

As the number of jammer increases, a volumetric-based algorithm, which has higher computational complexity, can be applied. This can be seen from Table 7.2. Note that, to eliminate the effects of X jammers, at least X+1 antenna is needed. However, with a fixed number of jammers, if more antennas are employed using the corresponding cost function, a better performance can be achieved, and this is shown in Fig. 6.9. When the power of all the jammers are at a very low level (SJR>25dB), ML becomes the best choice.

Table 7.2: Computational complexity of Volumetric-based algorithm

2 jammers/3 antenna	$19NM + 12M$
3 jammers/4 antenna	$106NM + 81M$

[58] estimates the jamming signals and the jamming fading gains. As the number of jamming increases, more parameters need to be estimated which in turn leads to less accurate results and a much more complicated implementation. VSM and volumetric-based algorithm utilize the spatial correlation of the jamming components as the cost function. Both the analytical complexity and computational complexity are reduced. ML and SMI have relatively low computational complexity, but the performance is not good when the power of jamming is large.

7.2 Future Works

The three proposed anti-jamming algorithms, the MLBB, VSM, and volumetric-based algorithms, assume that the perfect channel information is known to the receiver. However, if the jamming signal is too fast for the receiver to obtain or estimate the channel parameters, these algorithms may fail to work.

Pilot symbol-assisted algorithms can be used to estimate the channel for various transmission systems. However, in the presence of a jamming signal, those algorithms will not work. Research work can be extended to estimate the channel information based on pilot symbol in the presence of a jamming signal.

As an example, Fig. 7.1 assumes that there are eight symbols in one hop.

The first symbol is a pilot symbol and the rest are data symbol. In addition, assume that the channel parameters are constant in one hop duration time.

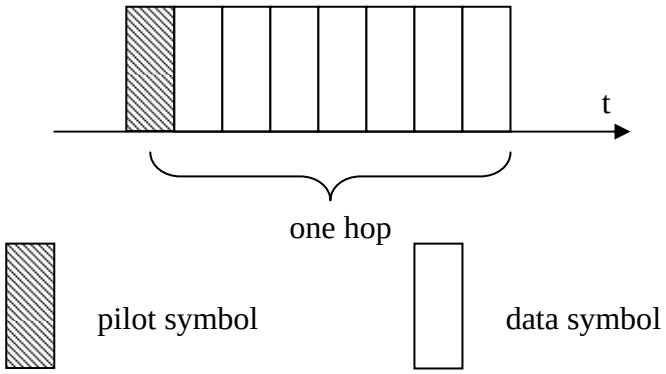

Fig. 7.1: Pilot-aided symbol in one hop

From (3.5), the receiver data for the pilot symbol part can be wirtten as

$$\mathbf{r}_p^{'} = \alpha_p \mathbf{s}\left(d_p\right) + \sum_{k=1}^{X} \beta_{kp} \mathbf{J}_k^T + \mathbf{w}_p, \tag{6.46}$$

where d_p is the pilot symbol and is known to the receiver. The estimation of the channel parameters, α_p, in the presence of jamming and white noise is an interesting research topic.

Because the principle of vector similarity can be applied to other applications such as searching, face authentication and fuzzy set systems, the proposed VSM and volumetric-based algorithms can also be used in those systems and a better performance may be obtained.

Modern communication systems need to consider multiuser transmission

(multi-access) or multiuser reception (broadcast) in their designs [71]. Significant effort has been spent to find the capacity of such channels for AWGN and Rayleigh fading scenarios [72-75]. Eliminating MAI in OFDM systems is still an interesting research topic now. For future work, implement VSM or volumetric-based algorithms in orthogonal frequency-division multiplexing (OFDM) system to mitigate MAI and combat multiple intentional jamming signals can be considered.

BIBLIOGRAPHY

[1] E. Z. Rodger and L. P. Roger, Introduction to Digital Communications, 2nd ed. New Jersey: Prentice Hall, 2000.

[2] J. Proakis, Digital Communications, 4th ed. New York: McGraw-Hill, 2001.

[3] T. Salonidis, P. Bhagwat, L. Tassiulas, and R. LaMaire, "Distributed topology construction of Bluetooth wireless personal area networks", IEEE Journal on Selected Areas in Communications, Vol. 23, Issue 3, pp. 633-643, Mar. 2005.

[4] L. Simone, N. Salerno, and M. Maffei, "Frequency-hopping techniques for secure satellite TT&C: system analysis & trade-offs", IEEE International Workshop on Satellite and Space Communications, pp. 13-17, Sept. 2006.

[5] D. L. Herrick, P. K. Lee, and L. L. Ledlow, Jr., "Correlated frequency hopping-an improved approach to HF spread spectrum communications", Proceeding of the Tactical Communications Conference, pp. 319-324, Apr. 1996.

[6] M. Pursley, "Frequency-hop transmission for satellite packet switching and terrestrial packet radio networks", IEEE Transactions on

Information Theory, Vol. 32, Issue 5, pp. 652-667, Sept. 1986.

[7] S. Barbarossa and A. Scaglione, "Parameter estimation of spread spectrum frequency-hopping signals using time-frequency distributions", IEEE Signal Processing Workshop on Signal Processing Advances in Wireless Communications, pp. 213-216, Apr. 1997.

[8] N. Khalil and R. Hippenstiel, "Wavelet transforms of correlation functions of frequency hopped signals", Conference Record of the Thirtieth Asilomar Conference on Signals, Systems and Computers, pp. 964-967, Nov. 1996.

[9] J. E. Kleider, G. Maalouli, S. Gifford, and S. Chuprun, "Preamble and embedded synchronization for RF carrier frequency-hopped OFDM", IEEE Journal on Selected Areas in Communications, Vol. 23, Issue 5, pp. 920-931, May 2005.

[10] C. C. Ko, Wanjun Zhi, and F. Chin, "ML-based frequency estimation and synchronization of frequency hopping signals", IEEE Transactions on Signal Processing, Vol. 53, Issue 2, pp. 403-410, Feb. 2005.

[11] J. S. Min and H. Samueli, "Analysis and design of a frequency-hopped spread-spectrum transceiver for wireless personal communications", IEEE Transactions on Vehicular Technology, Vol. 49, Issue 5, pp. 1719-1731, Sept. 2000.

[12] J. S. Min and H. Samueli, "Synchronization techniques for a frequency hopped wireless transceiver", IEEE Vehicular Technology Conference, Vol. 1, pp. 183-187, Apr. 1996.

[13] S. Glisic, Z. Nikolic, N. Milosevic, and A. Pouttu, "Advanced frequency hopping modulation for spread spectrum WLAN", IEEE Journal on Selected Areas in Communications, Vol. 18, pp. 16-29, Jan. 2000.

[14] L. Xie, L. Gan, and J. Guo, "Design and implementation of a novel bit synchronization method in short-wave frequency hopping communication networks", International Conference on Wireless Communications, Networking and Mobile Computing, pp. 504-507, Sept. 2005.

[15] Q. Ling and T. Li, "A spectrally efficient frequency hopping scheme", 41st Annual Conference on Information Sciences and Systems, pp. 190-195, Mar. 2007.

[16] J. Liang, L. Gao, and S. Yang, "Frequency estimation and synchronization of frequency hopping signals based on reversible jump MCMC", Proceedings of 2005 International Symposium on Intelligent Signal Processing and Communication Systems, pp. 589-592, Dec. 2005.

[17] J. E. Kleider, G. Maalouli, S. Gifford, and S. Chuprun, "Channel

estimation performance for frequency hopped OFDM using embedded synchronization", IEEE Military Communications Conference, pp. 1611-1617, Nov. 2004.

[18] F. Dominique and J. H. Reed, "Robust frequency hop synchronisation algorithm", Electronics Letters, Vol. 32, pp. 1450-1451, Aug. 1996.

[19] F. Tong, J. Lu, H. Zhang, and X. Xu, "Frequency hopping underwater data communication system's synchronization processing", Proceedings of the 2003 International Conference on Neural Networks and Signal Processing, Vol. 2, pp. 960-964, Dec. 2003.

[20] K. Defly, X. Wang, G. Wu, and M. Lecours, "Synchronization in FH-MFSK spread spectrum systems", IEEE 38th Vehicular Technology Conference, pp. 385-389, June 1988.

[21] W. Li, J. Wang, and Y. Yao, "Synchronization design of frequency-hopping communication system", International Conference on Communication Technology Proceedings, Vol. 1, pp. 115-119, Oct. 1998.

[22] O. Mi-Kyung, J. Byunghoo, and P. Dong-Jo, "Low-complexity hop timing synchronization in frequency hopping systems", IEEE International Symposium on Circuits and Systems, pp. 2045-2048, May 2006.

[23] A. Pouttu, M. Raustia, and H. Saarnisaari, "Synchronization of FH/DS signal with interference suppression diversity", IEEE Ninth International Symposium on Spread Spectrum Techniques and Applications, pp. 69-73, Aug. 2006.

[24] H. M. Kwon, L. E. Miller, and J. S. Lee, "Evaluation of a partial-band jammer with gaussian-shaped spectrum against FH/MFSK", IEEE Transactions on Communications, Vol. 38, pp. 1045-1049, July 1990.

[25] K. C. Teh, A. C. Kot, and K. H. Li, "Performance study of a maximum-likelihood receiver for FFH/BFSK systems with multitone jamming", IEEE Transactions on Communications, Vol. 47, Issue 5, pp. 766-772, May 1999.

[26] J. Wang and C. Jiang, "Analytical study of FFH systems with square-law diversity combining in the presence of multitone interference", IEEE Transactions on Communications, Vol. 48, Issue 7, pp. 1188-1196, July 2000.

[27] C. Jiang and J. Wang, "Performance analysis of FFH/MFSK receivers with self-normalization combining in the presence of multitone jamming", IEEE Transactions on Communications, Vol. 51, Issue 5, pp. 1120-1127, Sept. 2002.

[28] Y. Han and K. C. Teh, "Error probabilities and performance

comparisons of various FFH/MFSK receivers with multitone jamming", IEEE Transactions on Communications, Vol. 53, Issue 5, pp. 769-772, May 2005.

[29] B. K. Levitt, "FH/MFSK performance in multitone jamming", IEEE Journal on Selected Areas in Communications, Vol. 5, Issue 3, pp. 627-643, Sept. 1985.

[30] X. Wu, C. Zhao, X. You, and S. Li, "Robust diversity-combining receivers for LDPC coded FFH-SS with partial-band interference", IEEE Communications Letters, Vol. 11, Issue 7, pp. 613-615, July 2007.

[31] J. S. Bird and E. B. Felstead, "Anti-jam performance of fast frequency-hoped M-ary NCFSK-an overview", IEEE Journal on Selected Areas in Communications, Vol. 4, Issue 2, pp. 216-233, Mar. 1986.

[32] Y. Han and K. C. Teh, "Performance study of asynchronous FFH/MFSK communications using various diversity combining techniques with MAI modeled as alpha-stable process", IEEE Transactions on Wireless Communications, Vol. 6, Issue 5, pp. 1615-1618, May 2007.

[33] Y. C. Chen, "Optimum and joint-suboptimum maximum-likelihood detection for FH/BFSK in multitone jamming", IEEE Consumer Communications and Networking Conference, Vol. 2, Issue 8, pp.

849-853, Jan. 2006.

[34] Y. Han and K. C. Teh, "Maximum-likelihood receiver with side information for asynchronous FFH-MA/MFSK systems over Rayleigh fading channels", IEEE Communications Letters, Vol. 10, Issue 6, pp. 435-437, June 2006.

[35] Y. Han and K. C. Teh, "Performance study of suboptimum maximum-likelihood receivers for FFH/MFSK systems with multitone jamming over fading channels", IEEE Transactions on Vehicle Technology, Vol. 54, Issue 1, pp. 82-90, Jan. 2005.

[36] T.-M. Wu, "A sub-optimal maximum-likelihood receiver for FFH/BFSK systems with multitone jamming over frequency-selective Rayleigh fading channels", IEEE Transactions on Vehicle Technology, Vol. 57, Issue 2, pp. 1316-1322, Mar. 2008.

[37] Y. Chen, G. Li, S. Li, and Y. Cheng, "A new anti-jam receiver for MFSK/FFH system with multitone jamming", IEEE International Conference on Communication Systems, pp. 451-455, Nov. 2008.

[38] K. C. Teh, A. C. Kot, and K. H. Li, "Performance analysis of an FFH/BFSK product-combining receiver with multitone jamming over Rician-fading channels", IEEE Vehicle Technology Conference Proceedings, Vol. 2, pp. 1508-1512, May 2000.

[39] K. C. Teh, A. C. Kot, and K. H. Li, "Error probabilities of an FFH/BFSK self-normalizing receiver in a Rician fading channel with multitone jamming", IEEE Transactions on Communications, Vol. 48, Issue 2, pp. 308-315, Feb. 2000.

[40] Y. S. Shen and S. L. Su, "Performance analysis of an FFH/BFSK receiver with ratio-statistic combining in a fading channel with multitone interference", IEEE Transactions on Communications, Vol. 51, Issue 10, pp. 1643-1648, Oct. 2003.

[41] Z. Yu, T. T. Tjhung, and C. C. Chai, "Independent multitone jamming of FH/MFSK in Rician channels", IEEE Transactions on Communications, Vol. 49, Issue 11, pp. 2006-2015, Nov. 2001.

[42] R. C. Robertson and J. F. Sheltry, "Multiple tone interference of frequency-hopped noncoherent MFSK signals transimitted over Rician fading channels", IEEE Transactions on Communications, Vol. 44, Issue 7, pp. 867-875, July 1996.

[43] T. T. Tjhung and C. C. Chai, "Multitone jamming of FH/BFSK in Rician channels", IEEE Transactions on Communications, Vol. 47, Issue 7, pp. 974-978, July 1999.

[44] G. Katsoulis and R. C. Robertson, "Performance bounds for multiple tone interference of frequency-hopped noncoherent MFSK systems",

Proceedings of MILCOM 97, Vol. 1, pp. 307-312, Nov. 1997.

[45] K. C. Teh, K. H. Li, and A. C. Kot, "Performance analysis of an FFH/BFSK linear-combining receiver against multitone jamming", IEEE Communications Letters, Vol. 2, pp. 205-207, Aug. 1998.

[46] C. Jiang and J. Wang, "Multitone interference of fast FH/MFSK systems over Rician fading channels", IEEE International Conference on Communications, Vol. 1, pp. 309-313, 1999.

[47] J. J. Chang and L. S. Lee, "An exact performance analysis of the clipped diversity combining receiver for FH/MFSK systems against a band multitone jammer", IEEE Transactions on Communications, Vol. 42, pp. 700-710, Feb. 1994.

[48] G. Li, Q. Wang, V. K. Bhargava, and L. J. Mason, "Maximum-likelihood diversity combining in partial-band noise", IEEE Transactions on Communications, Vol. 46, Issue 12, pp. 1569-1574, Dec. 1998.

[49] J. S. Lee, R. H. French, and L. E. Miller, "Probability of error analyzes of a BFSK frequency-hopping system with diversity under parial-band jamming interference--Part I: Performance of square-law linear combining soft decision receiver", IEEE Transactions on Communications, Vol. 32, Issue 6, pp. 645-654, June 1984.

[50] J. S. Lee, L. E. Miller, and Y. K. Kim, "Probability of error analyzes of a

BFSK frequency-hopping system with diversity under parial-band jamming interference--Part II: Performance of square-law nonlinear combining soft decision receiver", IEEE Transactions on Communications, Vol. 32, Issue 12, pp. 1243-1250, Dec. 1984.

[51] L. E. Miller, J. S. Lee, and A. P. Kadrichu, "Probability of error analyzes of a BFSK frequency-hopping system with diversity under parial-band jamming interference--Part III: Performance of square-law self-normalizing soft decision receiver", IEEE Transactions on Communications, Vol. 34, Issue 7, pp. 669-675, July 1986.

[52] C. M. Keller and M. B. Pursley, "Clipped diversity combining for channels with partial-band interference--Part I: Clipper linear combining", IEEE Transactions on Communications, Vol. 35, Issue 12, pp. 1320-1328, Dec. 1987.

[53] C. M. Keller and M. B. Pursley, "Clipped diversity combining for channels with partial-band interference--Part II: Radio-statistic combining", IEEE Transactions on Communications, Vol. 37, Issue 2, pp. 145-151, Feb. 1989.

[54] K. C. Teh, A. C. Kot, and K. H. Li, "Partial-band jamming rejection of FFH/BFSK with product combining receiver over a Rayleigh fading channel", IEEE Communications Letters, Vol. 1, Issue 3, pp. 64-66,

May 1997.

[55] R. Viswanathan and K. Taghizadeh, "Diversity combining in FH/BFSK systems to combat partial band jamming", IEEE Transactions on Communications, Vol. 36, Issue 9, pp. 1062-1069, Sept. 1988.

[56] F. Eken, "Use of antenna nulling with frequency-hopping against the follower jammer", IEEE Transactions on Antennas Propagation, Vol. 39, Issue 9, pp. 1391-1397, Sept. 1991.

[57] C. C. Ko, H. Nguyen-Le, and L. Huang, "Joint Interference Suppression and Symbol Detection in Slow FH/MFSK Systems with an Antenna Array", IEEE Vehicular Technology Conference Proceedings, Vol. 6, pp. 2691-2695, May 2006.

[58] C. C. Ko, H. Nguyen-Le, and L. Huang, "ML-based follower jamming rejection in slow FH/MFSK systems with an antenna array", IEEE Transactions on Communications, Vol. 56, Issue 9, pp. 1536-1544, Sept. 2008.

[59] H. Kriegle, S. Brechelsen, P. roger, and M. feifle, "Using sets of feature vectors for similarity search on voxelized CAD objects", Proceedings of the ACM SIGMOD International Conference on Management of Data, pp. 587-598, June 2003.

[60] O. Ozturk and H. Ferhatosmanoglu, "Effective indexing and filtering for

similarity search in large biosequence databases", Third IEEE Symposium on Bioinformatics and Bioengineering, pp. 359-366, Mar. 2003.

[61] F. K. P. Chan, A. W. C. Fu, and C. Yu, "Haar wavelets for efficient similarity search of time-series: with and without time warping", IEEE Transactions on Knowledge and Data Engineering, Vol. 15, Issue 3, pp. 686-705, May 2003.

[62] A. Tefas, C. Kotropoulos, and I. Pitas, "Using support vector machines to enhance the performance of elastic graph matching for frontal face authentication", IEEE Transactions on Pattern Analysis and Machine Intelligence, Vol. 23, Issue 7, pp. 735-746, July 2001.

[63] D. Wu and M. Mendel, "A vector similarity measure for interval type-2 fuzzy sets", IEEE International on Fuzzy Systems Conference, pp. 1-6, July 2007.

[64] D. Wu and J. M. Mendel, "A vector similarity measure for linguistic approximation: Interval type-2 and type-1 fuzzy sets", Information Sciences, Vol. 178, Issue 2, pp. 381-402, Jan. 2008.

[65] Ivanovic V., Dakovic M., Djurovic I., and Stankovic L., "Instantaneous frequency estimation by using time-frequency distributions", Proc. IEEE ICASSP, Vol. 6, pp. 3521-3524, 2001.

[66] R. L. Peterson, R. E. Ziemer, and D. E. Borth, Introduction to Spread Spectrum Communications. New York: Prentice-Hall, 1995.

[67] S. Ahmed, L.-L. Yang, and L. Hanzo, "Erasure insertion in RS-coded SFH/MFSK subjected to tone jamming and Rayleigh fading", IEEE Transactions on Vehicle Technology, Vol. 56, Issue 6, pp. 3563-3571, Nov. 2007.

[68] M. Lei, A. Duel-Hallen, and H. Hallen, "Reliable adaptive modulation and interference mitigation for mobile radio slow frequency hopping channels", IEEE Transactions on Communications, Vol. 56, Issue 3, pp. 352-355, Mar. 2008.

[69] K. Scharnhorst, "Angles in complex vector spaces", Acta Applicandae Mathematicae, Vol. 69, pp. 95-103, Oct. 2001.

[70] F. Liu, H. Nguyen-Le, and C. C. Ko, "Vector Similarity-Based Detection Scheme for Multi-antenna FH/MFSK Systems in the Presence of Follower Jamming," IET on Signal Processing, Vol. 2, Issue 4, pp346-353, Dec. 2008.

[71] J. Kazemetabar and H. Jafarkhanmi, "Multiuser interference cancellation and detection for users with more than two transmit antennas", IEEE Transactions on Communications, Vol. 56, Issue 4, pp. 574-583, Apr. 2008.

[72] L. Li and A. Goldsmith, "Capacity and optimal resource allocation for fading broadcast channels-part I: ergodic capacity", IEEE Transactions on Information Theory, Vol. 47, Issue 3, pp. 1083-1102, Mar. 2001.

[73] L. Li and A. Goldsmith, "Capacity and optimal resource allocation for fading broadcast channels-part II: outrage capacity", IEEE Transactions on Information Theory, Vol. 47, Issue 3, pp. 1103-1127, Mar. 2001.

[74] D. Tse and S. V. Hanly, "Multiaccess fading channels part I: polymatroid structure, optimal resource allocation and throughput capacities", IEEE Transactions on Information Theory, Vol. 44, Issue 7, pp. 2796-2815, Nov. 1998.

[75] D. Tse and S. V. Hanly, "Multiaccess fading channels part II: delay-limited capacities", IEEE Transactions on Information Theory, Vol. 44, Issue 7, pp. 2816-2831, Nov. 1998.

[76] Simon Haykin, Adaptive Filter Theory, New Jersey: Prentice Hall, 2002.

[77] R. E. Ziemer, R. L. Peterson and D. E. Borth, Introduction to Spread Spectrum Communications, Englewood Cliffs, NJ: Prentice-Hall, 1995.

[78] O. Besson, P. Stoica and Y. Kamiya, "Direction finding in the presence of an intermittent interference", IEEE Transactions on Signal Processing, Vol. 50, pp. 1554–1564, July 2002.

[79] E. B. Felstead, "Follower jammer considerations for frequency hopped spread spectrum", IEEE Proceedings in MILCOM 98, Oct. 18-21, 1998, Vol. 2, pp. 474 –478.

[80] Y. Kamiya and O. Besson, "Interference rejection for frequency hopping communication systems using a constant power algorithm", IEEE Transaction on Communications, Vol. 51, pp. 627–633, Apr. 2003.

[81] B. Boashash, “Time-Frequency Concepts”, Chapter 1, pp. 3–28, in B. Boashash, ed,, Time-Frequency Signal Analysis & Processing: A Comprehensive Reference, Elsevier Science, Oxford, 2003

[82] B. Boashash, “Heuristic Formulation of Time-Frequency Distributions”, Chapter 2, pp. 29–58, in B. Boashash, editor, Time-Frequency Signal Analysis and Processing: A Comprehensive Reference, Elsevier Science, Oxford, 2003

[83] B. Boashash, "Note on the Use of the Wigner Distribution for Time Frequency Signal Analysis", IEEE Transactions on Acoustics, Speech, and Signal Processing, Vol. 36, No. 9, pp. 1518–1521, Sept. 1988

[84] B. Boashash, “Time-Frequency Signal Analysis & Processing: A Comprehensive Reference”, Elsevier, Oxford, 2003

[85] V. Katkovnik;L. Stankovic, “Instantaneous frequency estimation using the Wigner distribution with varying and data-driven window length”,

IEEE Transactions on Signal Processing, Volume: 46, Issue: 9, pp2315 - 2325

[86] L. Stankovic;V. Katkovnik, “The Wigner distribution of noisy signals with adaptive time-frequency varying window”, IEEE Transactions on Signal Processing, Volume: 47, Issue: 4 , pp1099 - 1108

[87] I. Djurovic;L. Stankovic, “Robust Wigner distribution with application to the instantaneous frequency estimation”, IEEE Transactions on Signal Processing, Volume: 49, Issue: 12 , pp2985 – 2993

[88] L. Stankovic and V. Katkovnik, "Algorithm for the Instantaneous Frequency Estimation Using Time-Frequency Distributions with Adaptive Window Width", IEEE Signal Processing Letters, Vol. 5, Issue. 9, 1998, pp 224 – 227

[89] K. M. Wong and Q. Jin, "Estimation of the time-varying frequency of a signal: the Cramer-Rao bound and the application of Wigner distribution", IEEE Transactions on Acoustics, Speech and Signal Processing, Vol. 38 , Issue. 3, Mar 1990, pp 519-436

[90] E. Sejdic, I. Djurovic and L. Stankovic, "Quantitative PerformanceAnalysis of Scalogram as Instantaneous Frequency Estimator", IEEETransactions on Signal Processing, Vol. 56 , Issue. 8, 2008, pp3837-3845

APPENDIX A: A BRIEF INTRODUCTION TO TFD

In the field of time-frequency analysis, the goal is to have signal formulations that are used for representing the signal in a joint time-frequency domain [81]. There are several methods and transfors under time-frequency distributions" (TFDs) [82]. The most useful and used methods form a class known as "quadratic" or bilinear time-frequency distributions. A core member of this class is the Wigner-Ville distribution (WVD) [83], as all other TFDs can be written as a smoothed version of the WVD. Another popular member of this class is the spectrogram which is the square of the magnitude of the short-time Fourier transform (STFT). The spectrogram has the advantage of being positive and is easy to interpret, but has disadvantages like being irreversible which means that once the spectrogram of a signal is computed, the original signal cannot be extracted from the spectrogram. The theory and methodology for defining a TFD that verifies certain desirable properties is given in the "Theory of Quadratic TFDs" [84].

Research on WVD can be found in [7; 65; 85-90]. In [85], The WVD with a data-driven and time-varying window length is developed as an adaptive estimator of the IF. The choice of the window length is based on the

intersection of the confidence intervals of the IF estimates with the increasing window lengths. The developed algorithm uses only the formula for the variance of the estimate obtained for the relatively high sampling rate and white noise. Simulations show that the adaptive algorithm has good accuracy. [87] introduces a robust WD for processing signals corrupted by additive impulse noise. It produces significantly better results than the standard WD in the impulse noise environment, whereas the results are slightly worse in a pure Gaussian environment. Two different forms of the robust WD are considered. The robust WD, based on a combination of the squared absolute error and the absolute error, improves iteration convergence with respect to the case when only the absolute error is used as a loss function. Both of these forms behave similarly, and both are better than the standard WD.

Error analysis can be found in [65; 88-90]. In [89], the authors reviewed the performance of the Wigner distribution in the estimation of the time-varying instantaneous frequency of a signal. Several examples of linear and quadratic FM signals in white Gaussian noise are used, and the Cramer-Rao lower bounds (CRLB) for these examples are also juxtaposed to facilitate comparison.

The estimation algorithm proposed by [7] can estimate hop timing, hop frequencies and time offset of FH signals embedded in AWGN. A fairly good

closeness is also observed between the CRLB and the estimated variances of the frequency estimation when SNR is greater than 0.

APPENDIX B: DERIVATION OF (4.8) AND (4.9)

Differentiating (4.7) with respect to η and $\mathbf{v}$, respectively, and then setting the result to zero, we get

$$\left(\mathbf{z}_2(d)-\eta\mathbf{v}\right)^H \mathbf{v}=0 \tag{B.1}$$

and

$$\left(\mathbf{z}_1(d)-\mathbf{v}\right)+\eta^*\left(\mathbf{z}_2(d)-\mathbf{v}\right)=0\,. \tag{B.2}$$

After solving (B.1) and (B.2), we get

$$\eta=\frac{\mathbf{v}^H\mathbf{z}_2(d)}{\left\|\mathbf{v}\right\|^2} \tag{B.3}$$

and

$$\mathbf{v}=\frac{\mathbf{z}_1(d)+\eta^*\mathbf{z}_2(d)}{1+\left|\eta\right|^2}. \tag{B.4}$$

Substituting (B.4) into (4.7), we get

$$\begin{aligned}\Gamma(d)&=\frac{\left\|\left|\eta\right|^2\mathbf{z}_1(d)-\eta^*\mathbf{z}_2(d)\right\|^2+\left\|\mathbf{z}_2(d)-\eta\mathbf{z}_1(d)\right\|^2}{\left(1+\left|\eta\right|^2\right)^2}\\&=\frac{\left|\eta^*\right|^2\left\|\eta\mathbf{z}_1(d)-\mathbf{z}_2(d)\right\|^2+\left\|\mathbf{z}_2(d)-\eta\mathbf{z}_1(d)\right\|^2}{\left(1+\left|\eta\right|^2\right)^2},\\&=\frac{\left\|\mathbf{z}_2(d)-\eta\mathbf{z}_1(d)\right\|^2}{1+\left|\eta\right|^2}\end{aligned} \tag{B.5}$$

which is the same as (4.10).

By substituting (B.4) into (B.3), we find

$$\frac{\left\|\mathbf{z}_1(d)+\eta^{*}\mathbf{z}_2(d)\right\|^2}{\left(1+|\eta|^2\right)^2}\eta=\frac{\left(\mathbf{z}_1(d)+\eta^{*}\mathbf{z}_2(d)\right)^H}{1+|\eta|^2}\mathbf{z}_2(d)\,. \tag{B.6}$$

After expanding (B.6) and eliminating the same terms on the two sides of the equation, we get

$$\mathbf{z}_2^H(d)\mathbf{z}_1(d)\eta^2+\left(\left\|\mathbf{z}_1(d)\right\|^2-\left\|\mathbf{z}_2(d)\right\|^2\right)\eta-\mathbf{z}_1^H(d)\mathbf{z}_2(d)=0\,, \tag{B.7}$$

which is the same as (4.11).

APPENDIX C: DERIVATION OF (4.29) and (4.30)

With (4.27) and (4.28) being the received signal when the correct decision is made, (4.6) can be written as

$$\mathbf{z}_1(d) = \mathbf{v} + \mathbf{w} \tag{C.1}$$

and

$$\mathbf{z}_2(d) = \eta\mathbf{v} + \mathbf{w}\,. \tag{C.2}$$

By substituting (C.1) and (C.2) into (4.18), we get

$$\hat{\eta}(0) = \frac{\| \mathbf{a} \|^2 - \| \mathbf{b} \|^2 + \sqrt{(\| \mathbf{a} \|^2 - \| \mathbf{b} \|^2)^2 + 4 | \mathbf{a}^H \mathbf{b} |^2}}{2\mathbf{a}^H \mathbf{b}} \tag{C.3}$$

where

$$\mathbf{a} = \mathbf{v} + \mathbf{w} \tag{C.4}$$

and

$$\mathbf{b} = \eta\mathbf{v} + \mathbf{w}\,. \tag{C.5}$$

Then by substituting (C.3), (4.23) and (4.24) into (4.26), $f(0)$ can be written as

$$\begin{aligned} f(0) &= \left\| \frac{\hat{\eta}(0)\mathbf{r}_1 - \mathbf{r}_2}{\hat{\eta}(0)\alpha_1 - \alpha_2} - \mathbf{s}(0) \right\|^2, \\ &= \left\| \frac{\hat{\eta}(0)\mathbf{b} - \mathbf{a}}{\hat{\eta}(0)\alpha_1 - \alpha_2} \right\|^2 \end{aligned} \tag{C.6}$$

which is the same as (4.29).

Similarly, (4.30) can be calculated by the same procedure.

APPENDIX D: DESCRIPTION OF TRADITIONAL ML AND SMI

D.1 Traditional ML

ML decision is based on the likelihood between the received signal and transmitted signal. Thus the cost function is given by

$$\Gamma_{ML}(d) = \sum_{k=1}^{X} \left\| \mathbf{r}_k(d) - \alpha_k \mathbf{s}(d) \right\|^2 . \quad \text{(D.1)}$$

The transmitted symbol can be detected by using

$$d_0 = \arg\min_d \left\{ \Gamma_{ML}(d); d = 0,1,\cdots M-1 \right\} . \quad \text{(D.2)}$$

D.2 SMI

Based on [56], SMI minimizes the mean squared error (MSE) between the output of an N-element adaptive array and a desired reference signal.

Assume that **h** is the weighting vector and

$$\mathbf{R} = [\mathbf{r}_1 \ \mathbf{r}_2 \ \mathbf{r}_3 \ \ldots \ \mathbf{r}_{X+1}] . \quad \text{(D.3)}$$

Then, the cost function of SMI can be

$$\Gamma_{SMI}(d) = \left\| \mathbf{hR} - \mathbf{s}(d) \right\|^2 . \quad \text{(D.4)}$$

The optimum weight for this is [76]

$$\mathbf{h}_{opt} = \mathbf{R}^{-1}\mathbf{s}(d)\,. \tag{D.5}$$

Substituting (D.5) into (D.4), the cost function can be rewritten as

$$\Gamma_{SMI}(d) = \left\| \mathbf{R}^{-1}\mathbf{s}(d)\mathbf{R} - \mathbf{s}(d) \right\|^2 . \tag{D.6}$$

Thus, the transmitted symbol can be detected by using

$$d_0 = \arg\min_{d} \left\{ \Gamma_{SMI}\left(d\right); d = 0,1,\cdots M-1 \right\} . \tag{D.7}$$

AUTHOR'S PUBLICATIONS

[1] Fangming Liu, C. C. Ko, "Volumetric-based Detection Scheme for multi-Antenna FH/MFSK Systems in the Presence of Multi Follower Jamming", Signal Processing, Volume 90, Issue 6, pp 2031-2042, June 2010.

[2] Fangming Liu, H. Nguyen-Le, C. C. Ko, "Vector Similarity-Based Detection scheme for Multi-Antenna FH/MFSK Systems in the Presence of Follower Jamming", IET on Signal Processing, Vol. 2, Issue 4, pp346-353, Dec. 2008.

[3] Fangming Liu, H. Nguyen-Le, C. C. Ko, "ML-based beamforming for follower jamming rejection in slow FH/MFSK systems", Proceeding of 9th IASTED InternationalConference on Signal and Image Processing, Aug. 20-22 2007, Honolulu, USA, pp335-340.